Mechanistic Studies on Flavocytochrome c_3

Katherine L. Pankhurst

THESIS PRESENTED FOR THE DEGREE OF

DOCTOR OF PHILOSOPHY

UNIVERSITY OF EDINBURGH

OCTOBER 2002

The work presented in this thesis is the original work of the author, except where specific reference is made to other sources. It has not been submitted in part, or in whole, for any other degree. Some of the results have already been published.

Acknowledgements

I would like to thank my supervisors Steve and Graeme, for all their guidance and support. Thanks also to all the members of the Chapman and Reid groups (past and present) for making the lab such an enjoyable place to work. Particular thanks go to Dr. Caroline Miles for the fcc_3 mutagenesis, Ruth Moysey and to Dr. Chris Mowat for solving all those crystal structures. Thanks so much to Emma for her work on fcc_3 and for being the best flatmate a stressed-out thesis writer could hope to live with!

Finally, a huge thank you to my family for always being there for me and always believing in me. I hope you know how much I appreciate it.

Abstract

Flavocytochrome c_3 is a soluble, periplasmic, fumarate reductase from *Shewanella frigidimarina* which consists of three domains. Four *c*-type hemes in a cytochrome domain supply electrons to a non-covalently bound FAD in a flavin domain. The third, clamp, domain undergoes conformational changes to allow substrate access. Fumarate is reduced to succinate by hydride transfer from the flavin N5 and protonation by Arg402, the active site acid (Doherty; 2000). Arg402 is reprotonated by a proton pathway involving Glu378 and Arg381. This thesis reports an investigation into the enzyme mechanism by site directed mutagenesis.

Fumarate is bound in the active site via important interactions with the side chains of His504, His365, Thr377 and Arg544. The substitution of Thr377 by alanine causes a 13-fold decrease in k_{cat} and a 27-fold increase in K_M, consistent with a role purely in substrate binding. Substituting Arg544 with methionine dramatically lowers the k_{cat} by 10^4-fold and raises the K_M 29-fold. This residue is involved in substrate binding but is likely to have an additional role polarising the substrate molecule, for hydride attack.

A structural sodium ion is located close to both the active site and the FAD tail group. It is bound in approximately octahedral geometry by five backbone carbonyls (Thr506, Met507, Gly508, Thr536 and Glu534) and a water molecule. Substituting Glu534 results in an inability to retain FAD. His505 hydrogen bonds to the water molecule ligating the sodium and is also next to His504, which is one of the substrate binding residues. The pH-activity profile of wild-type fits to a single pK_a value of 7.5 ± 0.1 which is attributed to His504 stabilising the build up of charge in the reaction intermediate. This pK_a is raised to 8.2 ± 0.1 by the substitution H505Y and to 9.0 ± 0.2 by H505A. The k_{cat} value is lowered 2-fold and 20-fold for these mutants respectively. In the mutant enzymes His504 has become a weaker acid and is less able to enhance the rate at low pH. The role of His505 may be to moderate the effect of the negative charge of Glu534 on His504.

The active site acid, Arg402, has a dual role as both a Lewis acid (stabilising the build up of charge after hydride transfer) and a Brønsted acid (delivering a proton to

the substrate C3). The structure of the mutant enzyme R402A revealed a water molecule at the active site (Mowat; 2001), but this is too far from the substrate C3 to act as the acid catalyst and the enzyme is completely inactive (Doherty; 2000). The double mutant Q363F/R402A, however, is active, but at a level 10^4-fold lower than wild-type. The structure shows that the water molecule is now close enough to the substrate C3 to act as an acid catalyst.

Wild-type fcc_3 has an overall solvent isotope effect, k_H/k_D, of 8.2 ± 0.4 and its proton inventory fits to a model for multiple exchangeable hydrogenic sites, consistent with a complex transition state involving a proton pathway. Q363F/R402A has double the solvent isotope effect of wild-type and the proton inventory indicates that the transition state remains complex. So the active site water is trapped and requires reprotonation by the proton pathway.

Substituting Arg402 by glutamine lowers the k_{cat} 10^5-fold. Not only is glutamine a poor Lewis acid but the structure shows that the shorter side chain results in an increased proton transfer distance. The mutant R402F is completely inactive as phenylalanine is unable to protonate the substrate.

Substitution of either of the proton pathway residues dramatically decreases the activity of the enzyme. E378A is completely inactive. Substituting Glu378 with aspartate or glutamine lowers the k_{cat} 10^2-fold or 10^3-fold respectively. Arg381 is close to the protein surface but substitution with lysine or methionine lowers k_{cat} 10-fold or 10^2-fold respectively. The solvent isotope effect is only slightly increased for E378Q, R381K and R381M, but for E378D it is double that of wild-type, indicating compromised proton transfer in this mutant. The structure of R381K has two water molecules in the proton pathway, which may mediate in proton transfer. E378D has no water in the pathway so the increased isotope effect must be a direct result of the substitution.

Contents

Chapter 1: Introduction   1

Chapter 2: Materials and Methods 46

Chapter 3: Substrate Binding

Chapter 4: The Sodium Site and the Role of His505

Chapter 5: The Active Site Acid Catalyst 88

Chapter 6: The Proton Pathway 110

Appendices 129

List of Figures

Chapter 1
Introduction

1.0 Introduction

Flavocytochrome c_3 (fcc_3) is the fumarate reductase from *Shewanella frigidimarina*. It catalyses the two-electron reduction of fumarate to succinate (Figure 1.1) in the terminal step of a common anaerobic respiratory pathway. Fcc_3 is a member of a large family of fumarate reductases and succinate dehydrogenases (which catalyse the reverse reaction) from a wide variety of organisms. The entire family have structurally similar catalytic domains with high sequence identity, implying a common mechanism for fumarate reduction/succinate dehydrogenation. The majority of fumarate reductases are membrane bound, multi-subunit complexes. Fcc_3, however is a soluble, single-subunit enzyme (Pealing *et al*, 1992) and is therefore ideal for establishing a mechanism for fumarate reduction which can be applied throughout the family.
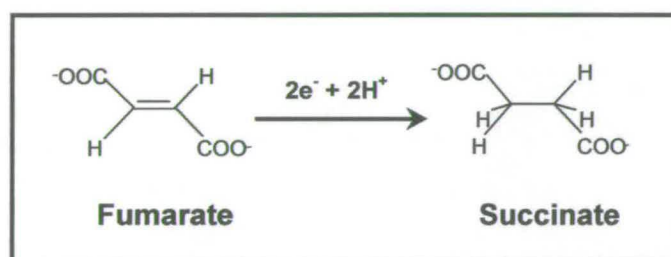
Figure 1.1: The reduction of fumarate to succinate, involving the transfer of two electrons and two protons.

1.1 Redox Centres

Page *et al* (1999) searched the protein data bank for structures of redox proteins with known function and analysed the electron transfer distances between redox centres. They found that there is a physiological range of 4-14 Å, within which electron transfer may occur. Beyond that, a chain of redox cofactors spaced $\leq$ 14 Å can mediate fast electron transfer over great distances.

Nature has evolved a wide variety of redox centres, for example: Heme, flavin, metal ions such as iron and copper, NAD^+/NADH, quinones/quinols and even amino acid residues may be redox active. Of these, heme, flavin and metal ions are usually bound within a protein complex, while NADH and quinols are mobile electron carriers. The latter are hydrophobic and located inside the cell membranes.

1.1.1 Heme

The heme moiety consists of an iron bound by four ring nitrogens at the centre of a porphyrin macrocycle. Hemeoproteins have several different roles in nature. These include electron transfer (eg. cytochrome *c*), storage (such as oxygen storage by myoglobin) or in catalysis (eg. P450s). Heme is generally a one-electron cofactor, with iron accessing the two most stable oxidation states, Fe^{2+} and Fe^{3+}, but some mechanisms have been shown to involve ferryl intermediates (Fe^{4+}), such as the P450 and heme-copper oxidase reaction cycles.

Hemes are classed according to the nature of the porphyrin ring, hemes *a-c* are shown in Figure 1.2. Each type has a characteristic UV-visible absorption spectrum which arises from $\pi \rightarrow \pi^*$ electronic transitions of the porphyrin ring. The *b*-type hemes are also called iron protoporphyrin IX with the other naturally occurring porphyrin types being modifications of this. A *c*-type heme is an iron protoporphyrin IX that is covalently bound to the protein via thioether links formed by the condensation of cysteine with the vinyl groups of the porphyrin. Heme *a* is less common and has two modified side chains: a formyl group and a seventeen carbon sidechain. Heme *a* is, to date, only found in the family of heme-copper terminal oxidases (section 1.2.3.4).
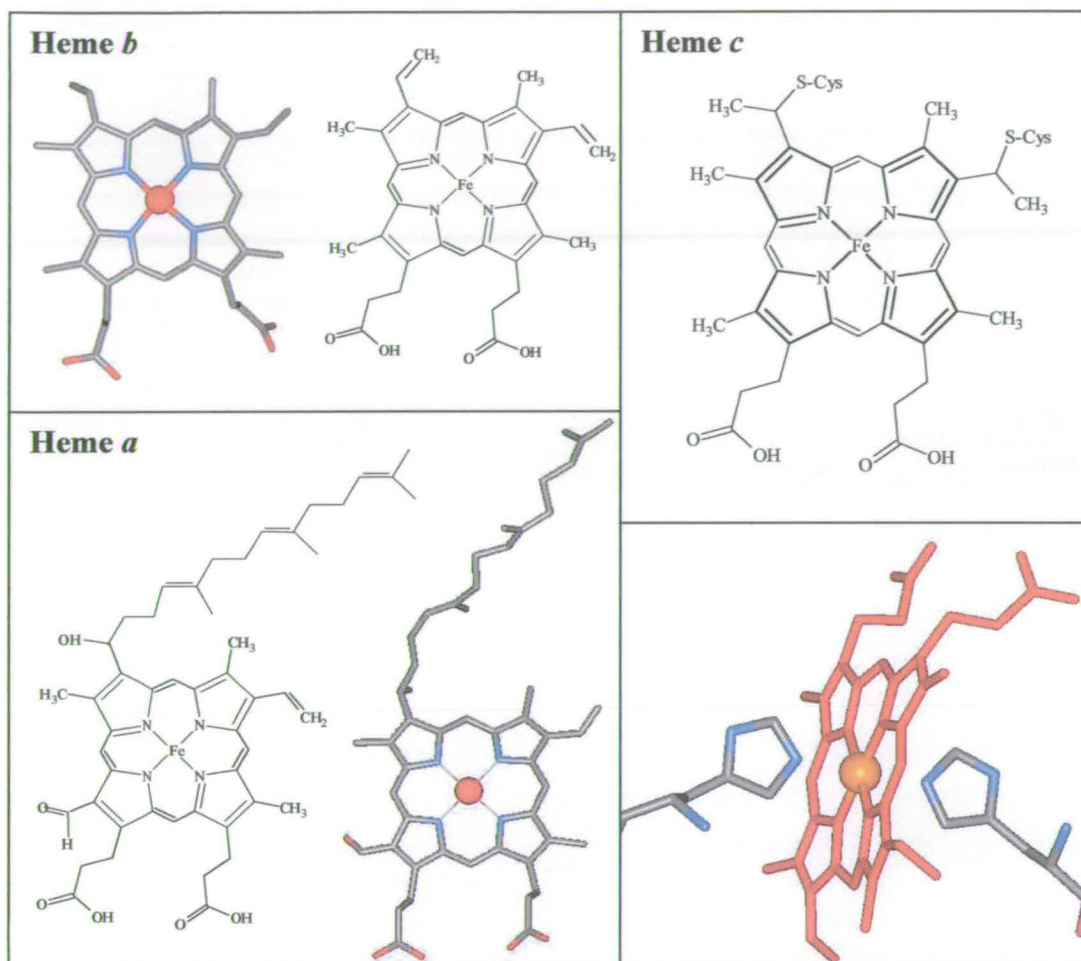
Figure 1.2 Heme types. Heme b, or iron protoporpyrin IX, is shown in the top left of the diagram. Heme c differs from heme b in that it is covalently bound to the protein via two cysteine residues. Heme a has two modified side chains, a formyl group and a seventeen carbon chain. Heme a is only known to be a cofactor in the family of heme-copper terminal oxidases. An example of heme axial ligation, by two histidine residues, is shown in the bottom right.

1.1.2 Flavin

Flavin is an extremely versatile cofactor. The redox active section is the isoalloxazine ring, which has three redox states (Figure 1.3c), fully oxidised, semiquinone and a fully reduced or hydroquinone. Depending on the protonation state, either a blue or a red semiquinone is formed. The availability of three oxidation states means that the flavin can act as a transceiver, receiving electrons singly and performing a two electron reduction, or vice versa.

Flavin occurs in biology as either flavin adenine dinucleotide (FAD) or flavin mononucleotide (FMN) (Figure 1.3), both of which are derived from vitamin B_2, riboflavin. They undergo almost identical electron-transfer reactions but the difference between them is in their tail groups, which serve to anchor the flavin to the protein (Figure 1.3b,c) by hydrogen bonding interactions with surrounding residues. Flavin may also be bound into the protein by a covalent link with the isoalloxazine ring (Scrutton, 1999). The flavin binding motifs are shown in Figure 1.3d. Known examples of covalently bound flavin involve linkage of the 8α or 6 carbon to a histidine, cysteine or tyrosine residue.
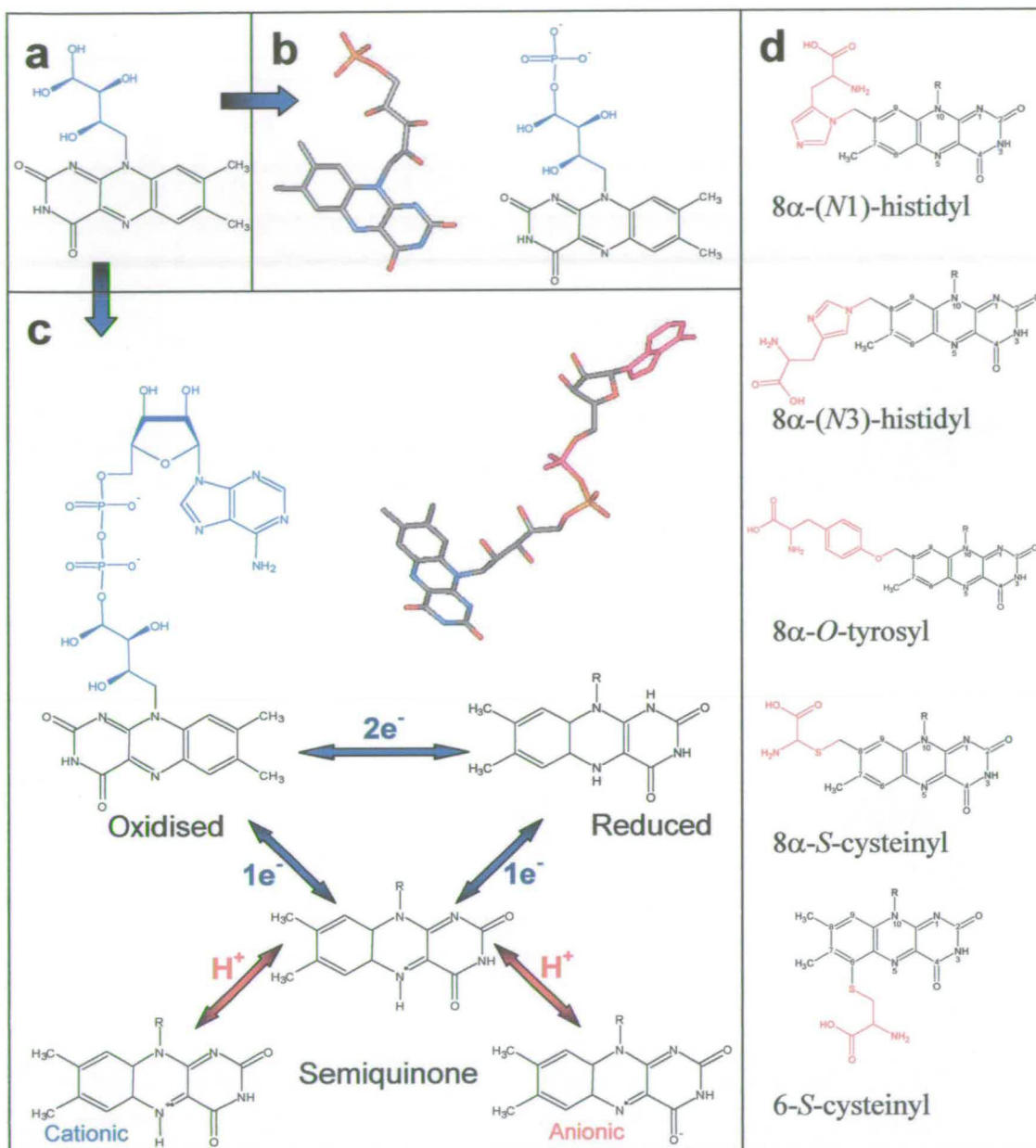
Figure 1.3: Flavins. (a) Riboflavin, vitamin B2, from which both FAD and FMN are derived. (b) Flavin mononucleotide (FMN) (c) Flavin adenine dinucleotide (FAD). The redox states of a flavin isoalloxazine ring are shown. Flavin may act either as a two-electron or one-electron donor/acceptor as it can access three redox states; fully oxidised, fully reduced and semiquinone. Depending on the protonation of the semiquinone it may be cationic (blue), neutral (colourless) or anionic (red). (d) Flavin covalent binding motifs.

1.1.3 Iron Sulfur Clusters

Iron is important for many protein redox reactions, cycling between Fe^{2+} and Fe^{3+}. It may be incorporated as mononuclear iron co-ordinated largely by 4 cysteine residues, or as an iron sulfur cluster. Iron in a cluster is covalently bound to the protein by cysteine residues and within the cluster, iron atoms are bridged by inorganic sulfur atoms. Typical examples of mononuclear iron binding and iron sulfur clusters are shown in Figure 1.4. Although they generally have 2-4 iron atoms, overall the clusters only act as one electron centres.

$Fe(S^{\gamma}_{cys})_4$

$[Fe_2S_2](S^{\gamma}_{cys})_4$

$[Fe_3S_4](S^{\gamma}_{cys})_3$

$[Fe_4S_4](S^{\gamma}_{cys})_4$
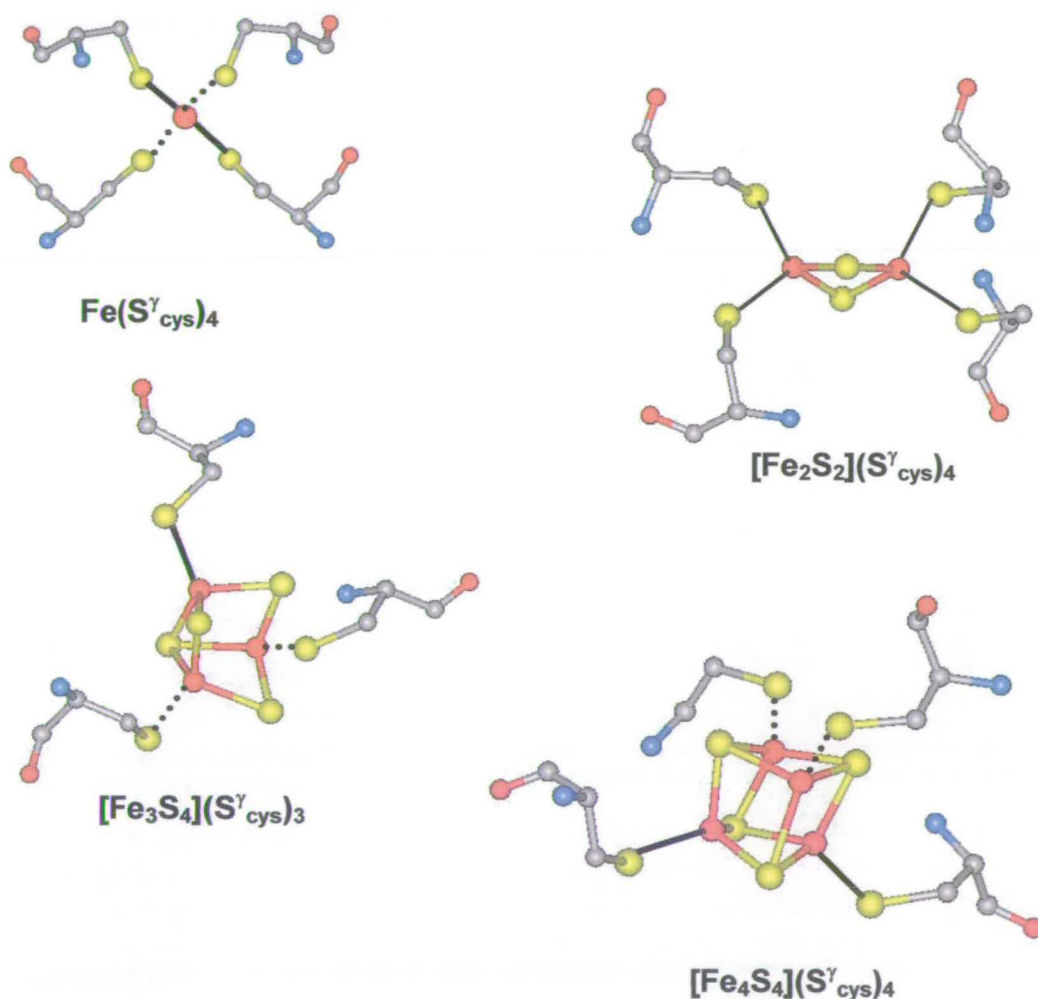
Figure 1.4: Examples of mononuclear iron binding and iron sulfur clusters. Iron is usually bound to the protein by the sulfur atoms of cysteine residues (an exception being the Rieske centre with two cysteine and two histidine ligands) and within the cluster is bridged to other irons by sulfur.

1.1.4 Quinones

Quinones are extremely hydrophobic molecules, owing to their long isoprenoid tail groups and they act as two electron carriers within the membrane. They occasionally also undergo more integral roles with binding sites within the protein, notably in the Q-cycle of complex III (section 1.3.3.1) and possibly in other respiratory complexes. The length of the tail groups varies depending on the organism, usually 10 isoprene units in mammalian cells and 6 in bacterial cells.

Mitochondria tend to use ubiquinone (UQ) in the electron transport chain, whereas bacteria utilise menaquinone (MK) (Figure 1.5a). Both can undergo $2e^- + 2H^+$ reduction to form quinol or partial reduction to a semiquinone.

1.1.5 NADH

Nicotinamide adenine dinucleotide (NAD^+) is a redox coenzyme. The nicotinamide ring is easily reduced and acts as an oxidising agent. NADH is widely used as a mobile reductant in respiratory pathways. The reduction of NAD^+ can be thought of as hydride transfer because, formally, two electrons and one proton are lost from the nicotinamide ring (figure 1.5b). In enzymes such as NADH dehydrogenase there are specific binding sites so that NADH is acting as a second substrate, which is constantly recycled in the cell.
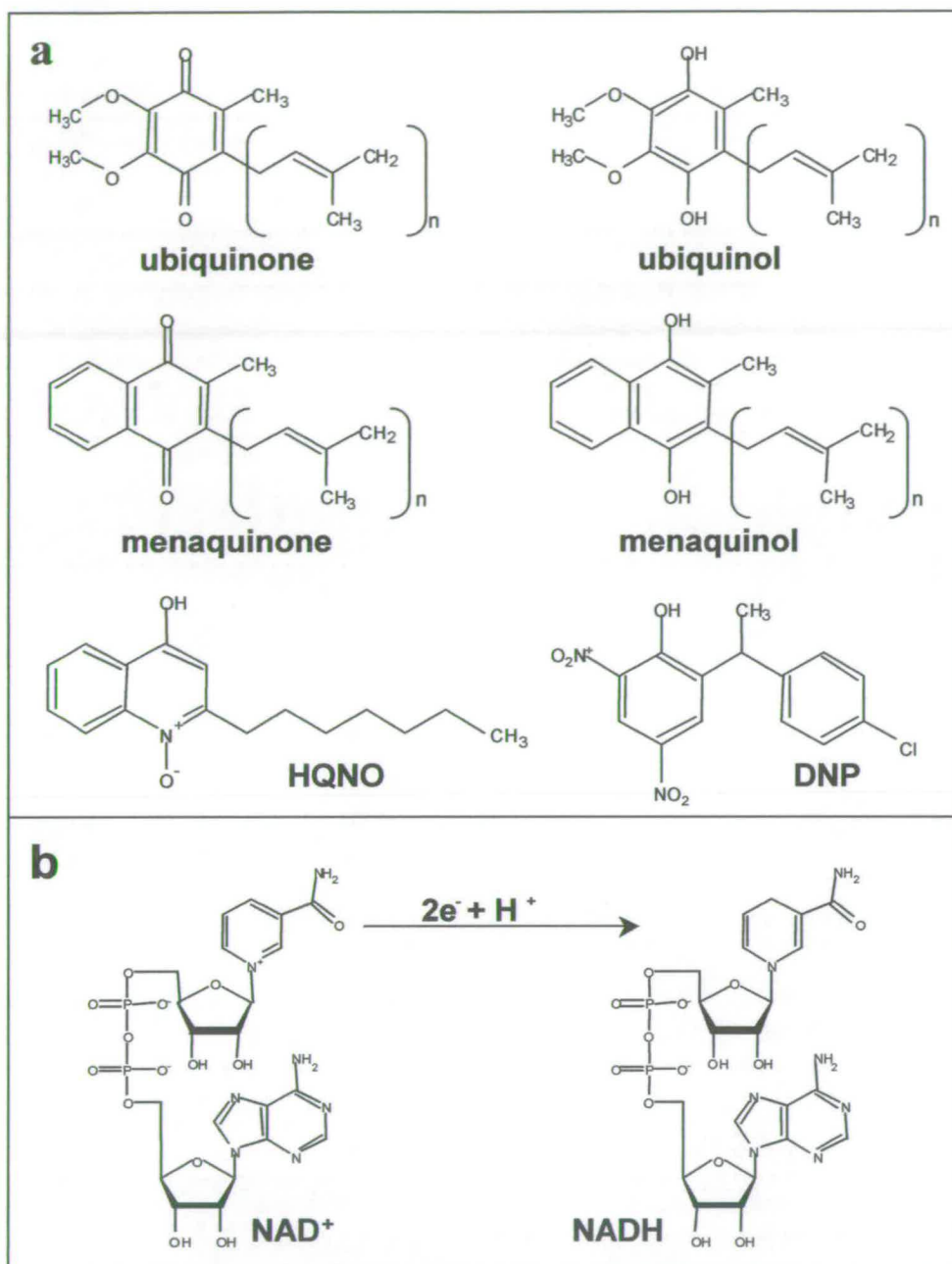
Figure 1.5: (a) Structures of quinone(ol)s and two quinone binding inhibitors; 2-heptyl 4-hydroxy quinoline N-oxide (HQNO), thought to be a semiquinone mimic, and 2-[1-(p-chlorophenyl)ethyl] 4, 6-dinitrophenol (DNP). Organisms respiring aerobically tend to utilise ubiquinone, whereas anaerobic organisms sometimes use menaquinone. (b) The reduction of NAD$^+$ to NADH.

1.2 Respiration

Cellular energy requirements are fulfilled by coupling with the hydrolysis of ATP (adenosine triphosphate), to ADP (adenosine diphosphate) and inorganic phosphate (Figure 1.6a). ATP is maintained in the cell at a concentration 7-10 orders of magnitude above its equilibrium level. Taking the typical concentrations of Pi (10^{-2} M) and ADP (10^{-3} M) in the cytoplasm would give an ATP concentration, at equilibrium, of only 10^{-10} M. The mitochondria, however, manage to maintain ATP around 10^{-2} M. It is this displacement from equilibrium that gives ATP the capacity to do work (Nicholls and Ferguson, 1992).

ATP is synthesised as a result of the breakdown of nutrient molecules such as carbohydrates. The sum of the processes involved in the catabolism of nutrients and the consequent release of energy is termed respiration. In eukaryotes, respiration is an aerobic process carried out in mitochondria. Bacteria may respire either aerobically or anaerobically, the latter will be discussed in sections 1.4 - 1.8.

1.2.1 Glycolysis

In glycolysis, 6-carbon sugar molecules are split into two 3-carbon pyruvate molecules, in the mitochondrial matrix. It is a multi-step, enzyme catalysed process but, overall, glycolysis is anaerobic and undergoes no net oxidation or reduction. The first five steps are an energy-investment-phase with two moles of ATP used to produce two moles of 3-carbon sugar phosphate from one mole of sugar. The next five steps are an energy generation phase resulting in four moles of ATP and two moles of pyruvate. Two reducing equivalents in the form of NADH also result from glycolysis:

$$2NAD^+ + \text{sugar (6C)} + 2ADP + 2P^i \rightarrow 2 \text{ pyruvate (3C)} + 2ATP + 2NADH$$
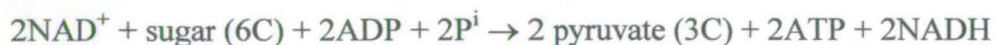
Pyruvate is then decarboxylated by the enzyme system 'pyruvate dehydrogenase complex' using coenzyme A to form acetyl CoA which then enters the citric acid cycle. A further reducing equivalent (NADH) is generated in the process.

1.2.2 The Citric Acid Cycle

The organic metabolites from glycolysis are oxidised in the citric acid cycle, which is another enzyme catalysed, multi-step, pathway (Figure 1.6b). Carbon enters the cycle as acetyl-CoA. In one cycle the acetyl group (originally from pyruvate) is oxidised to CO_2. In three of the four oxidation steps NAD^+ is the cofactor, reduced to NADH. In the fourth, the FAD cofactor of succinate dehydrogenase is used to oxidise the saturated carbons of succinate.

ATP is generated indirectly via GTP at one step in the cycle, the formation of succinate from succinyl-CoA. The oxidation of sugar to CO_2 through glycolysis and the citric acid cycle yields, in total, four moles of ATP per mole of sugar:

$$Sugar + 6H_2O + 10NAD^+ + 2FAD + 4ADP + 4P^i$$
$$\rightarrow 6CO_2 + 10NADH + 10H^+ + 2FADH_2 + 4ATP$$
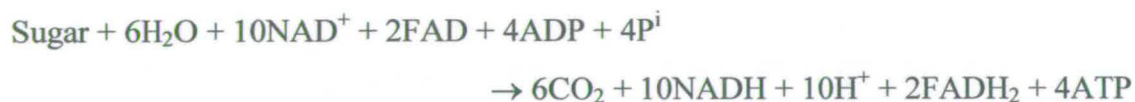
The reducing equivalents, NADH and $FADH_2$, are then reoxidised by a chain of membrane bound protein complexes which transfer electrons, ultimately reducing dioxygen to water. The electron transfer is coupled to the synthesis of further ATP.
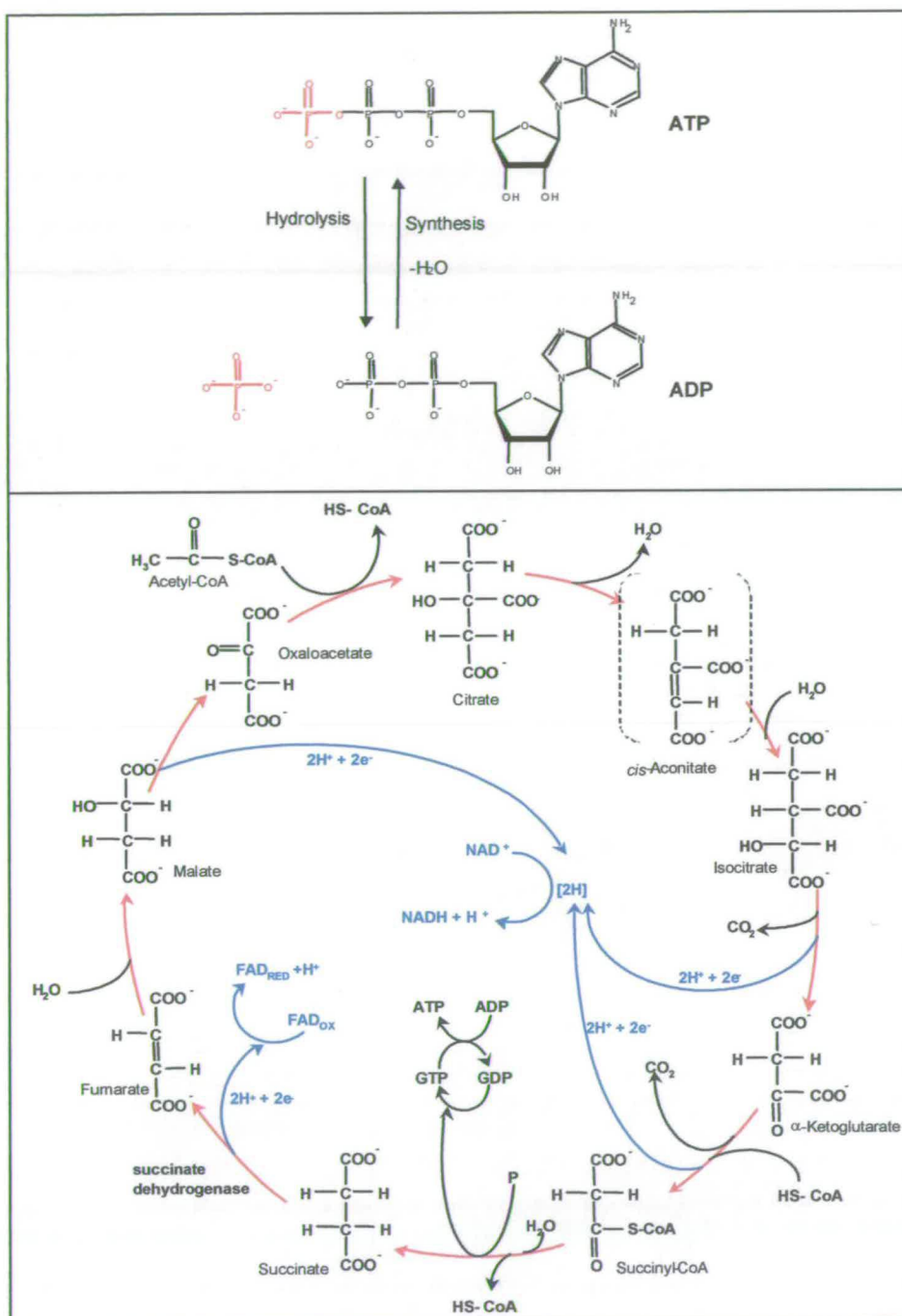
Figure 1.6: (a) Synthesis/hydrolysis of ATP. (b) The citric acid cycle. The organic metabolites from glycolysis enter the cycle as acetyl-coA and are ultimately oxidised to CO_2.

1.2.3 Oxidative Phosphorylation

The electron transport pathway consists of protein complexes anchored to the inner mitochondrial membrane (or the inner cell membrane of aerobic bacteria). Figure 1.7 shows the essential electron transfer complexes I-IV. Complexes I, III and IV generate a transmembrane proton electrochemical gradient which is utilised by complex V (ATP synthase) for the production of ATP. Electrons enter the chain either as NADH at complex I (NADH:quinone oxidoreductase), or directly from the citric acid cycle enzyme succinate:quinone oxidoreductase (SQR, complex II).

Figure 1.7 (following page): Oxidative Phosphorylation. (a) Schematic representation of the electron transport complexes I-IV showing the cofactors and the flow of electrons. Complexes I, III, and IV pump protons across the membrane, setting up an electrochemical gradient that is used by Complex V to drive ATP synthesis. (b) Crystal structures of the oxidative phosphorylation complexes. No structure is available for NADH dehydrogenase. The structure shown for succinate dehydrogenase is that of the closely related fumarate reductase (W.succinogenes).

a

2H⁺ (/e⁻)

UQ

N2 FeS

UQH₂

UQH₂

UQ

UQH₂

UQH₂

UQ

2Fe2S

2H⁺ (/e⁻)

c

c₁

Qₒ

bₗ

Qᵢ

bₕ

Cu_A Cu_A

a

Cu_B

a₃

H⁺ (/e⁻)

UQH₂

N1, N5, N4

FeS

FMN

NADH

NAD⁺ + 2H⁺

b

FAD

Succinate   Fumarate + 2H⁺

½ O₂ + 2H⁺   H₂O

c_{6-10}   a

3   b₂

γ

α

β

ADP + Pⁱ   ATP

3H⁺ (/ATP)

**Complex I
NADH dehydrogenase**

**Complex II
succinate
dehydrogenase**

**Complex III
cytochrome
*bc₁***

**Complex IV
cytochrome *c* oxidase**

**Complex V
ATP synthase**

b
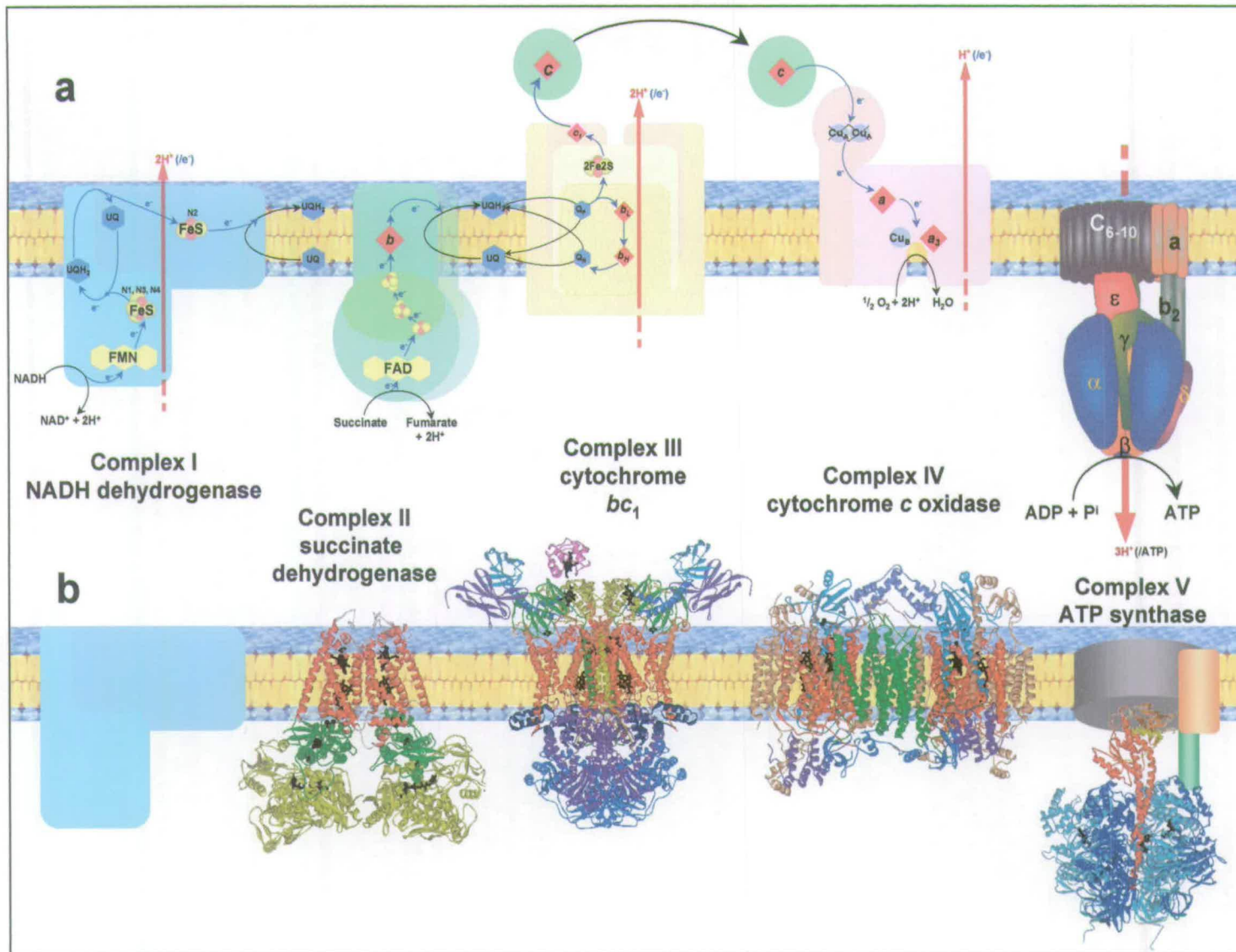
1.2.3.1 Complex I: NADH:Quinone Oxidoreductase

(NADH Dehydrogenase)

NADH dehydrogenase is the largest and most complex of the electron transport proteins with >30 subunits, which is reflected in the lack of a crystal structure to date. Complex I catalyses the oxidation of NADH and the reduction of quinone in the membrane. It translocates protons across the inner membrane with a stoichiometry of $4H^+/2e^-$ (Nicholls and Ferguson, 1992). The complex contains one FMN cofactor and possibly as many as seven iron sulfur clusters, four of which are well characterised:

N1	2Fe:2S	low potential	
N2	4Fe:4S	high potential	Probably donor to UQ
N3	4Fe:4S	low potential	
N4	4Fe:4S	low potential	

The complex may also contain an internal quinone that is involved in proton translocation but not exchangeable with the quinone pool.

NADH dehydrogenase can be degraded into three different fractions by disrupting the water structure with chaotropic agents, such as NaBr. The flavoprotein and the iron sulfur protein are both soluble but the remainder of the protein forms a hydrophobic fraction. The flavoprotein fraction is comprised of three subunits and contains the NADH binding site, FMN, N1, and a 4Fe:4S cluster. This fraction can catalyse the transfer of electrons from NADH to non-physiological acceptors. The iron sulfur protein consists of six polypeptides and contains three iron sulfur clusters. The rest of the enzyme makes up the hydrophobic fraction, which contains an unknown number/type of iron sulfur clusters. The high potential 4Fe:4S cluster N2 is thought to be located in the membrane section of the protein and to be the electron donor to quinone.

Low resolution electron microscopy data suggest that the enzyme is L-shaped (Weiss *et al*, 1990). A smaller NADH dehydrogenase is expressed in the fungus *Neurospora*

crassa when protein synthesis is inhibited by chloramphenicol. This corresponds to the hydrophilic arm of the molecule and suggests that the larger enzyme evolved from the combination of the small enzyme with another pre-existing collection of subunits, perhaps to enable the complex to pump protons across the membrane.

A mechanism for complex I has been proposed (Figure 1.7a) whereby NADH binds and passes electrons to the FMN which then transfers them sequentially to an 'electron pool' consisting of the low potential iron sulfur clusters, N1, N3 and N4. The electrons then enter an internal theoretical Q-cycle before passing to the high potential cluster N2 and finally reduce free quinone to quinol (Weiss *et al*, 1990).

1.2.3.2 Complex II: Succinate:Quinone Oxidoreductase

(SQR, Succinate Dehydrogenase)

As mentioned previously, SQR is one of the enzymes from the citric acid cycle and it passes electrons directly into the electron-transport chain. The protein consists of two domains. Figure 1.7a includes a schematic of complex II and the flow of electrons. In the soluble domain, succinate is oxidised by FAD and electrons are passed along three iron sulfur clusters (2Fe:2S, 4Fe:4S, 3Fe:4S). Quinones are then reduced at the hydrophobic domain. The complex II family is discussed in further detail in section 1.5, including structural information about fumarate reductase which is of the complex II family.

1.2.3.3 Complex III: Quinone:Cytochrome c Oxidoreductase

(Cytochrome bc₁)

Cytochrome bc_1 catalyses the reduction of the small soluble electron transport protein cytochrome *c*, taking electrons from the quinol pool. It also translocates protons across the membrane with $4H^+/2e^-$ stoichiometry (Trumpower, 1990). Crystal

structures have been solved for complex III from bovine (Iwata *et al*, 1998) and chicken heart mitochondria (Zhang *et al*, 1998) and also from yeast (Lange and Hunte, 2002).

The number of subunits in this complex varies greatly between organisms, but the cofactors are all located in three essential subunits, an iron sulfur protein (ISP, Rieske), cytochrome c_1 and cytochrome b. The ISP is a soluble, globular protein located in the inter-membrane space, but anchored to the membrane by the hydrophobic N-terminus (Rieske fold). It contains a single 2Fe:2S cluster where one iron is co-ordinated by two cysteine residues and the other by two histidines. The crystal structure shown in Figure 1.7b is a dimer. In this figure, the Rieske protein is coloured green, cytochrome c_1 is yellow and cytochrome b is red. The remaining membrane spanning subunits are in orange and the subunits that lie in the matrix or inter-membrane space are in blue and purple. The structure shown is from *Saccharomyces cerevisiae* (Lange and Hunte, 2002) and was solved with the physiological electron acceptor; cytochrome c bound (pink). The redox cofactors are shown in black for clarity. Different crystal forms have yielded three conformationally different structures with regard to the Rieske protein. The iron sulfur cluster binding fold can either be positioned for fast electron transfer with cyt c_1 or cyt b or may adopt an intermediate configuration (Zhang *et al*, 1998; Iwata *et al*, 1998).

Cytochrome c_1 is also located in the inter-membrane space but is anchored to the membrane by its C-terminus. This subunit is entirely α-helical and contains one heme which is His, Met ligated. The cytochrome b subunit consists of transmembrane helices. It contains two hemes, one at each side of the membrane. The heme on the matrix side (b_H) is of high potential, +50 mV and the heme located near the inter-membrane space (b_L) is of low potential, -100 mV. Proton translocation is coupled to electron transfer in a Q-cycle:

1) Quinol binds on the outer side of the membrane (inter-membrane space) at a binding site called Q_P, from where an electron is transferred to the iron sulfur cluster in the Rieske protein. During this step two protons are released into the inter-membrane space. This first electron is then passed down the chain to cyt c_1 and cyt c.

A second electron is transferred from the semiquinone radical at Q_P, but this time to heme b_L and quinone leaves Q_P. The electron passes from b_L to b_H which is near a second quinol binding site Q_N at the matrix side of the membrane. Quinol binds at Q_N and receives the electron from b_H to form a semiquinone.

2) Another quinol binds at Q_P with the two electrons distributed as before. The second electron is given eventually to the semiquinone at Q_N to form quinol, with two protons taken from the matrix. So overall only two protons are taken from the matrix but four are given out to the inter-membrane space.
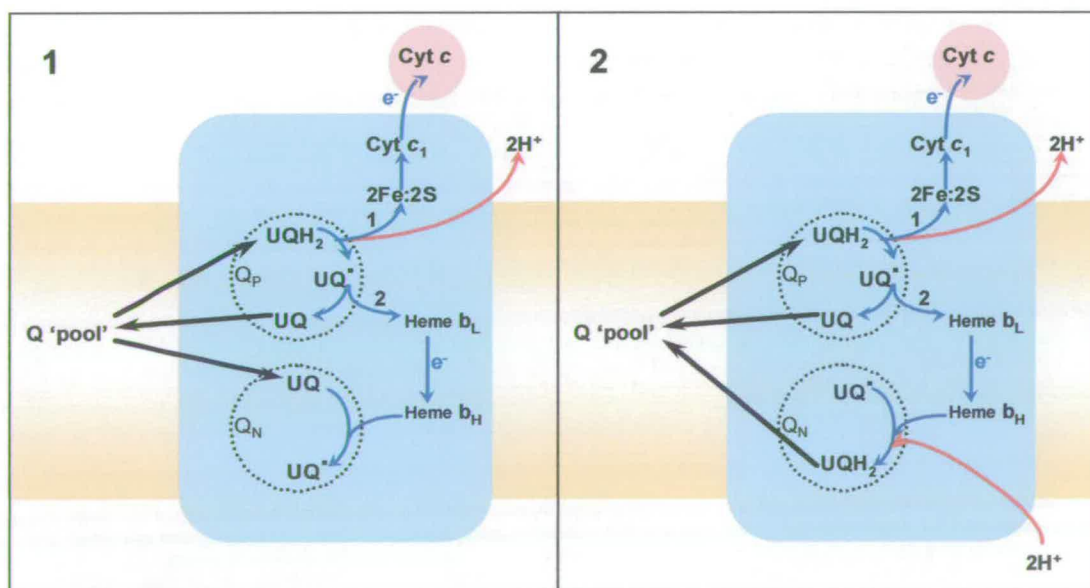
Figure 1.8: The Q-cycle. The diagram shows the electron transfer and proton transfer events occurring at the two quinol binding sites in complex III (Q_P and Q_N).

1.2.3.4 Complex IV: Ferrocytochrome:O_2 Oxidoreductase

(cytochrome c oxidase)

The terminal complex in the electron-transport chain is cytochrome c oxidase, which takes electrons from cytochrome *c* in the inter-membrane space and reduces O_2 to water in the matrix. Protons are pumped across the membrane with $4H^+/4e^-$ stoichiometry (Ferguson-Miller and Babcock, 1996). Crystal structures have been solved from *Paracoccus denitrificans* (Iwata *et al*, 1995) and bovine heart mitochondria (Tsukihara *et al*, 1996), both to 2.8 Å. The bovine structure is a dimer and shown in Figure 1.7b.

Bacterial complex IV is generally comprised of only three subunits but the mammalian complex may have up to thirteen. Sequences of the subunits making up the catalytic core are highly conserved throughout the family. The major catalytic subunit is embedded in the membrane (Figure 1.7b, red) and consists of twelve membrane spanning helices arranged in three semicircles of four helices with C_3 symmetry. There are three metal centres in this subunit, a copper ion (Cu_B) and two *a* type hemes (*a* and a_3). Heme *a* is bis-His ligated and as a result, low spin. Heme a_3 has only a proximal histidine and is thought to be high spin. Cu_B has three histidine ligands. These six histidines are completely conserved throughout the family. Cu_B and the high spin heme form a dinuclear site of O_2 reduction. O_2 is thought initially to form a short-lived bridged ferrous-oxy intermediate and to proceed via peroxide bridged and ferryl intermediates. The steps involving oxidation of the latter two species are coupled to proton translocation.

The second subunit is a ten strand β-barrel soluble domain, anchored to the membrane by two transmembrane helices (cyan). This subunit contains a mixed valence dinuclear copper centre bridged by two cysteine residues (Cu_A). One copper ion is also ligated by histidine and methionine residues and the other by glutamate and histidine. Cu_A is the first metal site to be reduced and is thought to pass electrons first to heme *a*, from where they are transferred to the dinuclear site (Figure 1.7a).

1.2.3.5 Complex V: F₁F₀-ATP Synthase

Electrons are transported by complexes I-IV whilst protons are pumped across the membrane perpendicular to the direction of electron transfer. This generates a proton gradient, $\Delta\mu H^+$, across the inner mitochondrial (or bacterial) membrane. Complex V, ATP synthase uses this electrochemical proton gradient to drive the synthesis of ATP from ADP and inorganic phosphate (Figure 1.6a).

ATP synthase is referred to as F_1F_0-ATP synthase. F_1 is the extra-membranous soluble fraction of the enzyme, located in the matrix and F_0 is embedded in the membrane. The structure varies little between organisms. The simplest ATP synthase is prokaryotic, which has subunit stoichiometry of $\alpha_3\beta_3\gamma\delta\epsilon ab_2c_{10-14}$. The likely arrangement of these subunits is shown in Figure 1.7a. F_1 consists of $\alpha_3\beta_3\gamma\delta\epsilon$ and several crystal structures of this portion of the protein are available. The most recent from bovine mitochondria, (Gibbons *et al*, 2000, 2.0Å) is shown in Figure 1.7b. The α (blue) and β (cyan) subunits have similar structures, with an N-terminal β-barrel domain furthest from the membrane and they alternate in a ring around the γ subunit (red).

An electron density map for an F_1c_{10} complex from yeast mitochondria has been obtained by Stock *et al* (1999), which clearly shows the c subunits forming a ring at the foot of the γ subunit. The resolution is unfortunately insufficient for the residue side chains to be discerned.

The c-ring forms a motor in the membrane that converts the proton gradient energy into rotational energy (Suzuki *et al*, 2002). There is currently no structure for subunit a but it is thought that the interface between a and c is important for proton translocation down the gradient. The b_2 and δ subunits are thought to form a 'stator stalk', anchored to subunit a at the membrane and α at the other end of the protein. Subunits γ and ϵ form a 'rotor stalk', connected to the c-ring at one end. This transmits energy to the catalytic domain, rotating within the $\alpha\beta$ ring. There are three

catalytic sites located at the interfaces between α and β pairs, where the rotational energy is used for the formation of a chemical bond between ADP and P^i.

The recent bovine mitochondrial ATP synthase structure (Gibbons *et al*, 2000) is the first to be solved with all three exchangeable sites occupied. The nucleotides are coloured black in Figure 1.7b. The crystals were grown in the presence of MgADP and AlF_3. In the structure two sites contain MgADP.AlF_4^- with the site in a closed conformation. The third site contains MgADP and is in a half closed conformation. This final site also contains a sulfate ion which is thought to mimic the binding of inorganic phosphate.

The three sites are thought to act sequentially (Boyer, 1993). In a recent review, Senior *et al* (2002) proposed a tri-site model, whereby catalysis at each site is at a different step in the cycle:

1) ATP synthase is reversible, also capable of catalysing the hydrolysis of ATP. The active site is modified for binding of ADP and P^i by movement of αArg376 into the catalytic site, resulting from changes at the αβ interface caused by rotation. αArg376 creates a P^i binding pocket and prevents ATP binding, so ADP binds in a complex with Mg^{2+}.

2) The αβ interface closes, forcing P^i and ADP together, overcoming their charge repulsion and forming the catalytic transition state. Upon complete closure of the site the ADP-P^i distance shortens and ATP is formed, leaving product water bound to βGlu181.

3) Further rotation of γ rearranges αArg376 so the catalytic transition state cannot reform and allow hydrolysis of the ATP.

4) ATP is released from the catalytic site.

1.3 Anaerobic Respiration

Many bacteria respire anaerobically as well as, or instead of, aerobically. A wide range of organic molecules and metal ions may be utilised as terminal electron acceptors. A common terminal electron acceptor for anaerobic respiration is fumarate, which is reduced to succinate (Figure 1.1) by quinol:fumarate reductase, QFR. A typical electron transport chain is shown in Figure 1.9. The chain has fewer components than those of the aerobic respiration electron transport chain, with hydrogenase and/or formate dehydrogenase reducing quinones in the membrane and fumarate reductase as the terminal reductase.
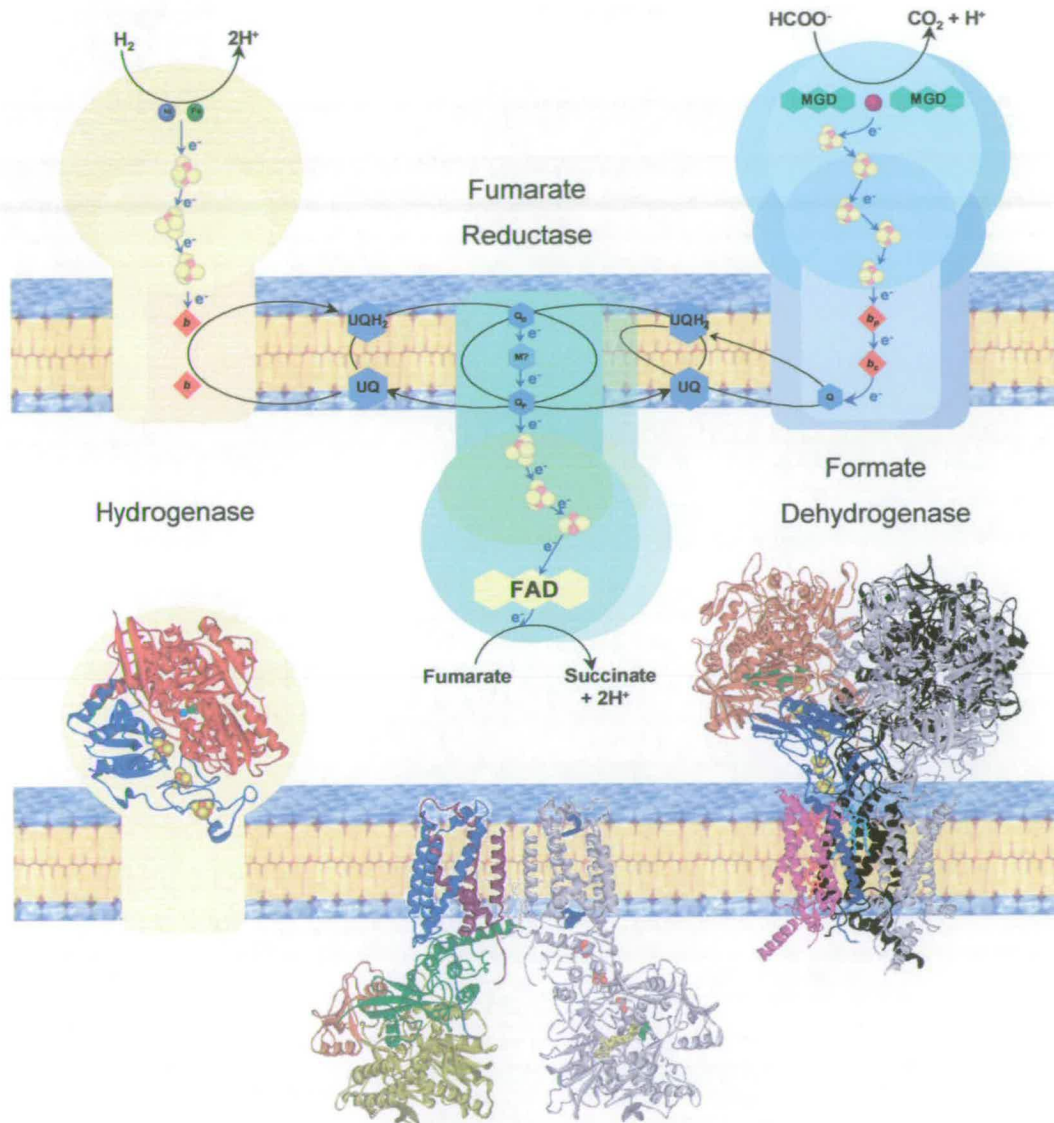
Figure 1.9: A typical anaerobic electron transport pathway. Quinones in the membrane are reduced by formate dehydrogenase (Fdh) and/or hydrogenase (Hyd). Fumarate reductase (QFR) takes electrons from the quinol pool for the reduction of fumarate. The top part of the diagram shows in schematic form the cofactors and flow of electrons and the lower part shows crystal structures of the enzymes. For hydrogenase the structure of the soluble enzyme from Desulfovibrio desulfuricans Miyazaki F (Higuchi et al, 1997) is included to illustrate the structure of the two most highly conserved subunits.

1.4 The Complex II Family

During aerobic respiration succinate dehydrogenase operates as part of the citric acid cycle, oxidising succinate to fumarate and feeding electrons directly into the electron-transport chain. Under anaerobic conditions, in the presence of fumarate, many bacteria express a quinol:fumarate reductase (QFR) that is analogous to SQR, but preferentially catalyses the reverse reaction (Cole *et al*, 1985; Van Hellemond and Tielens, 1994; Maklashina *et al*, 1998). The enzymes are structurally similar and are capable of catalysing both the reduction of fumarate and the oxidation of succinate.

The complex II family of enzymes (SQR and QFR) have very similar soluble domains, consisting of a flavoprotein and an iron sulfur protein (Cecchini *et al*, 2002; Lancaster *et al*, 2002). There are differences in the membrane anchors between members of the family and they are divided in 5 types depending on the number of subunits and their heme content (Figure 1.10). Type A tend to be 'classical' archaeal enzymes and have two hydrophobic subunits of transmembrane helices and two *b* hemes. Type B enzymes, such as *Wolinella succinogenes* QFR, have only one membrane spanning subunit, which has two hemes. Type C have two subunits and only one heme, an example being *E.coli* SQR. *E.coli* QFR, however, is of type D, which has two subunits but no heme. The final type of enzyme included in the complex II family is a little different. Enzymes of this type are 'non-classical' archaeal SQRs (Schäfer *et al*, 2002) and contain no heme in two hydrophobic subunits, which bear little resemblance to other members of the family.

There are as yet no crystal structures available for SQR, although structure of the *E. coli* enzyme is currently being refined (Tornroth *et al*, 2002). In 1999 five crystal structures of fumarate reductases were solved. Two were from complex II type QFRs (*E. coli* and *W. succinogenes*) and three were from *Shewanella* strains that express soluble periplasmic fumarate reductases. The highest resolution structure is that of fcc₃ from *S. frigidimarina*, at 1.8 Å (section 1.10).
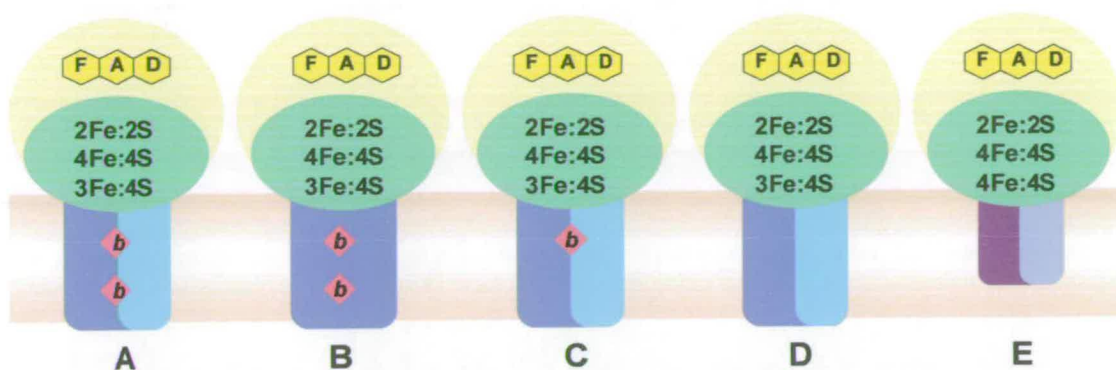
Figure 1.10: Classification of the complex II family of enzymes, SQRs and QFRs. There is great similarity in the hydrophilic domains but classification is based on the hydrophobic domains and their heme content.

1.4.1 The Structure of *E.coli* QFR

E.coli fumarate reductase is composed of 4 subunits, FrdABCD, and has a molecular weight of 121 kDa. The crystal structure was solved in 1999 by Iverson *et al* to 3.3 Å resolution (Figure 1.11a). The structure is of a dimer, however it is not thought that *E. coli* QFR is a physiological dimer, as the contact region is small and mediated by two detergent molecules. A QFR monomer has two distinct domains; the hydrophilic catalytic domain containing the flavin subunit (FrdA) and the iron sulfur subunit (FrdB), and the membrane anchor (FrdC and FrdD).
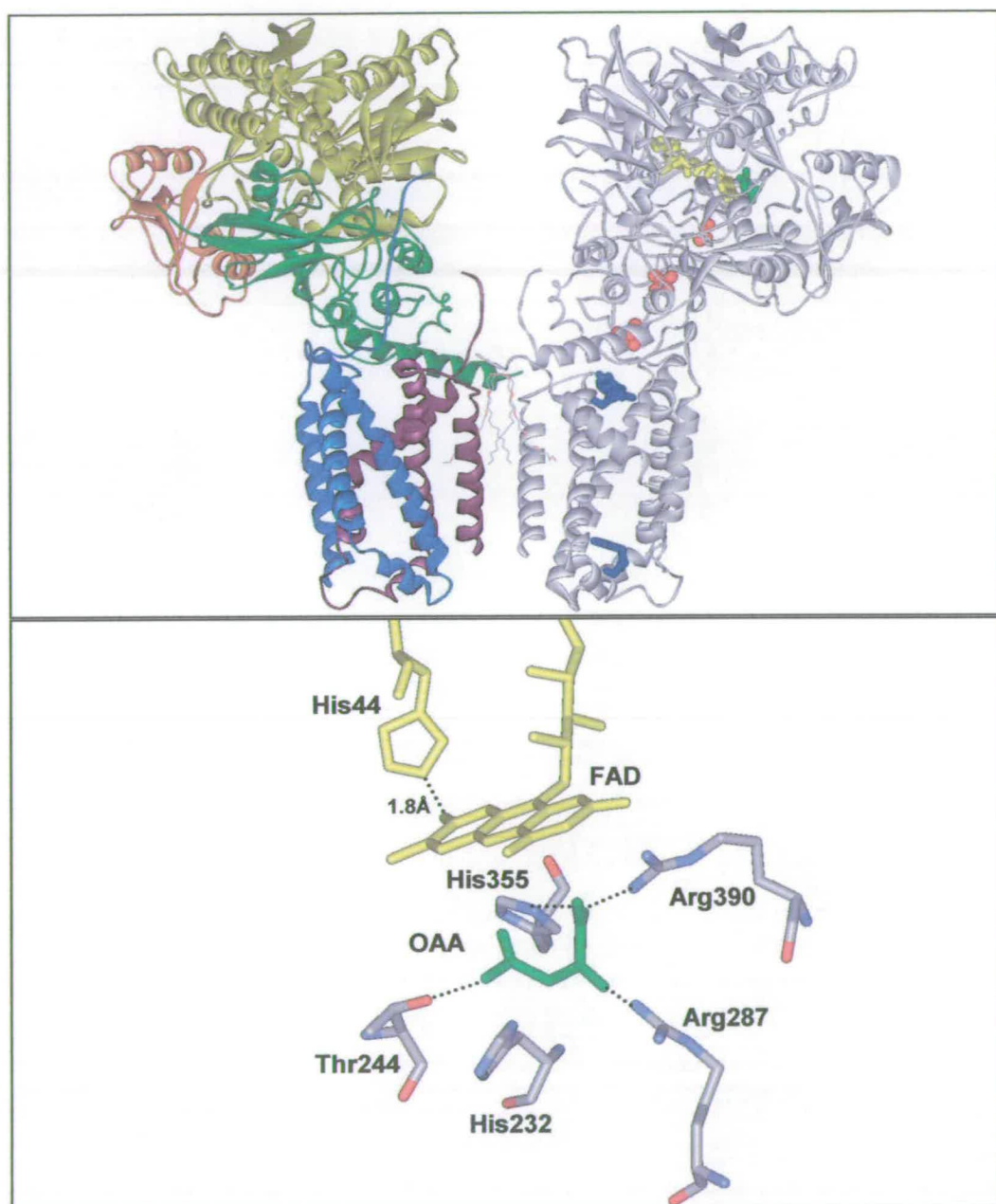
Figure 1.11: (a) The crystal structure of E. coli QFR. The monomer on the left is coloured according to subunits and domains. The flavin subunit is in yellow with the capping domain highlighted in orange. The iron sulfur subunit is in green and the membrane anchor subunits in blue and purple. The monomer on the right shows the cofactor locations within the protein. (b) Active site residues. The FAD in E. coli QFR is covalently bound to the protein by His44. The diagram shows the conserved residues involved in substrate binding, in green is the physiological inhibitor oxaloacetate.

1.4.1.1 Flavin Subunit (FrdA)

The flavoprotein subunit, as in all fumarate reductases and succinate dehydrogenases, consists of two domains; a capping domain is connected to the flavin binding domain by a short β sheet hinge. The active site lies at the interface between these two domains.

Fumarate is reduced to succinate by FAD that is covalently bound to the protein via His44 (Ackrell *et al*, 1989, Figure 1.11b). The covalent linkage and protein environment raise the flavin reduction potential to around –50 mV (Léger *et al*, 2001; Heering *et al*, 1997; Sucheta *et al*, 1993), compared to –219 mV for free FAD. This increase in potential is thought to be responsible for the reversibility of the complex II type enzymes (Blaut *et al*, 1989). The active site residues of *E. coli* QFR are shown in Figure 1.11b. The enzyme was crystallised with the inhibitor oxaloacetate bound at the active site. This ligand is bound by hydrogen bonds with His355, Arg390, Thr244, His232 and Arg287 (Figure 1.11b), all of which are strictly conserved throughout the family. Substituting His232 for Ser resulted in a drop in turnover rate from 133 s^{-1} to 33 s^{-1} (menaquinol:fumarate oxidoreductase assay). Before the crystal structure was solved it was suggested that His232 was the proton donor but that alternate donors could substitute for it when mutated, but it is clear now that it is only involved in substrate binding.

1.4.1.2 Iron Sulfur Subunit (FrdB)

The second soluble subunit, FrdB, contains three iron sulfur clusters that are arranged in a linear chain with edge-edge distances ideal for fast, efficient electron transfer (Figure 1.12). At the edge of the membrane is a 3Fe:4S cluster, 11.2 Å from a 4Fe:4S cluster which is in turn 7.6 Å from a 2Fe:2S cluster. This third cluster is ideally positioned close to the flavin domain to pass electrons to the FAD (9.2 Å). All the clusters are Cys ligated with typical iron sulfur cluster binding motifs: CxxxxCxxC...C (2Fe:2S), CxxCxxC...CP (4Fe:4S) and CxxxxxC...CP (3Fe:4S) (Werth *et al*, 1990). These sequences are largely conserved throughout the SQR/QFR family.

Before the crystal structure was solved the low midpoint potential of the 4Fe:4S (Figure 1.12) cluster had led to the suggestion that it was not involved in electron transfer, but the structural arrangement of the clusters clearly points to a role in electron transfer for all the clusters. With the distances concerned, the electron tunnelling rates will be sub millisecond despite the low potential of the 4Fe:4S cluster. For the observed turnover rate of 133 s^{-1}, electrons would only need to arrive every 0.004 seconds.
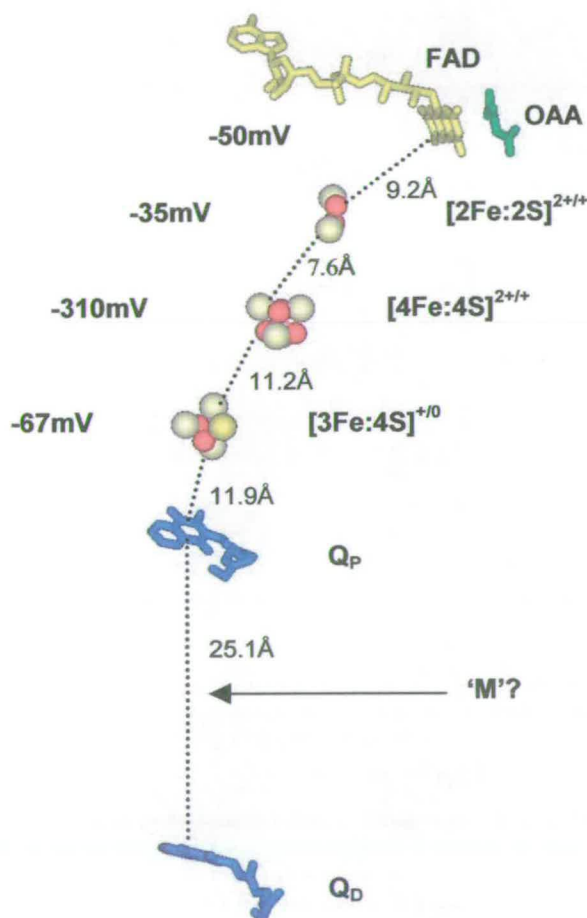
Figure 1.12: The chain of cofactors in E. coli QFR. The closest distances for electron transfer are shown. There is some evidence for the presence of a third quinol binding site, 'M', between Q_P and Q_D (Iverson et al, 2002). The midpoint potentials for FAD and the iron sulfur clusters are shown on the left (Léger et al, 2001).

1.4.1.3 The Membrane Anchor (FrdCD)

The hydrophobic domain of *E. coli* QFR is two subunits, each of which consists of three membrane spanning helices (Figure 1.11a) connected by extra membrane loops. As mentioned previously, *E. coli* QFR has no heme in its membrane spanning region to mediate electron transfer from menaquinol to the 3Fe:4S cluster. Two quinol binding sites were observed in the crystal structure, one on either side of the membrane, Q_P (proximal, near 3Fe:4S) and Q_D (distal) (Iverson *et al*, 1999; Cecchini *et al*, 1986a, b, Rothery and Weiner, 1998). Further crystal structures of *E. coli* QFR were solved by Iverson *et al* (2002) with the quinol binding inhibitors (Figure 1.5a) 2-heptyl 4-hydroxy quinoline N-oxide (HQNO) at 2.7 Å and 2-[1-(p-chlorophenyl)ethyl] 4, 6-dinitrophenol (DNP) at 3.6 Å. Both inhibitors are found at the Q_P binding site. The sites exhibited anti-cooperative binding behaviour with the inhibitors, as no density was observed at Q_D, although density was observed for the physiological quinol in both sites of the original structure.

Q_P and Q_D are positioned too far apart for direct electron transfer (~25 Å). It was suggested that Q_P alone was involved in electron transfer and that Q_D played a structural role, but with inhibitor bound at Q_P, Q_D is empty and the structure is uncompromised. A third quinol binding site ('M') has been postulated between the two sites to mediate electron transfer, based on some unassigned density and a cavity, but at 3.3 Å resolution this is speculative. It has been suggested that the Q_P site expands, incorporating the 'M' site for double occupancy, but Iverson *et al* are of the opinion that the helical structure will not allow movement of the intervening residues. There is, however, evidence to suggest that the 'M' site is important in some capacity, as the residues in that region have been shown by mutagenesis to be essential for enzyme function (Westenberg *et al*, 1990). The cavity also has the hydrophobicity characteristics of a quinol binding pocket.

1.4.2 The Structure of *Wolinella succinogenes* QFR

The structure of QFR from *W. succinogenes* was originally solved to 2.2 Å by Lancaster *et al* (1999, Figure 1.7b). The overall topology is very similar to that of *E. coli* QFR. The only obvious difference being the single subunit membrane anchor of four membrane spanning helices (Simon *et al*, 1998). Looking more closely, however, there are conformational differences around the active site, particularly to Arg301 (equivalent to Arg287 in *E. coli* and Arg 402 in *S. frigidimarina*. See Table 1.1). Water is now included at the active site (Figure 1.13a). Lancaster *et al* proposed a mechanism whereby water was the proton donor. A further crystal form later led them to conclude that their original structure was an open and inactive conformation (Lancaster *et al*, 2001, Figure 1.13b). The distances between Arg301 and the substrate cannot be compared between the two conformations as unfortunately the second structure has malonate bound at the active site instead of fumarate. The arrangement of active site residues in the new structure closely mirror those of *S. frigidimarina* fcc3, *S. oneidensis* MR1 fcc3, *S. frigidimarina* ifc3 and *E. coli* QFR. All of the above have very similar active site architecture and all exclude water.
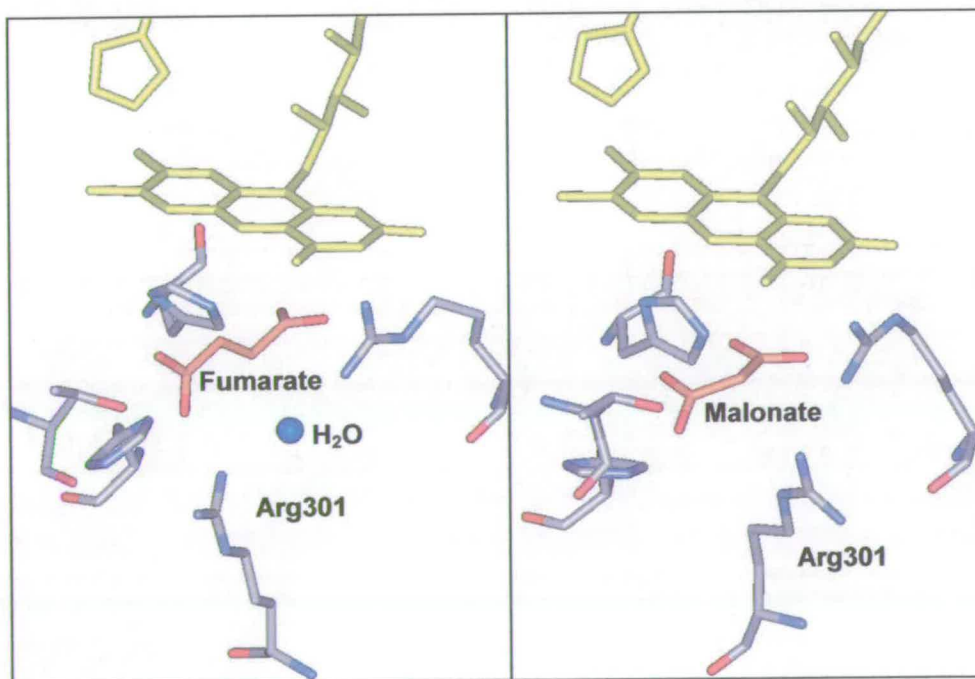
Figure 1.13: The active site of W. succinogenes QFR. (a) Open conformation including water (Lancaster et al, 1999) (b) A further crystal form contained the active site in a closed conformation (Lancaster et al, 2001). No water is now present.

1.5 Formate Dehydrogenase

The crystal structure of formate dehydrogenase from *E. coli* has been solved by Jormakka *et al* (2002) to 1.6 Å resolution. Formate dehydrogenase transfers electrons to the quinol pool for nitrate and fumarate respiration. The protein appears to be a trimer, each monomer comprised of three subunits. For clarity, only one monomer in Figure 1.9 is coloured according to subunit composition, the second and third monomers are coloured black and white. The structure is not dissimilar to QFR, with the α (orange) and β (blue) subunits forming a soluble domain, and the γ subunit (purple) is a membrane anchor of four transmembrane helices. The protein is bound to the inner membrane with the soluble domain located in the periplasm. The α subunit has two molybdopterin guanine dinucleotide cofactors, a 4Fe:4S cluster and a functionally relevant Se-cys. The β subunit has four 4Fe:4S clusters. The γ subunit has two *b*-hemes and a quinol binding site, located near the cytoplasmic side of the membrane.

1.6 Hydrogenase

There are three main types of hydrogenases; NiFe, Fe only and metal free. The NiFe type generally consist of one large catalytic subunit and a smaller iron sulfur subunit, they may, however, be anchored to the inner membrane by a third subunit (Kroger *et al*, 2002; Sawers, 1994). The membrane bound NiFe hydrogenases participate in the anaerobic electron transport chains of such bacteria as *W. succinogenes* and *E. coli*. The two hydrophilic subunits are similar throughout the family. Crystal structures have been published of soluble enzymes from *Desulfovibrio gigas* (Volbeda *et al*, 1996), *Desulfovibrio desulfuricans Miyazaki F* (Higuchi *et al*, 1997), *Desulfovibrio desulfuricans ATCC 27774* (Matias *et al*, 2001), *Desulfovibrio fructosovorans* (Rousset *et al*, 1998) and *Desulfomicrobium baclatum* (Garcin *et al*, 1999).

The structure shown in Figure 1.9 is from *Desulfovibrio desulfuricans Miyazaki F* (Higuchi *et al*, 1997). The large subunit (red) contains the NiFe active site and the

smaller subunit (blue) has three iron sulfur clusters; 4Fe:4S, 3Fe:4S and 4Fe:4S. In the membrane bound enzyme the catalytic subunit is HydB, the iron sulfur subunit is HydA which is anchored to the membrane by the hydrophobic C-terminus (Groβ *et al*, 1998). The third subunit, HydC, is hydrophobic and contains two *b*-type hemes (Figure 1.9).

1.7 $\Delta\mu H^+$ formation by the anaerobic electron transfer chain?

Jormakka *et al* (2002) proposed a mechanism by which formate dehydrogenase and nitrate reductase together translocate protons. Formate dehydrogenase converts $HCOO^-$ to CO_2 in the periplasm, releasing two protons on that side of the membrane. It also reduces menaquinone to menaquinol for which two protons are taken up from the cytoplasm. Nitrate reductase then uses protons from the cytoplasm as it reduces nitrate to nitrite. It takes electrons from menaquinol and releases protons into the periplasm.

Liposome experiments by Kröger have established that *W. succinogenes* complexes are capable of generating a transmembrane electrochemical proton gradient and that it can drive ATP synthesis (Kröger *et al*, 2002; Lorenzen *et al*, 1993; Lancaster *et al*, 2000, Ohnishi *et al*, 2000). So it might be imagined that a similar mechanism to the one outlined above might be in operation. However, it has been shown that the membrane potential created during fumarate respiration is entirely due to electron transfer from hydrogen or formate to menaquinone and not from menaquinol to fumarate. Additionally, the stoichiometry involved is H^+/e^-, which conflicts with the loop mechanism above, which would have stoichiometry of $2H^+/e^-$. A possible mechanism of $\Delta\mu H^+$ generation with the correct stoichiometry is shown in Figure 1.14. Hydrogenase converts H_2 to $2H^+$ in the periplasm and reduces menaquinone, taking protons from the cytoplasm. In doing so, this complex effectively translocates protons with stoichiometry of H^+/e^-. Fumarate reductase, however, takes two protons

from the cytoplasm to form succinate but also releases two into the cytoplasm on menaquinol oxidation. So there is no further proton translocation.

Despite the evidence from liposome experiments for *W. succinogenes* complexes, it is not certain that all anaerobic respiration electron transport pathways generate membrane potentials and drive ATP synthase *in vivo*. The metabolic ATP requirements of a bacterium may be supplied by glycolysis.
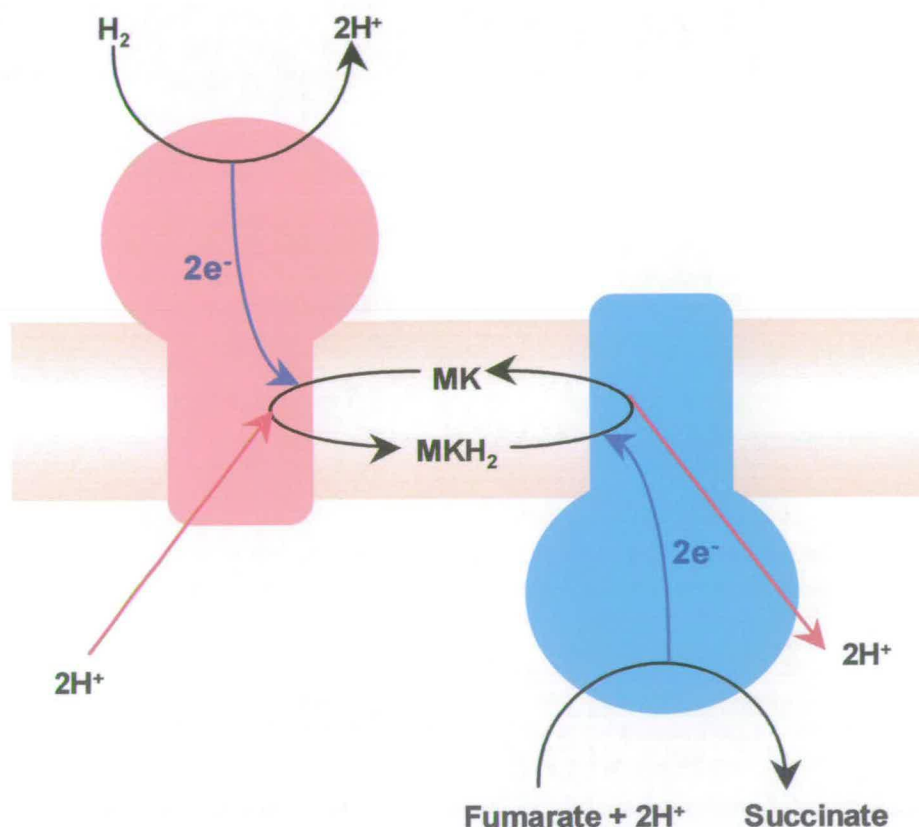
Figure 1.14: Possible mechanism for energy transduction in W. succinogenes by fumarate reductase and hydrogenase. Hydrogenase oxidises H₂ to 2H⁺ in the periplasm and reduces menaquinone to menaquinol in the membrane, taking two protons from the cytoplasm. Fumarate reductase oxidises menaquinol to menaquinone, releasing two protons into the cytoplasm and also reducing fumarate to succinate in the cytoplasm. So the net effect of the two complexes is the translocation of two protons from the cytoplasm to the periplasm.

1.8 *Shewanella frigidimarina*

Shewanella is a gram negative facultative anaerobe. Its range of terminal electron acceptors for anaerobic respiration is broad (Saffarini and Nealson, 1993; Saffarini *et al*, 1994), ranging from the metal ions Fe^{3+} and Mn^{4+} (Myers and Nealson, 1990; Baliaev and Saffarini, 1998; DiChristina and DeLong, 1994), to organic molecules such as TMAO (Ogdami *et al*, 1994), DMSO and fumarate and to nitrate, nitrite, sulfite, thiosulfate and elemental sulfur. This range of possible growth conditions makes *Shewanella* species extremely versatile bacteria, found in a wide range of environments. *Shewanella* strains have been isolated from many diverse environments. Two novel strains found in Antarctic sea ice samples were assigned as new species named *S. gelidimarina* and *S. frigidimarina* by Bowman in 1997. *S. oneidensis* was isolated from Lake Oneida, NY, USA (Myers and Nealson, 1988). *S. amazonensis* originated from sediment of the Amazon river delta (Venkateswaren *et al*, 1998). *Shewanella* species have even been observed in human clinical samples (Levin, 1972).

S.frigidimarina NCIMB 400 was first isolated from the North Sea, off the coast of Scotland. Originally classified as *S. putrefaciens*, it was re-classified by Reid and Gordon in 1999 to the recently defined *S. frigidimarina* species. As a marine bacterium it has been implicated in the corrosion of deep sea pipelines (Pickard *et al*, 1993). *Shewanella* is thought also to be involved in food spoilage, particularly fish, by the conversion of TMAO to TMA (Morris *et al*, 1990).

Anaerobic growth leads *Shewanella* to express a remarkable number of *c*-type cytochromes (Morris *et al*, 1990), the most abundant being flavocytochrome c_3, a fumarate reductase (Gordon *et al*, 1998; Morris *et al*, 1994; Reid *et al*, 1998; Pealing *et al*, 1992; 1995). When grown anaerobically in the presence of ferric iron an iso–enzyme of fcc_3 is produced (ifc_3) which is also a fumarate reductase, although strangely it is not expressed purely in the presence of fumarate (Dobbin *et al*, 1999).

Shewanella oneidensis MR1 also expresses an analogous fumarate reductase termed fcc_3-MR1.

1.9 Structure of Flavocytochrome c_3 from *Shewanella frigidimarina NCIMB 400*

Fcc_3 from *Shewanella frigidimarina* and its analogous enzymes from other *Shewanella* species are a novel class of fumarate reductases. They differ from the QFR-type fumarate reductase in several ways. Fcc_3 is a small soluble protein of 63 kDa. It reduces fumarate to succinate in the periplasm of the cell, whereas QFR is bound to the inner membrane and reduces fumarate in the cytoplasm. Fcc_3 is comprised of a single subunit unlike the three or four subunits required to make up complex II. There are also differences in the cofactor composition; although still a flavoprotein, fcc_3 is a flavocytochrome, and has no iron sulfur clusters.

The structure of fcc_3 was solved by Taylor *et al* at the University of Edinburgh in 1999, to 1.8 Å (Figure 1.15). The polypeptide is clearly divided into three domains. The heme domain is coloured red in Figure 1.15, with the four heme groups in atom type colours. The rest of the protein is similar to the flavin subunit of QFR, with a flavin domain (yellow) and a clamp domain (blue) and FAD at the active site between those two domains.
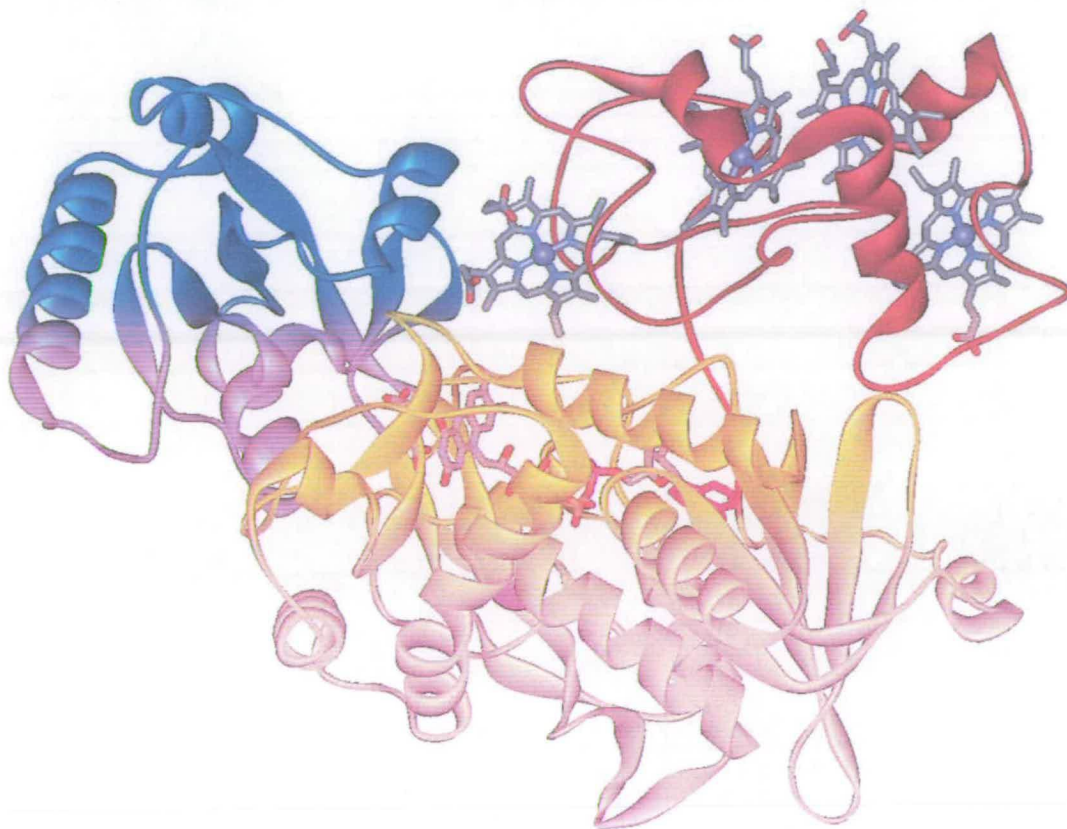
Figure 1.15: The crystal structure of fcc₃ from Shewanella frigidimarina. The flavin domain is in yellow, the heme domain in red and the clamp domain in blue. The heme groups, FAD and fumarate are all in atom type colours. In purple is the structural sodium ion located within the flavin domain.

1.9.1 Heme Domain

The C-terminal 104 residues form a cytochrome domain, containing four c-type hemes. Each heme is *bis*-His ligated and covalently linked to the protein by a CxxCH motif. The hemes supply electrons to the active site. They form a ~ 40 Å molecular wire for electron transfer, arranged in an unusual 'dog-leg' configuration. The edge-edge distances are all ≤ 8 Å (Figure 1.16a) so fast electron transfer is possible from heme I to heme IV, although hemes I-III are all clearly accessible to electron donors through the open protein structure. The midpoint potentials of the four hemes have been determined by potentiometric titration (-238, -196, -146, -102 mV, Turner *et al*,

1999). Assignment of potentials to specific hemes is not possible from potentiometric data alone.

Shewanella species also contain a periplasmic tetraheme cytochrome c_3, which is closely related to the heme domain of fcc₃ (Tsapin *et al*, 1996; Gordon *et al*, 2000). The hemes form the same unusual 'dog-leg' arrangement (Figure 1.16b) Although heme IV is slightly closer to the other hemes than in fcc₃, the heme core bears little resemblance to the well characterised c_3's from *Desulfovibrio* species (Picarra-Pereira *et al*, 1993; Turner *et al*, 1996). Heme assignment for this protein has been carried out by Passahna *et al* (2001) using 2D ^{1}H NMR. Heme IV was found to be the first to oxidise, followed by II, I and finally III. The extra protein bulk of fcc₃ and the nearby FAD group make comparison for the purposes of assignment impossible, but Passahna *et al* are currently undertaking a similar NMR assignment for fcc₃.
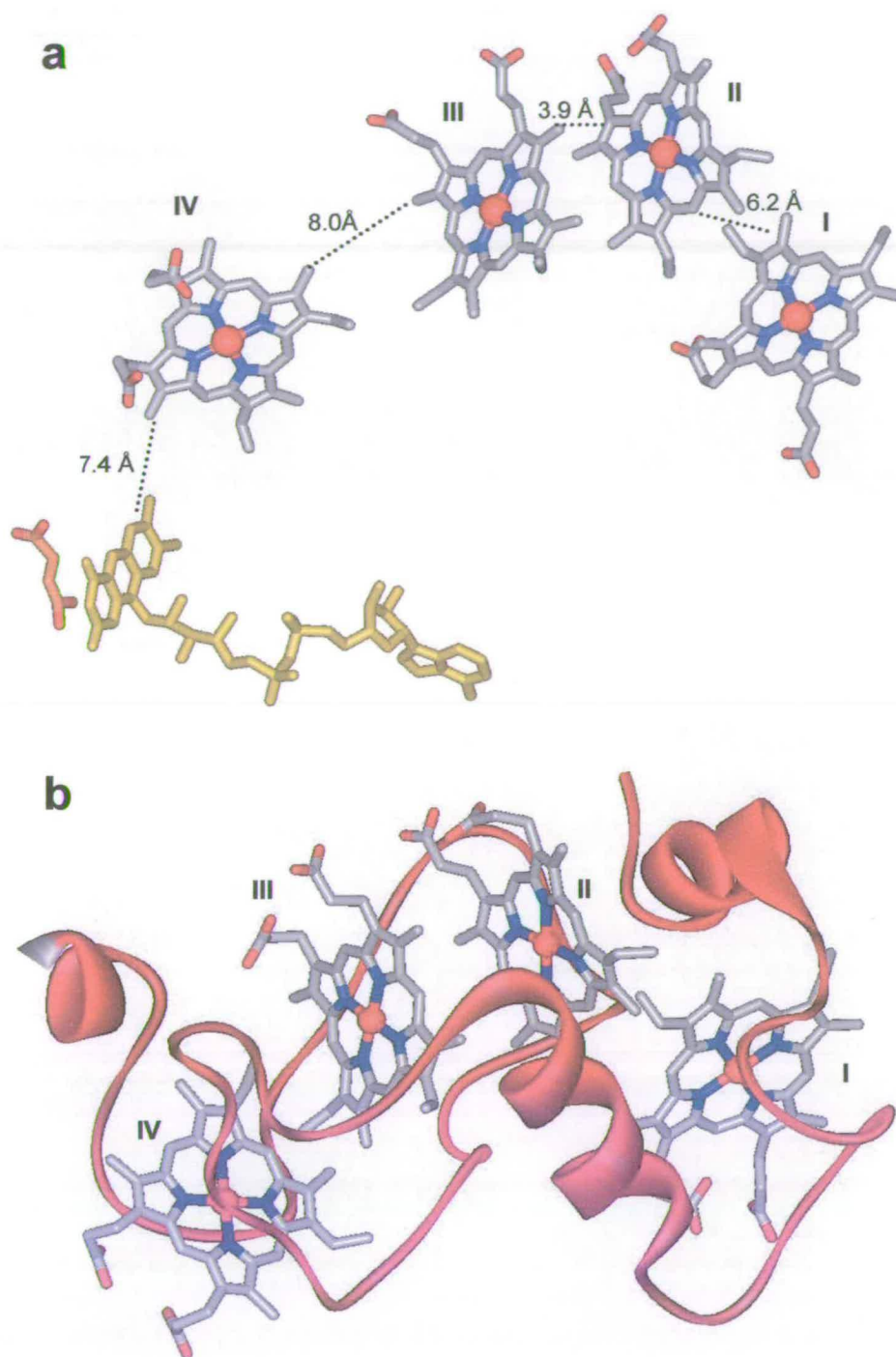
Figure 1.16: (a) The heme arrangement in fcc₃. The edge-edge distances are labelled. (b) c₃ is very similar to the heme domain of fcc₃. The structure shown is from MR1 (Leys et al, 2002) but the heme potentials for c₃ from S.frigidimarina have been assigned by NMR (Passahna et al, 2001).

1.9.2 Clamp Domain

The domain known as the clamp domain in fcc₃ is the equivalent of the 'capping domain' in QFR. This domain has significant freedom of motion. When open it allows substrate access to the active site, which is at the interface between the clamp and flavin domains. The active site is inactive until the clamp domain closes, as the substrate binding residues Thr377 and His365 are part of the clamp domain and hinge region respectively.

The structure of fcc₃-MR1 was solved in 3 different forms by Leys *et al* (1999); substrate free, fumarate bound and succinate bound. The three structures overlay well in the flavin and heme domains but some movement of the clamp domain is apparent in the substrate free structure. More conclusive evidence for active site access regulation by the clamp domain comes from open conformation of ifc₃.

1.9.2.1 Iron Induced Flavocytochrome c₃ (ifc₃)

Ifc₃ is a 63.9 kDa fcc₃ analogue, expressed by *S. frigidimarina* when grown anaerobically in the presence of ferric iron (Dobbin *et al*, 1999). Ifc₃ is the first observation of a protein being induced by growth on a metal ion. It has 43 % sequence identity with fcc₃ and similar heme and FAD potentials. Although ifc₃ is a fumarate reductase, it is not produced by the bacterium for fumarate respiration, even in the fcc₃ deficient strain EG301. When the ifc₃ gene is disrupted, *S. frigidimarina* NCIMB400 will still grow on Fe^{3+} but elevated levels of two other cytochromes are seen, a 35 kDa soluble protein and a 45 kDa membrane bound protein. There are multiple pathways to iron reduction, one involves ifc₃ but in its absence the other pathways can compensate.

The crystal structure of ifc₃ has been solved to 2.15 Å by Bamford *et al* (1999). The enzyme crystallised as homodimer, with the majority of the contact between the flavin domains. The protein is in the open conformation, in the absence of substrate. Ifc₃ (red) is overlaid with fcc₃ (blue) in Figure 1.17. The movement of the clamp

domain is clear, with ifc_3 in a more open conformation than fcc_3 by ~ 20°. Colouring by surface electrostatic potential clearly shows the basic fumarate binding pocket (Figure 1.17 inset).

Figure 1.17: Clamp domain movement. The structures of fcc₃ (blue) and ifc₃ are overlaid. The flavin and heme domains correspond well but the clamp domain of ifc₃ is in a significantly more open conformation. The fumarate bound in fcc₃ is in green. Inset (taken from Bamford et al, 1999): ifc₃ surface coloured according to electrostatic potential revealing the basic binding pocket.

1.9.3 Flavin Domain

The flavin domain is the largest section of the fcc₃ polypeptide. This domain does, in fact, bear great similarity to the flavin domains of the complex II enzymes, both structurally and in sequence identity. The FAD in fcc₃ is non-covalently bound with a potential of −152 mV. The enzyme is found to be essentially unidirectional. The fumarate is bound within the active site by hydrogen bonds with the residues Arg544, His504, His365 and Thr377 and Arg402 is positioned 3.0 Å from the fumarate C3 for proton transfer (Section 1.14, chapter 5). A summary of numbering for these conserved residues in the different proteins discussed in this chapter are in Table 1.1.

An interesting feature identified from the crystal structure of fcc₃ is the presence of a structural sodium ion close to the active site. It is visible in purple in Figure 1.15. The sodium ion and its environment is discussed in chapter 4.

Fcc₃	Fcc₃-MR1	Ifc₃	L-aspartate oxidase	E.coli QFR	W.succinogenes QFR
Arg402	Arg401	Arg397	Arg290	Arg287	Arg301
His365	His364	His360	His244	His232	His257
His504	His503	His499	His351	His355	His369
Thr377	Thr376	Thr372	Thr259	Thr244	Thr269
Arg544	Arg544	Arg539	Arg386	Arg390	Arg404

Table 1.1: Numbering of the catalytically important conserved active site residues for the members of the family for which crystal structures are available.

1.10 A Related Structure – L-Aspartate Oxidase

L-Aspartate oxidase (laspo) converts L-Asp to iminoaspartate as the first step in the biosynthesis of NAD^+. The enzyme is soluble with FAD as a cofactor, which is reoxidised by molecular oxygen, forming peroxide. Laspo may also use fumarate as an electron acceptor so the protein can function both aerobically and anaerobically.

The structure of laspo is very like that of fcc₃, with the active site situated between flavin and capping domains, but it has no requirement for hemes and instead has a C-terminal α-helical domain (Mattevi *et al*, 1999; Bossi *et al*, 2002, Figure 1.18). The protein has ~30 % sequence identity with members of the fumarate reductase/succinate dehydrogenase family. The active site contains all the conserved substrate binding residues and overlays well with that of fcc₃ (Tedeschi *et al*, 2001).
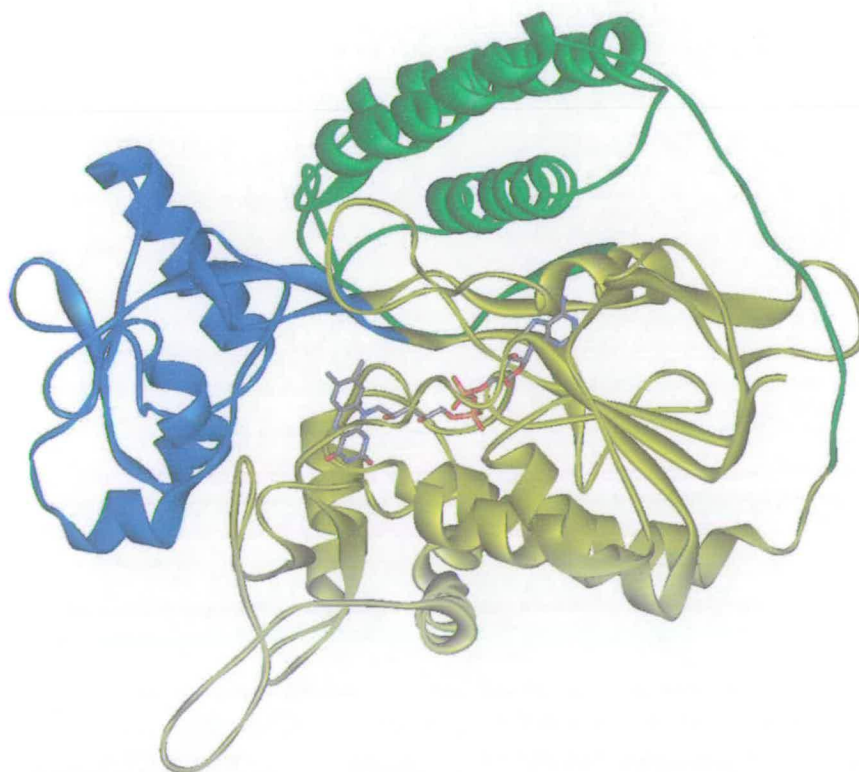
Figure 1.18: The structure of L-aspartate oxidase. L-aspartate oxidase bears great resemblance to the soluble fumarate reductases. All the residues important for catalysis are strictly conserved. The flavin domain is in yellow and the clamp domain is in blue. The FAD in L-aspartate oxidase is reoxidised by molecular oxygen so there is no requirement for heme groups. The third domain, in green, is referred to as the helical domain.

1.11 CymA: The Physiological Electron Donor to Fcc$_3$

QFRs receive electrons directly from quinols in the membrane pool. As fcc_3 is not associated with the membrane it must receive electrons from an alternate source. CymA is a 21 kDa *c*-type cytochrome from *S. oneidensis* MR1. It has a globular periplasmic tetra-heme domain that is anchored to the membrane by an N-terminal α-helix. The structural type is similar to the NapC/NirT family found in a range of facultative anaerobes (Myers and Myers, 1997; Simon *et al*, 2000). Another member of the family (NrfH) has been shown in liposome experiments to oxidise 1,4-napthoquinol and reduce NrfA, a periplasmic nitrite reductase from *W. succinogenes*.

Knock-out experiments have shown CymA to be essential for growth on nitrate, Fe^{3+}, Mn^{4+} and fumarate (Simon *et al*, 2000; Myers and Myers, 2000). It is proposed to act in a similar manner to NrfH, taking electrons from the membrane quinols and making them available to other electron transport proteins in the periplasm. In this way it may function in several pathways including fumarate respiration (Figure 1.19).

A solubilised form of CymA has been prepared (CymA$_{sol}$) and both fcc_3 and fcc_3-MR1 have been shown to receive electrons preferentially from CymA$_{sol}$ over cytochrome c_3, the soluble periplasmic electron transport protein (section 1.10.1). CymA$_{sol}$ transfers electrons to fcc_3 almost as fast as the artificial electron donor methyl viologen (Schwalb *et al*, 2002).
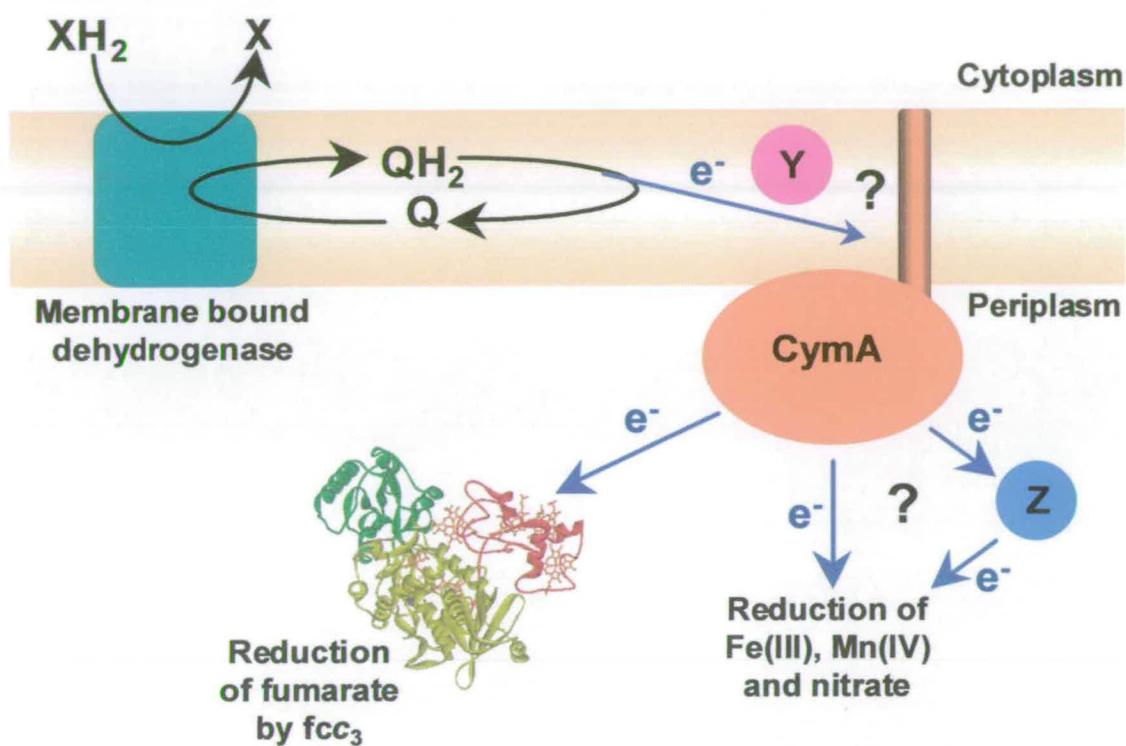
Figure 1.19: Schematic representation of the respiration pathways involving CymA. Quinones in the inner membrane are reduced by membrane bound dehydrogenases. It is not known whether CymA receives electrons directly from quinol or indirectly via a membrane integral electron transfer protein (Y) CymA is involved in the pathways of fumarate, Fe^{3+} and Mn^{4+} respiration. It may transfer electrons directly to the reductases or via a soluble electron transport protein in the periplasm (Z) (Schwalb et al, 2002).

1.12 Mechanism of Fumarate Reduction

Based upon the crystal structure of fcc$_3$, Taylor *et al* (1999) proposed a mechanism of fumarate reduction which is shown in Figure 1.20a.

1) A hydride is transferred from N5 of the fully reduced flavin to the fumarate C2. The resulting intermediate is thought to be stabilised by His504.

2) The intermediate C3 abstracts a proton from the nearby residue Arg402.

3) Arg402 is reprotonated by a proton pathway consisting of residues Glu378 and Arg381.

Fcc$_3$ was crystallised in the presence of fumarate but the species at the active site in the finished structure is malate. Figure 1.20b shows a proposed mechanism for hydroxylation at C2. During the crystallisation process the enzyme is oxidised so hydride transfer does not occur, but the substrate is activated so is susceptible to attack by water. This is purely an artefact of the crystallisation process.

All the residues involved in the above mechanism by substrate binding and proton transfer, including the active site acid Arg402 (Doherty *et al*, 2000), are strictly conserved throughout the soluble fumarate reductases and complex II family. L-aspartate oxidase also contains all the conserved residues implicated in the mechanism, so it appears to follow the same mechanism for dicarboxylate oxidation/reduction as the fumarate reductase/succinate dehydrogenase family. When Arg290 of laspo (Arg402 in fcc$_3$) was mutated to leucine the enzyme was completely inactive.

Fcc$_3$ is an ideal subject with which to study the mechanism of fumarate reduction/succinate oxidation as it is soluble and easier to prepare and crystallise. It is

also simpler to study kinetically because there is no quinone oxidation occurring simultaneously. The conservation of all important residues and the structural similarity between flavin domains of the whole family indicates that the catalytic mechanism of fcc_3 will be a universal mechanism for fumarate reduction. The work described in this thesis is an investigation into that mechanism by site directed mutagenesis. The detailed roles of the residues involved have been resolved by kinetic and crystallographic analysis of mutant forms of fcc_3.
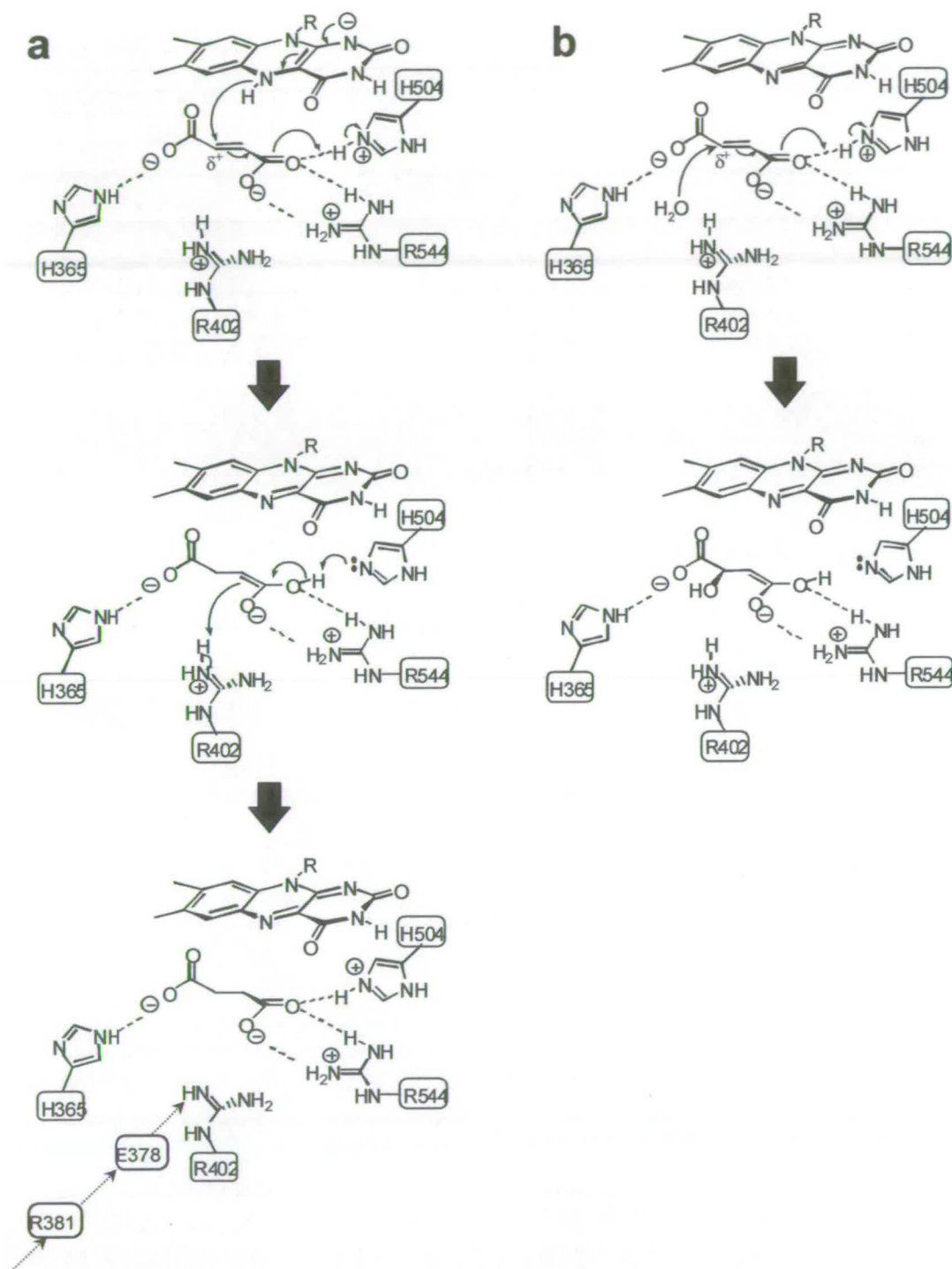
Figure 1.20: (a) Proposed mechanism for fumarate reduction by fcc₃. The first step is hydride transfer from the flavin N5, the resulting intermediate then abstracts a proton from Arg402 (Taylor et al, 1999). Arg402 is reprotonated by a proton pathway (Glu378 and Arg381). (b) Possible mechanism of substrate hydroxylation. The substrate is activated but the FAD is oxidised, so instead of hydride transfer occurring, a water molecule attacks the fumarate C2.

Chapter 2
Materials and Methods

2.0 Materials and Methods

2.1 Media and solutions

2.1.1 Luria Bertani High Salt Growth Media

Bacto tryptone	10 g/l
Yeast	5 g/l
NaCl	10 g/l

Filter sterilised antibiotics (50 mgl^{-1} kanamycin and 25 mgl^{-1} streptomycin) were added to the autoclaved media immediately prior to use.

2.1.2 Buffers

1M TRIS.HCl, I = 1M (Tris[hydroxymethyl]aminoethane)

dH$_2$O	500 ml
1M HCl	100 ml
NaCl	52.65 g

Adjusted to pH 8.4 with Trizma base and made up to 1 l.

Lysis Buffer

10 mM TRIS.HCl, I=10mM, pH 8.4

1 mM EDTA

0.2 mg/ml egg white lysozyme

50 mM MOPS, I = 50mM (3-[N-Morpholino]propanesulfonic acid)

dH2O	500 ml
1M NaOH	50 ml
NaCl	26.3 g

Adjusted to pH 7.8 with MOPS and made up to 1 l.

50mM TRIS.HCl (pH 7 - 9), I = 0.45M

dH$_2$O	500 ml
1M HCl	50 ml
NaCl	26.3 g
Methyl Viologen	0.5 g

Adjusted to the required pH at 25°C with Trizma base and made up to 1 l.

50mM MES.NaOH (pH 5.5 - 6.7), I = 0.45

(2-[N-Morpholino]ethanesulfonic acid)

dH2O	500 ml
1M NaOH	50 ml
NaCl	26.3 g
Methyl Viologen	0.5 g

Adjusted to the required pH at 25°C with MES and made up to 1 l.

**50 mM CHES.NaOH (pH 8.6-10), I = 0.45 (2-
[N-Cyclohexylamino]ethanesulfonic acid)**

dH2O	500 ml
1M NaOH	50 ml
NaCl	26.3 g
Methyl Viologen	0.5 g

Adjusted to the required pH at 25°C with CHES and made up to 1 l

2.2 Protein Purification

Site-directed mutants were prepared by Dr. Caroline Miles, ICMB, University of Edinburgh.

Recombinant enzyme was prepared using the pEGX₁/EG301 expression vector system (pEGX₁ plasmid - pMMB503EH fcc with signal sequence, EG301 – *Shewanella frigidimarina* NCIMB 400 Rif^R, Δfcc:ahp Km^R). Bacterial Strains were stored long term as DMSO stocks (-80 °C).

2.2.1 Growth of Recombinant and Mutant Forms of Fcc₃

- Starter flasks (50 ml Luria Broth) were inoculated with a single colony and grown overnight at 23°C, 150 rpm.
- 10 flasks (2l) containing 500 ml media were then inoculated with 5 ml portions of starter culture and grown for 8 hours as before.
- The Cultures were induced with IPTG (250 mgl^{-1}) and grown for a further 8-10 hours, 200 rpm.
- Cells were harvested by centrifugation (20 mins at 8,000 rpm, using a SLA-3000 rotor in a Sorvall RC-5B centrifuge).

2.2.2 Protein Extraction

The cells were re-suspended in the minimum volume of lysis buffer and stirred for 30 minutes at 4°C and then sonicated on ice at 10 microns for 3×20 seconds. The cell debris was pelleted by centrifugation (1 hr at 20,000rpm, using a SS-34 rotor in a Sorvall RC-26 Plus centrifuge). The supernatant was then 40% saturated with $(NH_4)_2SO_4$, re-centrifuged (20 minutes at 20,000 rpm) and the pellet discarded. The final supernatant was dialysed against 10mM TRIS.HCl, pH 8.4 (3×5l).

2.2.3 Anion Exchange Chromatography - DE52 (Whatman)

A 4×15 cm DE52 (Whatman) column was equilibrated with 10mM TRIS.HCl, pH 8.4 The protein solution was loaded, binding in a dark red band to the top 2 cm of the column. The protein was washed with the same buffer until the eluent absorption at 280 nm was minimal. The protein was eluted with a stepped gradient of NaCl in 0.1 M increments. Fcc_3 generally eluted at 0.2 M NaCl and was dialysed against 2×5l 10 mM TRIS.HCl.

2.2.4 Hydroxyapatite (Bio-Rad)

A 3×5cm column was equilibrated with 10mM TRIS.HCl, the protein was loaded and then washed with buffer until the absorption at 280nm was minimal. The protein was eluted with 0.1M K_2HPO_4.

2.2.5 FPLC (Fast Protein Liquid Chromatography)

For final purification the protein was dialysed into 10mM MOPS, pH 7.8 and further purified on an 1 ml Resource Q column (Pharmacia). All solutions were filtered prior

to use through a 0.45 µm Whatman nylon membrane. The pumps were equilibrated with the following solutions:

A: 10 mM MOPS

B: 10 mM MOPS, 0.5 M NaCl

The protein was filtered from a syringe through an FP point 45 ST filter unit, loaded through pump A and washed with 50 ml of buffer A at a flow rate of 4 ml/minute. The protein was eluted with a 20 ml linear gradient 0-0.5 M NaCl and collected in 1 ml fractions. The procedure is shown in schematic form in Figure 2.1.
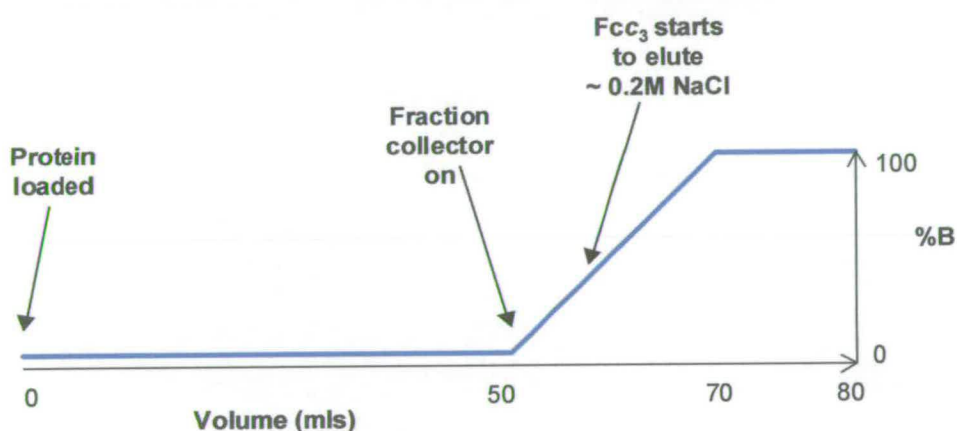
Figure 2.1: Elution profile used for final purification of fcc₃ by FPLC using a 1ml Resource Q column.

The column was regenerated as follows:

10 ml   1M NaCl

10 ml   Buffer A

10 ml   1M HCl

10 ml   Buffer A

10 ml   1M NaOH

10 ml   Buffer A

The column was stored in 20% ethanol, which was run through the column at a rate of 0.5 ml/min due to the greater viscosity.

2.3 Determination of Protein Purity and Concentration

2.3.1 Gel Electrophoresis

Pre-poured Invitrogen NuPAGE Novex 4-12 % Bis-Tris gels were used to determine the purity of the protein throughout the purification procedure and to ensure that protein of the correct molecular weight was obtained. Samples were prepared in NuPAGE LDS sample buffer (4×). The running buffer used was NuPAGE MES. Gels took approximately 35 min to run at a constant voltage of 200 V. SeeBlue Plus 2 pre-stained protein standard was used to mark the molecular weight. The approximate molecular weights for the markers in the buffer system described were:

Myosin	188 kDa
Phosphorylase B	98 kDa
BSA	62 kDa
Glutamic Dehydrogenase	49 kDa
Alcohol Dehydrogenase	38 kDa
Carbonic Anhydrase	28 kDa
Myoglobin Red	17 kDa
Lysozyme	14 kDa
Aprotinin	6 kDa
Insulin, B chain	3 kDa

The gels were stained with 1 % coomassie blue in 40 % MeOH, 10 % AcOH for 30 minutes and then the excess stain was removed with 40 % MeOH, 10 % AcOH. (Figure 2.2a)

2.3.2 UV-Visible Spectroscopy

A known volume of protein (typically 50-100 µl) was diluted to 1 ml with 10 mM TRIS.HCl and the oxidised protein spectrum between 240 and 650 nm was obtained using a Schimadzu UV-Vis scanning spectrometer. The relative intensities of heme

(409 nm) and total protein (280 nm) peaks were used to determine the purity of the protein. $Abs_{409}/Abs_{280} \sim 4.2$ indicated pure protein. (Figure 2.2b) The reduced spectrum was then obtained by addition of sodium dithionite. The soret peak at 419 nm was used to determine the protein concentration ($\varepsilon = 752{,}800$ $M^{-1}cm^{-1}$).
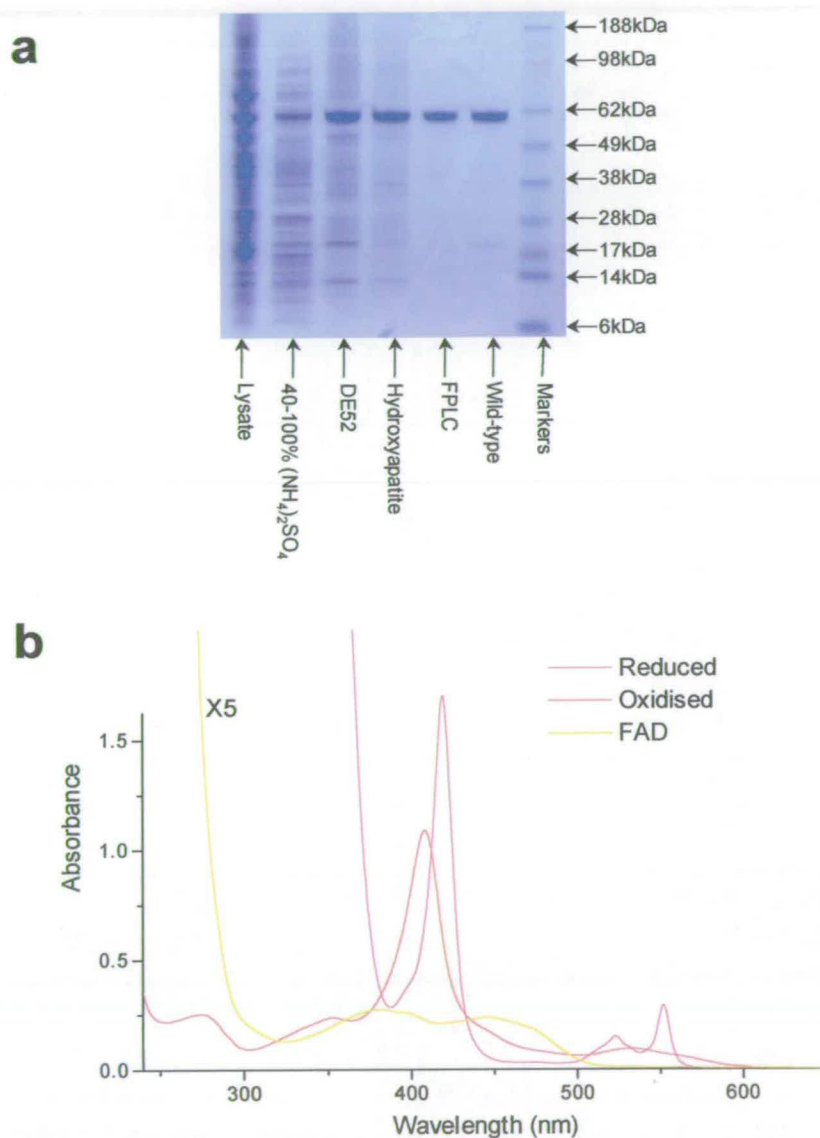
Figure 2.2: Determining the of purity of fcc₃ mutants. (a) Protein samples at each step of the purification procedure of an fcc₃ mutant, run against commercial markers and a sample of wild-type fcc₃. (b) The oxidised (red) and reduced (pink) spectra of fcc₃. The spectrum of FAD after protein precipitation is also shown (yellow).

2.4 Determination of FAD Content

The percentage of FAD incorporated into the protein was determined by the method of Macheroux *et al* (1999). A 1 ml aliquot of protein solution (~3.2 µM) was precipitated with 150 µl 50 % trichloroacetic acid. The protein was pelleted by microcentrifugation, leaving the FAD in solution (Figure 2.2b). The supernatant was removed and its pH was adjusted to 7 with solid sodium carbonate. The UV-visible spectrum was obtained, the FAD concentration was determined ($\varepsilon_{450nm} = 11,100\ M^{-1}cm^{-1}$) and expressed as a percentage of the total protein concentration. The average FAD content for recombinant wild-type protein was 73 %. All kinetic data were corrected to 100 % FAD.

2.5 Determination of Molecular Weight by Mass Spectrometry

2.5.1 Electrospray Mass Spectrometry

The molecular weights of wild-type and all mutants forms of fcc₃ were determined by electrospray mass spectroscopy. Protein samples 1of 0-20 µM were prepared in 5 mM ammonium acetate and 0.2 % formic acid was added to promote positive ionisation. Immediately prior to induction the samples were diluted 1:1 with acetonitrile. The samples were introduced to the instrument by direct infusion. Ten spectra were acquired over 500-2500 m/z using a cone ramp of 40-100 V over 700-1500 m/z. The raw data were baseline subtracted and smoothed, then centred to extract the charged ion series and transformed to give the total mass of the protein sample (Figure 2.3). Wild-type fcc₃ has a mass of 63,033 Da which indicates that the sodium ion is bound but the FAD does not fly with the protein in the spectrometer.

2.5.2 LC-MS

In order to desalt the protein for mass spectroscopy it can be eluted from a column directly into the spectrometer. The samples were loaded onto a 50×2mm Phenomenex jupiter C5 column. The protein was washed for 5min with solution A (95 % water, 5 % acetonitrile) at a flow rate of 0.2 ml/min. The protein was eluted with a 30 min gradient to solution B (5 % water, 95 % acetonitrile). The eluted protein passed into the mass spectrometer via a UV detector (280 nm). The protein spectra were combined and any surrounding features were subtracted. The spectra were processed as before.
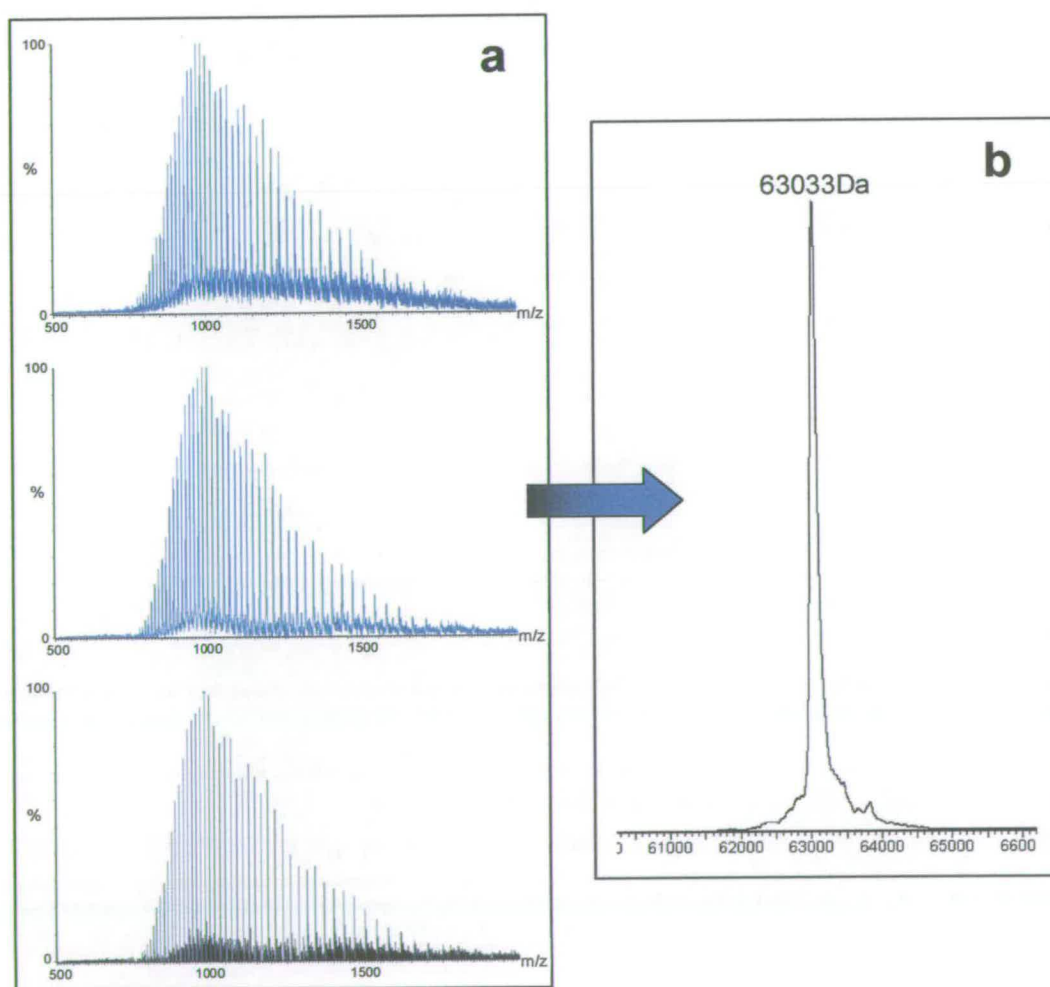
Figure 2.3: Mass Spectrum of fcc₃. (a) The raw data are shown at the top, below that are the subtracted and smoothed data and at the bottom are the centred data. (b) The transformed mass of wild-type fcc₃ is 63,033 Da.

2.6 Kinetic Analysis

2.6.1 Fumarate Reductase Assay

Enzyme activity was measured using a method adapted from Thorneley (1974). Assays were carried out under a nitrogen atmosphere in a Belle Technology glove box (< 2 ppm O_2) at 25°C, using a Shimidzu UV-PC1201spectrophotometer. 3 ml of 50 mM buffer (MES, TRIS or CHES), $I = 0.5M$ was placed in a disposable cuvette of 1cm pathlength and the methyl viologen (Figure 2.4a) was reduced with dithionite until the absorbance was 1-1.5. Protein was added and background activity was monitored at 600 nm to ensure that there was no re-oxidation by residual O_2. For wild-type the concentration was ~ 2 nM but for less active mutants concentrations of up to 5 μM were used. The reaction was initiated by the addition of fumarate and reoxidation of methyl viologen during fumarate reduction was monitored over 60-300 s (ε for methyl viologen at 600 nm = 13,000 $M^{-1}cm^{-1}$). A schematic representation of the assay is shown in Figure 2.4b. The rate of fumarate reduction over a range of substrate concentrations was fitted to the Michaelis-Menten equation (Appendix) by least squares regressional analysis in Microcal Origin, in order to determine the turnover number (k_{cat}) and the Michaelis constant (K_M).

The rate of turnover of fumarate by wild-type fcc_3 was tested and found to agree well with the data of Doherty *et al* (2000). In this thesis the turnover rates of the mutant forms of fcc_3 are compared to the published data.
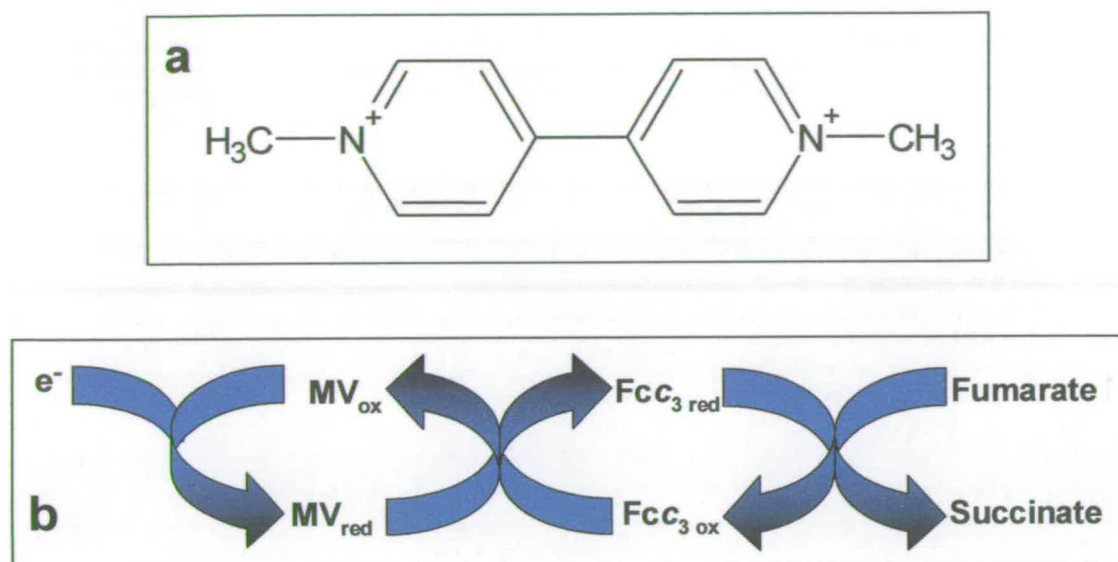
Figure 2.4: (a) The structure of methyl viologen. (b) Schematic representation of the fumarate assay. The blue arrows represent the flow of electrons. The methyl viologen is initially reduced by dithionite, it then passes electrons to fcc₃ which reduces fumarate to succinate.

2.6.2 Solvent Isotope Studies

Buffer and substrate solutions were prepared in both D_2O and H_2O for fumarate assays under substrate saturated conditions. The pH was adjusted with DCl or NaOD as required, applying the equation pD = pH* + 0.4, (where pH* is the pH meter reading) to correct for the acidity of the pH electrode itself (Glascoe and Long, 1960). Protein samples in H_2O were concentrated so that the minimum volume was added leaving the isotopic fraction essentially unaltered by the large dilution factor. Proton inventories (Appendix) were constructed by measuring the rate of fumarate reduction in a range of isotopic fractions, 0-100 %. The correct proportion was achieved by mixing H_2O and D_2O buffers in the assay cuvette. Isotopic exchange was fast; similar rates were observed 1 minute and 30 minutes after protein dilution.

2.6.3 Determining the Activity-pH Dependence

The pH dependences of wild-type mutant forms of fcc$_3$ were determined by measuring activity under conditions of fumarate saturation over the range pH 6-10 at intervals of 0.5 pH units. The profiles were fitted to one or two pK$_a$ values in Microcal Origin.

The pL (where L = H or D) dependence of the pK$_a$ values could be observed by constructing profiles in both H$_2$O and D$_2$O. Buffers were made up in the range of pH (meter reading) 5-10.

Chapter 3
Substrate Binding

3.0 Substrate Binding

Analysis of the fcc₃ sequence originally led to the proposal that fumarate would be bound in the active site by two arginines and two histidine residues (Arg381, Arg544, His365 and His504), all of which are completely conserved throughout the family. It was proposed that one of the histidines would act as the active-site acid catalyst, with arginine merely involved in substrate binding, since its pK_a (around 12) was thought to be prohibitive to the role of an active site acid. When the crystal structure of fcc₃ was solved it became apparent that Arg381 was not located at the active site, it was in fact found to be close to the surface of the protein, so participation in the proton pathway was suggested instead (introduced in section 1.12). It is clear from the structure that Arg402 is the residue ideally placed for proton transfer and that the two histidines are involved in hydrogen bonding at either end of the fumarate molecule (Figure 3.1).
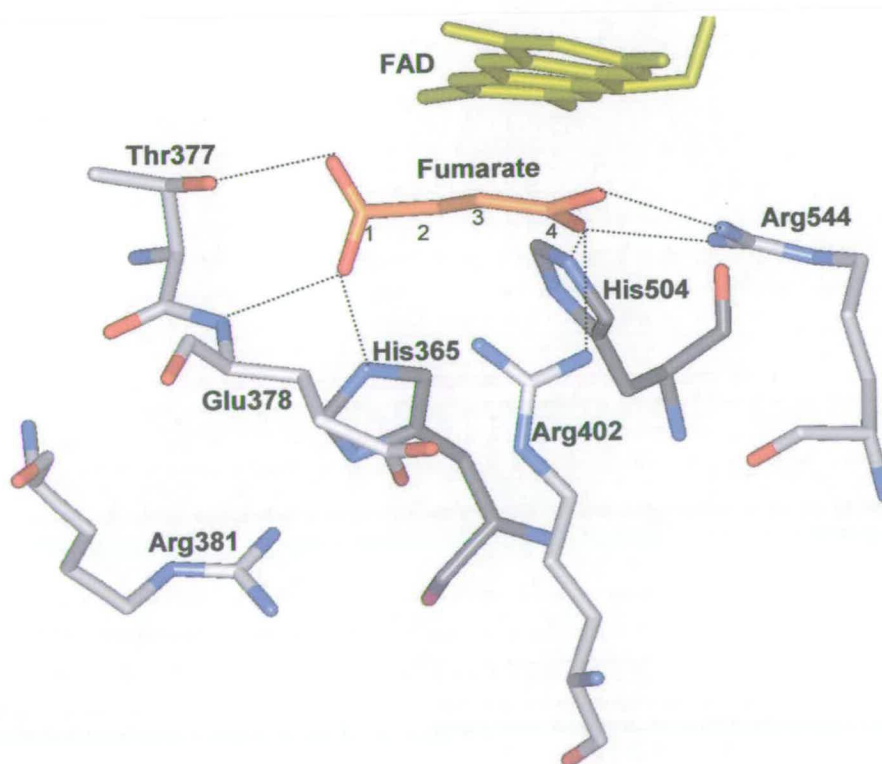
Figure 3.1: The active site of fcc₃. The substrate molecule (orange) is bound by hydrogen bonds to the side chains of residues His504, Arg544, Arg402, His365 and Thr377. There are also hydrogen bonds to some backbone amides, for example that of Glu378. The C1 carboxylate is twisted out of the plane of the molecule by the hydrogen bonding interactions.

The substrate molecule is bound within the active site by 11 hydrogen bonds (Taylor *et al*, 1999). Several of these bonds are interactions with protein backbone amides, such as that with Glu378 shown in figure 3.1. The amino acid side-chains important for substrate binding are those of His504, Arg544, His365 and Thr377. The latter two residues bind to the C1 fumarate carboxylate and the former to the C4 carboxylate. For all four residues the extent of their importance in hydrogen bonding and their involvement in fumarate reduction has been investigated by site directed mutagenesis. The residues and mutations made are shown in Table 3.1. All were substituted by alanine, with the exception of Arg544 which was replaced by methionine. In each case the hydrogen bonding capability of the residue was eliminated. Arg402 also participates in substrate binding via a hydrogen bond with the C4 carboxylate. Substitution of this residue is reported in chapter 5.
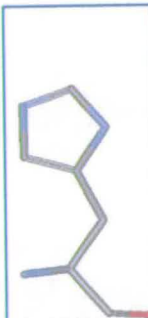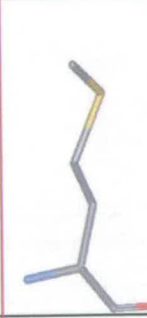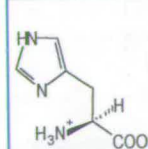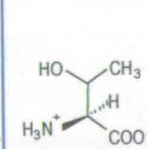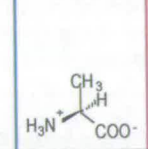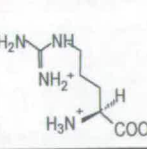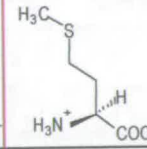
Table 3.1: Substrate binding residues and substitutions made. His365, His504 and Thr377 were all mutated to alanine, whereas Arg544 was substituted with methionine.

3.0.1 The Active Site Histidines.

Both His365 and His504 were mutated to alanine to remove their ability to form hydrogen bonds. A double mutation was also constructed (H365A/H504A). Kinetic characterisation of these mutants was carried out by Doherty and Moysey (Doherty *et al*, 2000; Doherty, 1999; Moysey, 2001) and the Michaelis parameters from these studies are shown in table 3.2. Both the single substitutions lower the activity of the enzyme to ~ 10 % of wild-type activity. They also affected Michaelis complex formation, with the K_M values increased 10-fold. So His365 and His504 are therefore involved in substrate binding and are important, but not crucial, for enzyme activity. Even substitution of both histidines does not entirely disable the enzyme, $k_{cat} \approx 1$ s^{-1}. The K_M value for the double mutant is elevated 50-fold. These results for the substitution of the active site histidines are consistent with a role in substrate binding. A more drastic loss of fumarate reductase activity would be expected if either His365 or His504 were the active site acid catalyst.

pH	k_{cat} (s^{-1})				K_M (µM)			
	WT	H365A	H504A	H365A/ H504A	WT	H365A	H504A	H365A/ H504A
6	658 ± 34	47 ± 2	26 ± 1	0.3 ± 0.1	43 ± 10	113 ± 20	38 ± 3	~280
7.2	509 ± 15	51 ± 2	65 ± 3	0.8 ± 0.1	25 ± 2	259 ± 20	256 ± 23	~1100
7.5	370 ± 10	54 ± 2	58 ± 2	0.9 ± 0.1	28 ± 3	143 ± 20	200 ± 15	~1800
9	210 ± 13	52 ± 2	76 ± 3	0.9 ± 0.2	7 ± 2	224 ± 20	635 ± 37	~1300

Table 3.2: Comparison of Michaelis parameters for H365A, H504A and H365A/H504A with wild-type. Values taken from Doherty et al, 2000.

The crystal structure of H365A was solved to 1.8 Å resolution (Doherty *et al*, 2000). The substitution was shown to have had an additional, conformational effect on two nearby residues, Arg402 and Met375 (Figure 3.2). The side chains of both of these residues have moved from their positions in the wild-type active site to partially

occupy the void left by the His365 imidazole ring. Arg402 was described in section 1.12 as the active site acid. The movement of this residue may contribute to the lower k_{cat} of H365A but it is no further away from the substrate molecule than it is in the wild-type structure and the proton pathway residues, Arg381 and Glu378, are conformationally unaltered by the substitution.
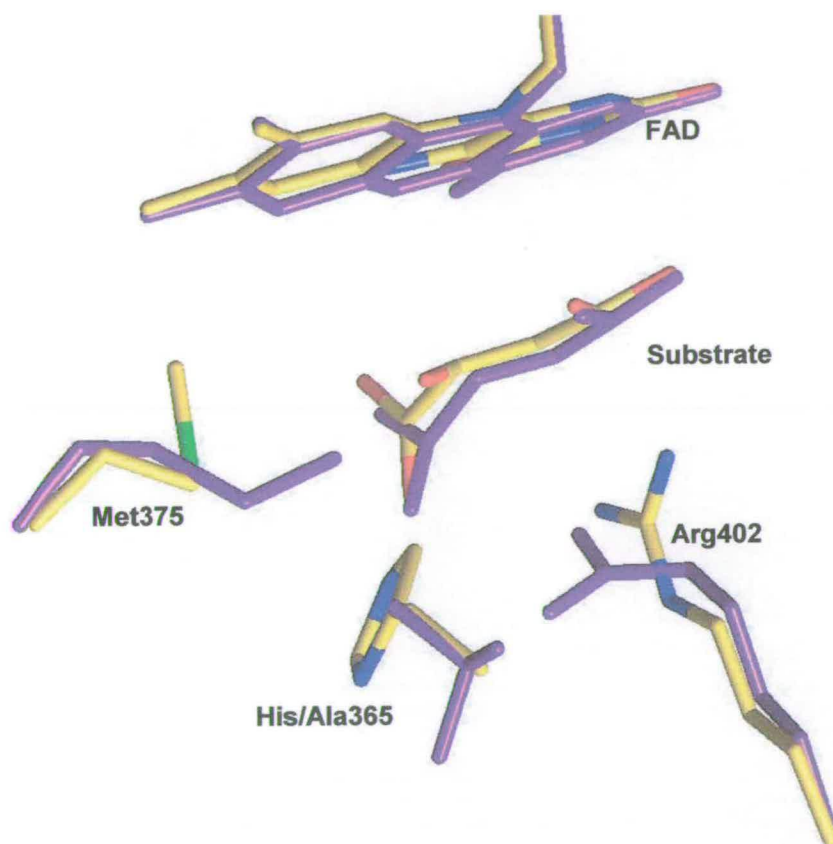
Figure 3.2: Crystal structure of H365A. The active site of H365A (purple) is overlaid with that of wild-type (atom type colours). The side chains of Arg402 and Met375 have altered their conformations in order to compensate for the removal of the His365 imidazole ring (Doherty et al, 2000). The pH of the crystal during data collection was 6.5 (due to the freezing solution).

3.1 Substitution of Thr377

Thr377 was mutated to alanine in order to assess its individual contribution to substrate binding. The active site is formed at the interface between the clamp and flavin domains. Thr377 is part of the clamp domain and His365 is on the hinge linking the clamp and flavin domains. These residues both hydrogen bond to the C1 end of the fumarate, so a double mutant was also constructed, H365A/T377A, removing two major interactions between the fumarate and the clamp domain.

The mutations were confirmed by DNA sequencing and electrospray mass spectroscopy. Wild-type fcc_3 has a mass of 63033 Da. The mass difference was found to be -38 Da for T377A (expected difference of -30 Da) and -103 Da for H365A/T377A (expected difference of -96 Da).

The average FAD contents were calculated to be 79 % for both T377A and H365A/T377A, which is comparable to the average recombinant wild-type FAD content of 73 %.

3.1.1 The kinetic Properties of T377A and H365A/T377A

The ability of the mutants to catalyse fumarate reduction was determined over a range of pH values. Michaelis plots were constructed by measuring the rate of fumarate reduction at increasing substrate concentration (Figure 3.3). Data were fitted by least-squares regressional analysis to the Michaelis-Menten equation and the resulting parameters; the turnover number, k_{cat}, and the Michaelis constant, K_M are shown in Table 3.3.

The single substitution of Thr377 to alanine has lowered the k_{cat} for the enzyme 10-50-fold from wild-type. The range reflects an alteration in the pH dependence. Wild-type protein is most active at pH 6 but T377A is least active at that pH. The substitution of T377A has had a greater effect on catalytic activity than either H365A

or H504A, the k_{cat} is slightly lower at 38 s^{-1} compared with 51 s^{-1} and 65s^{-1} respectively (pH 7.2). The double mutation, T377A/H365A, has had a more drastic effect on the activity of fcc$_3$, a 1000-2000-fold decrease. There is no crystal structure yet available for H365A/T377A but it is possible that conformational changes to surrounding residues, as seen in H365A, contribute to the low level of activity in this mutant. As the H365A/T377A mutation has no ability to hydrogen bond to the C1 carboxylate, several monocarboxylate molecules were tested to determine whether they could be reduced by the enzyme. No turnover, however, was detected for acrylate, butenoate or hexenoate.

The substitutions have also had a great effect on K_M. In T377A the K_M value is increased 10-200 fold over the pH range studied, with a reversal in the pH dependence. The K_M for wild-type fcc$_3$ ranges from 43 µM at pH 6 to 7 µM at pH 9. Conversely, the K_M of T377A increases from 0.5 mM at pH 6 to 1.4 mM at pH 9. Such a large increase in K_M is to be expected from the removal of a hydrogen bond to the substrate molecule. T377A/H365A removes two hydrogen-bonds to the substrate and accordingly the K_M is increased 100-600-fold. These changes are summarised in Table 3.3.

pH	k_{cat} (s^{-1})			K_M (µM)		K_M (mM)
	Wild-type	T377A	H365A/T377A	Wild-type	T377A	H365A/T377A
6	658 ± 34	14 ± 1	0.08 ± 0.003	43 ± 10	497 ± 101	1.8 ± 0.3
7.2	509 ± 15	38 ± 1	0.24 ± 0.02	25 ± 2	676 ± 27	2.0 ± 0.3
7.5	370 ± 10	38 ± 1	0.26 ± 0.03	28 ± 3	941 ± 121	3.3 ± 0.6
9	210 ± 13	35 ± 1	0.17 ± 0.02	7 ± 2	1444 ± 81	5.4 ± 1.0

Table 3.3: Comparison of Michaelis parameters for T377A and H365A/T377A with wild-type (Doherty et al, 2000). The rate of fumarate reduction has been decreased ≥ 10-fold by the single mutation T377A and ≥ 10^3-fold by the double mutation H365A/T377A. The substitutions have greatly affected Michaelis complex formation, particularly in the double mutant which has K_M values in the millimolar range. The errors quoted are the standard deviations of the data from the curves fitted.
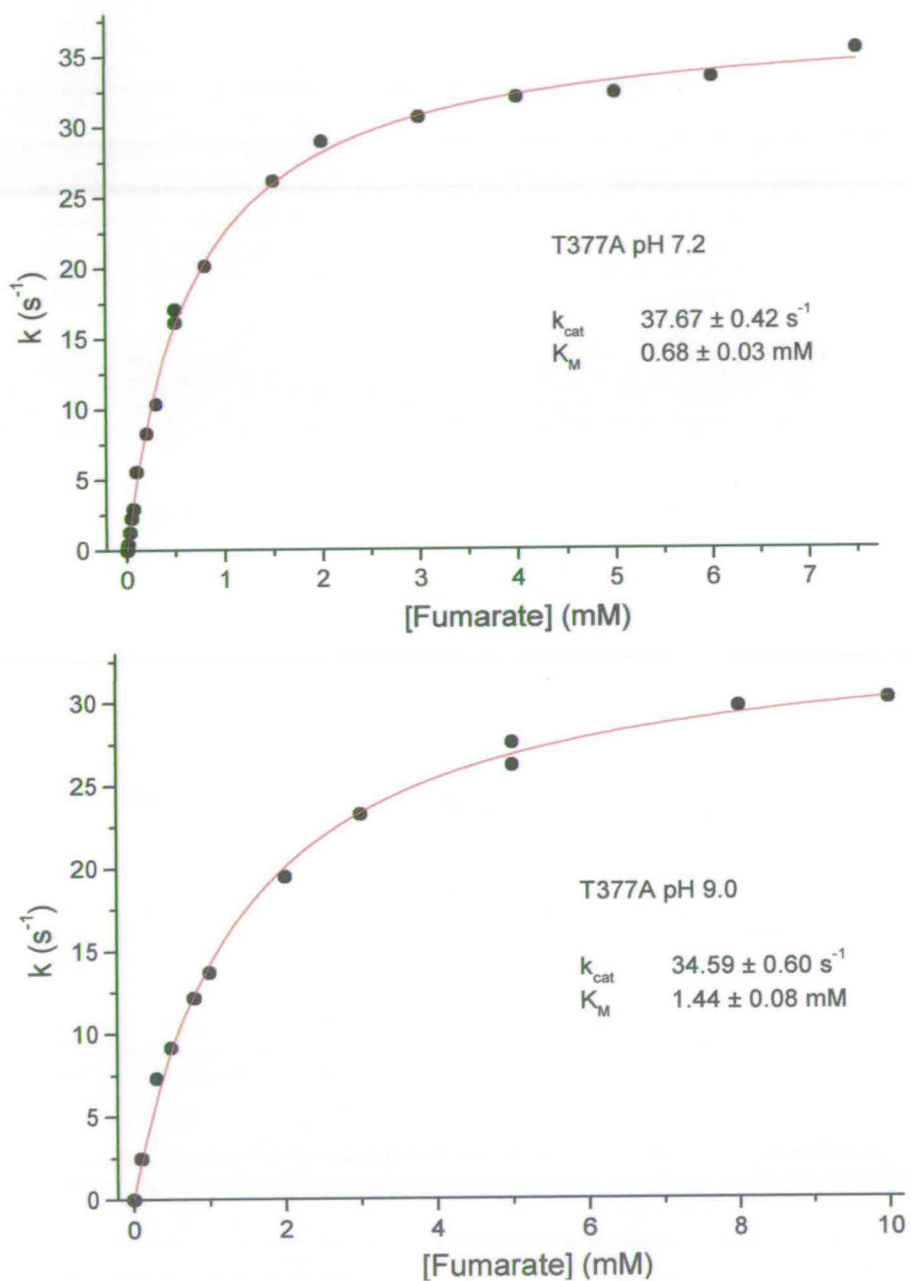
Figure 3.3: Michaelis plots for T377A at pH 7.2 (top) and 9.0 (bottom). At pH 9 the turnover number, k_{cat}, is slightly lower and the Michaelis constant, K_M, is double that at pH 7.2.

3.1.2 pH-Activity Profiles

The pH-activity profile for wild-type fcc$_3$ is shown in Figure 3.4a. The data fit to a single pK$_a$ of 7.5 ± 0.1, which is attributed to His504. This residue is thought to enhance the catalytic rate when protonated, by stabilising the build up of charge in the intermediate (Figure 1.20). The pH profile of H504A is a bell shaped curve that fits to two pK$_a$ values of 6.8 ± 0.2 and 10.3 ± 1.0 (Figure 3.4b). The maximum rate of fumarate reduction is reached at pH 8.5. All the substrate binding mutants have activity well below the wild-type minimum value, where different groups will influence the rate of fumarate reduction. At high pH, His504 will be deprotonated and so will be unable to stabilise the build-up of negative charge. The enzyme is seen to retain activity of ~200 s^{-1} ≥ pH 9, so the intermediate is still able to form at a considerable rate. The pH activity profiles of mutants that are less active than the wild-type minimum will not be affected by His504.

T377A has a broad pH profile, with the maximum rate at pH 7.2 with one discernible pK$_a$ value of 9.1 ± 0.1. It is not possible to determine the origins of the pK$_a$ values observed for the mutant enzymes.

The lower activity of the mutants T377A, H365A and especially T377A/H365A when compared with wild-type, may be due in part to poor activation of the substrate molecule. The twisted conformation prevents conjugation between the C1 carboxylate and the C2-C3 double bond. The driving force for this comes from the hydrogen-bonds formed, including those with His365 and Thr377. Removing one or both of these residues will make substrate activation less favourable and decrease the rate. Closure of the clamp domain is thought to be regulated by binding of the substrate in the twisted conformation. So the low rates observed when substitutions are made in the locality of the C1 carboxylate are likely to be the sum of multiple effects. Michaelis complex formation is compromised and there will be less driving force for the twisted conformation. Thus substrate activation and clamp domain movement are likely to be occurring at a lower rate.
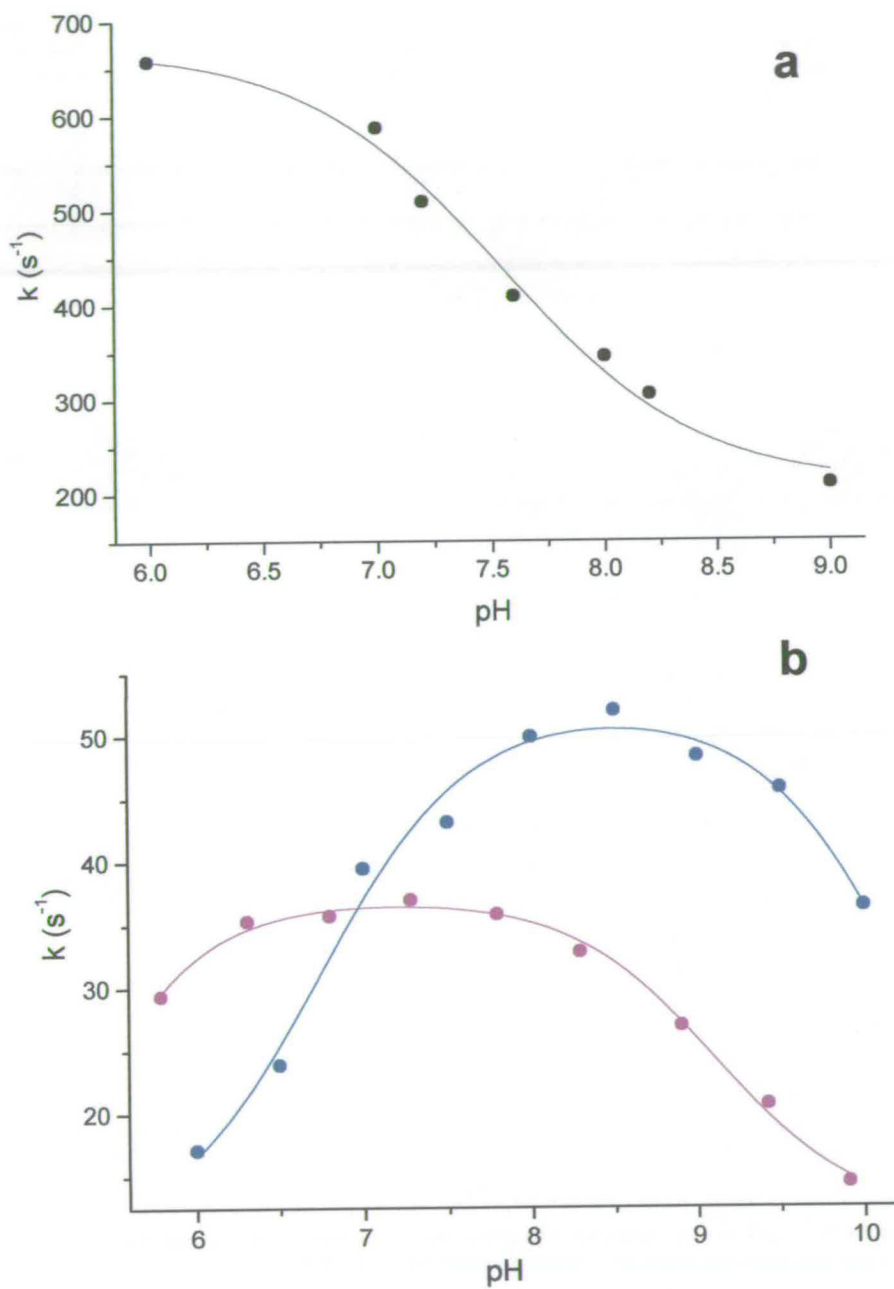
Figure 3.4: pH profiles of wild-type, H504A and T377A (a) The activity profile of wild-type fcc$_3$ fits to a single pK$_a$ of 7.5 ± 0.1. (b) pH profiles of H504A (blue) and T377A (purple). The pH profile of H504A is a bell-shaped curve that fits to two pKa values of 6.8 ± 0.2 and 10.3 ± 1.0. One pK$_a$ value of 9.1 ± 0.1 can be calculated for T377A.

3.2 Arginine 544

Arg544 contributes two hydrogen bonds to the substrate, one to each branch of the carboxylate. This residue was mutated to methionine. The mass difference of R544M was −23 Da from wild-type (expected difference of −25 Da). At 56 %, the FAD content of the mutant was a little lower than wild-type (73 %).

R544M was found to have a k_{cat} value of 0.15 ± 0.01 s^{-1} and a K_M of 714 μM at pH 7.2. The increase in K_M is large and consistent with Arg544 contributing two hydrogen bonds. What is more surprising is the very low level of activity observed for this mutant. When the other residues involved in substrate binding were substituted, the rate of fumarate reduction fell only ~10-fold, but in R544M the decrease is 3500-fold.

This residue clearly has an additional part to play in fumarate reduction, it is not purely involved in substrate binding. Analysis of the wild-type crystal structure shows Arg544 to be part of a very positively charged environment surrounding the C4 carboxylate (Figure 3.5). This must serve to polarise the substrate. The extensive loss of activity in R544M suggests that Arg544 is the major contributor in this polarisation. The twisted conformation of the substrate removes the C1 carboxylate from delocalisation and with the double bond polarised, the overall effect is to generate some positive charge at C2. This renders the molecule susceptible to hydride attack by the flavin N5. An additional effect of the substrate environment is likely to be modulation of the pK_a at C3 to be capable of abstracting a proton from Arg402.
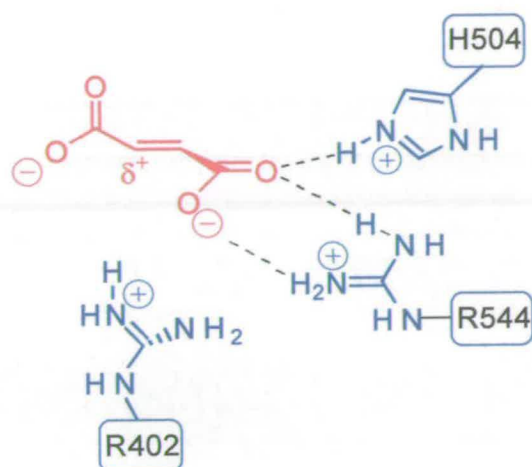
Figure 3.5: The fumarate environment. Substrate binding in a twisted conformation and the polar environment of the C4 carboxylate causes C2 to have significant positive charge. Arg544 is very important for polarisation of the molecule.

3.3 Hydrogen Bond Strengths

The elevated K_M levels that are observed when the residues His365, Thr377, His504 and Arg544 are substituted show them to be important in substrate binding. The strength of their hydrogen bonding contributions can be estimated from the K_M values, using equation 3.1. K_M has previously been shown by inhibition studies to be to be similar to K_D (Morris *et al*, 1994).

$$\Delta G = -RT\ln K_M \qquad\qquad \text{equation 3.1}$$

The difference in free energies between mutant and wild-type gives an estimate of the strength of the hydrogen bond (Table 3.4). The two histidine residues contribute equal strength hydrogen bond(s) and each end of the substrate has a stronger hydrogen bonding species, Thr377 at C1 and Arg544 at C4. Thr377 has by far the greatest individual hydrogen bond strength as Arg544 contributes two bonds. The combined effect of the double mutations on substrate binding is only slightly less than the sum of the individual mutations.

Residue(s)	H-Bonding Contribution ($KJmol^{-1}$)
His365	5.8
Thr377	8.1
His504	5.8
Arg544	8.3
His365/His504	9.4
His365/Thr377	11.6

Table 3.4: Estimation of hydrogen bonding contributions made by each residue. His365 and His504 make the same hydrogen bonding contributions to substrate binding. One residue at either end of the molecule has a greater effect (Thr377 and Arg544). The effect of the double substitutions appears to be slightly less than the sum of the single contributions.

3.4 The 'Clamp' Methionines

In the crystal structure of fcc₃, the fumarate molecule is in a twisted conformation, with the C1 carboxylate perpendicular to the plane of the molecule. The substrate occupies virtually all the available space in the active site (Figure 3.6a). Fumarate is ideally a planar molecule, if it is modelled into the active site as such, it sterically clashes with two methionine residues (Taylor *et al*, 1999), Met236 and Met375 (Figure 3.6b). Met236 is located in the flavin domain and Met375 is in the clamp domain. These residues are not, in fact, conserved throughout the family. Sequence alignment shows that in the QFRs and SQRs the residues are phenylalanine and leucine respectively. In all cases the two residues are hydrophobic and may play a similar steric role. By the C1 carboxylate twisting out of the plane to hydrogen bond with His365 and Thr377, steric clashing with the methionines is avoided. The effect of the twist is to remove this carboxylate from conjugation over the whole substrate molecule.

The methionine residues were both mutated individually to alanines. The mass differences were found to be –63 Da for M236A and –68 Da for M375A (expected difference – 60Da).
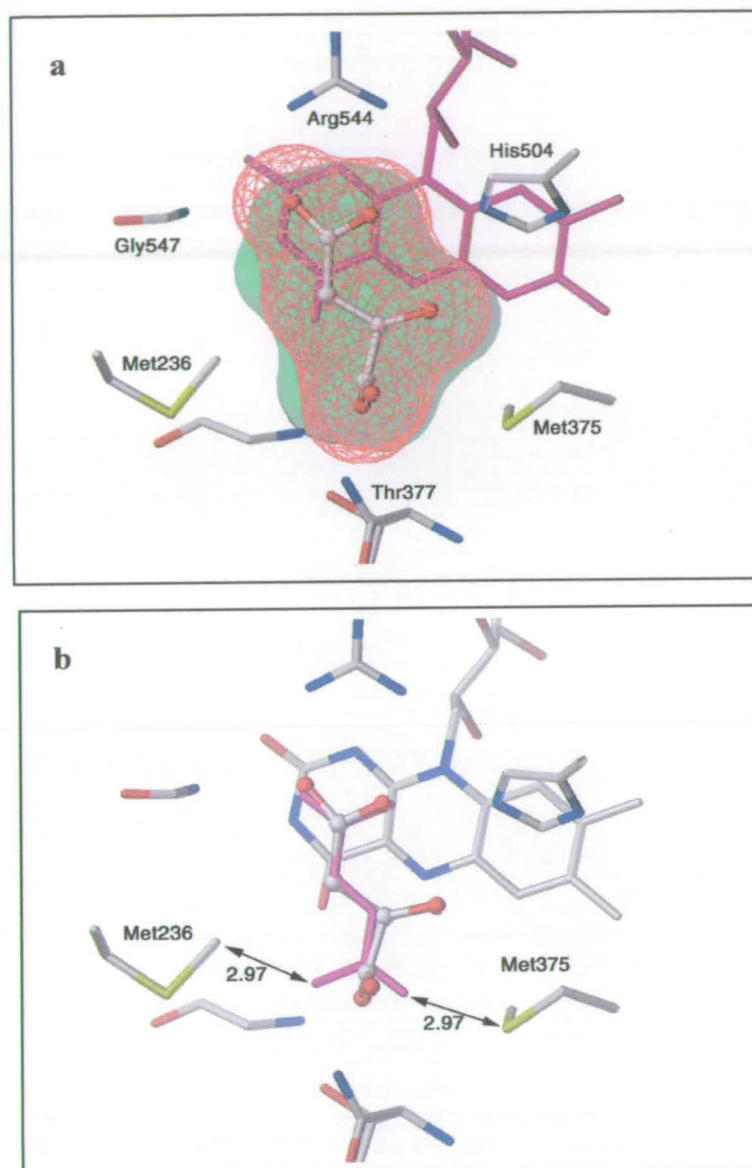
Figure 3.6: Orientation of the substrate within the active site. (a) The active site cavity. The Connolly surfaces show that fumarate (red) occupies virtually all the available space within the active site (green). (b) Planar fumarate (magenta) modelled into the active site. The C1 carboxylate sterically clashes with Met236 and Met375. (Figure taken from Taylor et al, 1999).

3.4.1 Loss of FAD in M375A

The FAD content of the M236A mutant was high, 84 % (average for wild-type 73 %). The FAD content for M375A was initially determined to be 55 %, but when the activity was tested a curve was obtained in a steady-state assay under fumarate-saturating conditions (Figure 3.7). The decrease in rate was not due to consumption of fumarate, as further addition of protein increased the rate again. To test whether the decrease in rate was due to loss of FAD, a protein sample was run through a gel filtration column after turnover. A yellow band (FAD) eluted after the protein band. The FAD content was found to be 42 %. This amount of FAD appeared to remain bound to the protein and straight lines were obtained in further assays. M375A was found to lose FAD without turnover, but samples were always found to retain ~40 % FAD and all rates were corrected to 100 % FAD.
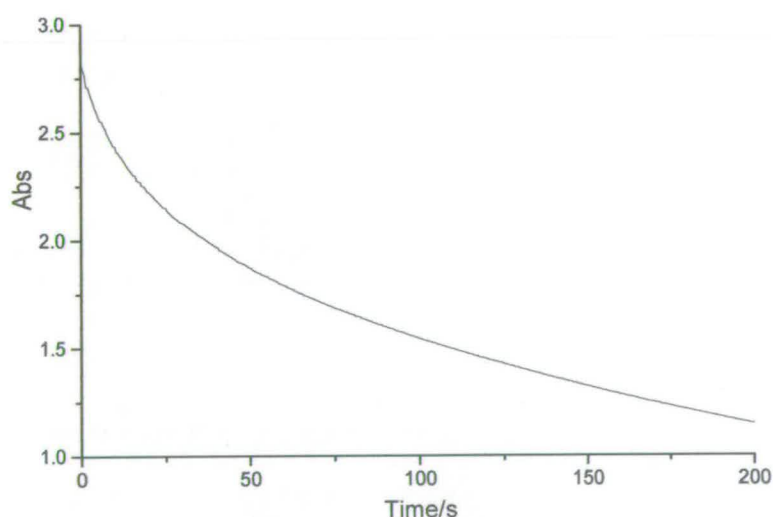
Figure 3.7: Loss of activity of M375A during turnover. The rate of change in absorbance decreases over the first 100 s of the assay, indicating a loss of activity. The rate of absorbance change then becomes virtually constant.

3.4.2 The Kinetic properties of M236A and M375A

Values of k_{cat} and K_M for the two mutants are shown in Table 3.5. They have similar levels of activity to wild-type at pH 9 but less activity at lower pH. At pH 7.2 the K_M of M375A is essentially the same as wild-type fcc₃ but the pH trend is reversed, activity increasing with basicity. The maximum K_M seen for M375A is less than twice that of the wild-type protein. In contrast, M236A has a K_M at pH 6 equivalent to wild-type but the values increase sharply with pH to ~2 mM at pH 9. This result is difficult to interpret as Met236 itself is not involved in hydrogen bonding. With no crystal structure available, it is impossible to tell how the mutation has affected the active site architecture.

pH	k_{cat} (s⁻¹)			K_M (μM)		
	Wild-type	M236A	M375A	Wild-type	M236A	M375A
6	658 ± 34	16 ± 1	85 ± 2	43 ± 10	38 ± 7	13 ± 2
7.2	509 ± 15	159 ± 4	117 ± 2	25 ± 2	705 ± 53	17 ± 1
7.5	370 ± 10	259 ± 8	148 ± 5	28 ± 3	498 ± 60	41 ± 5
9	210 ± 13	218 ± 10	160 ± 3	7 ± 2	1912 ± 245	70 ± 5

Table 3.5: Comparison of Michaelis parameters for M236A and M375A with wild-type (Doherty et al, 2000). Both substitutions have decreased activity at low pH. Only M236A has had a significant effect on K_M.

The methionine residues are thought to help regulate the movement of the clamp domain. When the substrate is effectively bound in the active site, the formation of hydrogen bonds being the driving force for the C1 carboxylate twist, Met236 and Met375 will not clash with the substrate when the clamp domain is in the closed (active) conformation. Substituting either methionine residue is likely to make this process less efficient, resulting in the decrease in rate of fumarate reduction.

3.5 Chapter 3 Summary

- Fumarate is bound at the active site by hydrogen bonds with surrounding residues, including interactions with the side chains of Arg544, His504, His365 and Thr377.

- Each of these residues was substituted with a non-hydrogen bonding residue (alanine or methionine) which resulted in large increases in the value of K_M.

- Thr377 and Arg544, at opposite ends of the fumarate molecule, make the greatest hydrogen bonding contributions.

- R544M is ~ 400-fold less active than the other substrate binding mutants. Arg544 has an additional role, polarising the double bond and causing the fumarate C2 to be slightly positive and susceptible to hydride attack.

- Hydrogen bonds from His365 and Thr377 to the C1 carboxylate cause the substrate to bind in a twisted conformation, removing that carboxylate from delocalisation with the rest of the molecule.

- The twisted conformation avoids steric clashing with Met236 and Met375, thus allowing the clamp domain to close.

Chapter 4

The Sodium Site

and the Role of His505

4.0 The Sodium Site and the Role of His505

The high resolution crystal structure of fcc$_3$ revealed an internally bound sodium ion (Taylor *et al*, 1999). It is coordinated by five backbone carbonyl oxygens (from Thr506, Met507, Gly508, Glu534 and Thr536) and a water molecule, in essentially octahedral geometry (Figure 4.1). The architecture of the site is conserved throughout the family but the assignment of the metal ion initially varied.
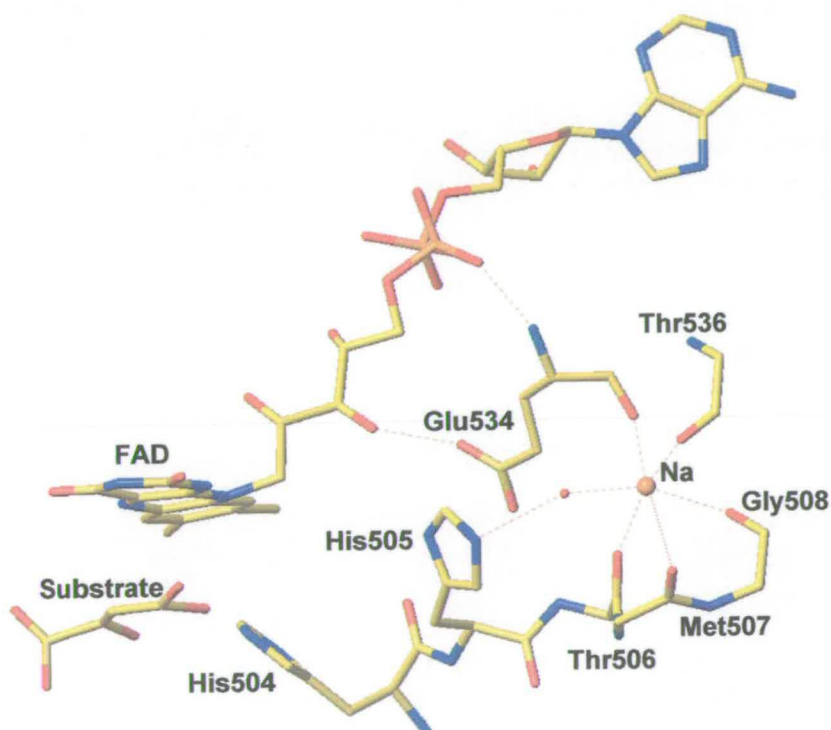
Figure 4.1: The sodium site. The crystal structure of fcc$_3$ revealed a structural sodium ion close to active site. It is bound in geometry close to octahedral by hydrogen bonds with 5 backbone carbonyl oxygens (Thr506, Met507, Gly508, Glu534 and Thr536) and a water molecule. The water molecule is in turn bound to His505.

In the structure of *Wolinella succinogenes* QFR, the ion was tentatively assigned as Ca^{2+} (Lancaster *et al*, 1999). In the more recent structure of the *Wolinella* enzyme, however, the metal ion is assigned as sodium (Lancaster *et al*, 2001). In the crystal structures of both *S. frigidimarina* ifc$_3$ (Bamford *et al*, 1999) and *S. oneidensis* MR1-fcc$_3$ (Leys *et al*, 1999), the density was interpreted as a water molecule. Neither a

metal ion nor a water molecule was included at the putative 'sodium' site in the original *E. coli* QFR structure (Iverson *et al*, 1999), but this is unsurprising at 3.3 Å resolution. The more recent structure of *E. coli* QFR, with the quinol binding inhibitor HQNO, is at 2.7 Å and a potassium ion has been assigned. The backbone arrangement is also conserved in L-aspartate oxidase. The original structure was of apo- L-aspartate oxidase and had no metal ion in the region next to the active site, however, the 2002 structure of the R386L mutant was found to contain FAD and had a sodium ion next to the active site in agreement with the fcc₃ structure. The 'sodium' sites from the different members of the fumarate reductase family and their metal/water assignments are shown in figure 4.2.
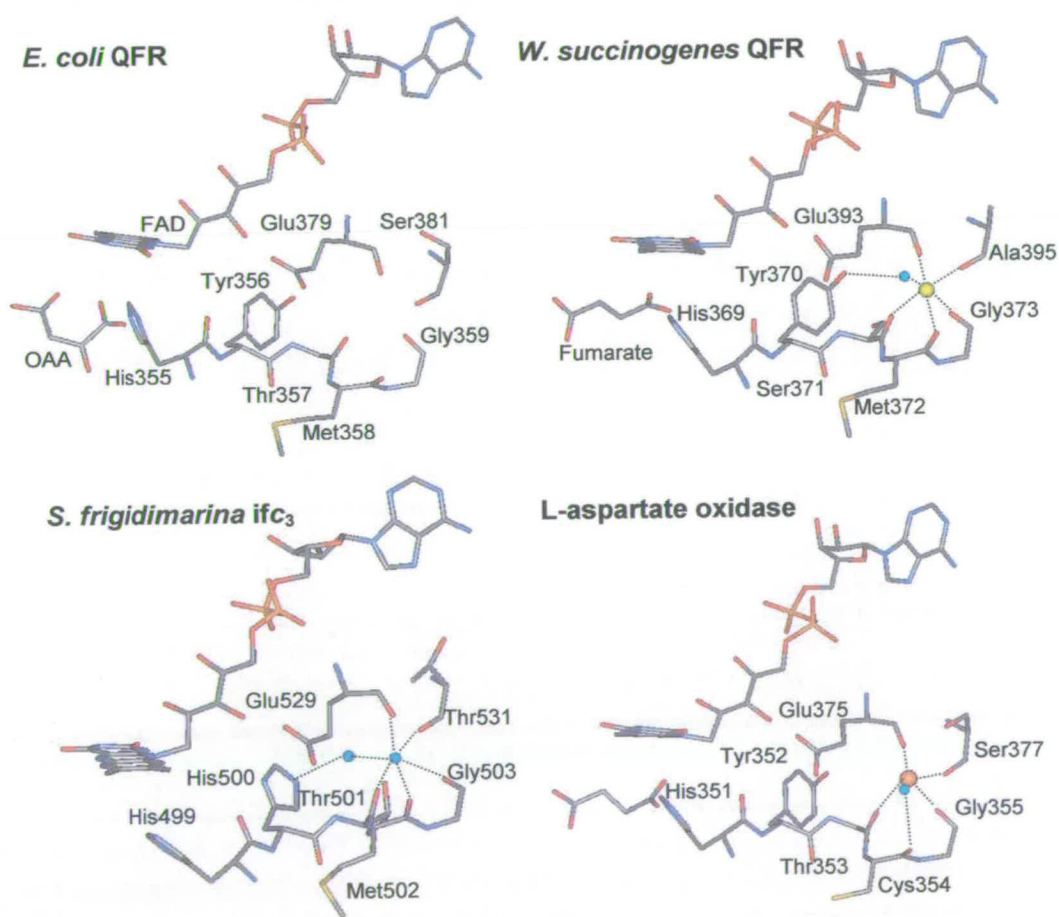
Figure 4.2: 'Sodium' sites of fumarate reductase family members. The original *E. coli* structure had no species assigned in that region. In ifc₃ (and MR1-fcc₃) the density was assumed to be due to water. A calcium ion was originally assigned in *W. succinogenes* QFR. A recent structure of L-aspartate oxidase has a sodium ion and apparently a water molecule only 0.9 Å away.

There are several known cases of sodium ions playing important roles within a protein structure. Many pyridoxal phosphate (PLP)-dependent enzymes, involved in amino-acid metabolism are activated by monovalent cations. Dialkylglycine decarboxylase has two alkali metal binding sites. The crystal structure of the enzyme from *Pseudomonas cepacia* (Hohenester *et al*, 1994; Toney and Kirsch, 1993; Toney *et al*, 1995, Maklashkevich *et al*, 1999), shows that it is a tetramer in the form of a dimer of dimers. The active site is at the dimer interface, composed of residues from both monomers. Metal site 1 is close to the catalytic active site and metal site 2 is near the protein surface. Site 1 can accommodate all alkali metal ions but K^+ has been shown to activate the enzyme whereas Li^+ and Na^+ have an inhibitory effect. The geometric alterations caused by the smaller ionic radii induce long range structural changes. Conversely, site 2 appears to select for Na^+ which fits well into a tight turn between α-helix and β-sheet. The Na^+ has octahedral coordination by carbonyl oxygens from a Pro-Pro-Gly-Leu sequence and also two water molecules (Toney and Kirsch, 1993). This site is thought to play a purely structural role within the protein.

Tryptophan synthase is from another family of PLP-dependent enzymes. It catalyses the last two reactions in the synthesis of L-tryptophan. The subunit stoichiometry is $\alpha_2\beta_2$. The α and β subunits catalyse different reactions:

α: indole-3-glycerol phosphate ↔   indole + D-glyceraldehyde 3-phosphate

β: L-serine + indole   →   L-tryptophan + H_2O
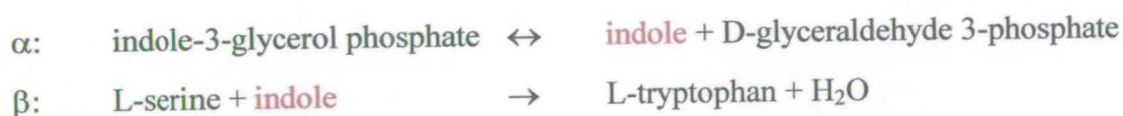
The two active sites are connected by a tunnel for the transport of the intermediate indole. A sodium binding site was observed in the β subunit between two domains (Rhee *et al*, 1996). The ion is coordinated by three backbone carbonyls and two water molecules. Replacing Na^+ with K^+ or Cs^+ induces changes in the coordination sphere leading to long range structural alterations. Sodium binding is thought to stabilise the structure of the β subunit.

The crystal structure of diaminopelargonic acid synthase (Käck *et al*, 1999) contains another example of a sodium ion largely coordinated by backbone carbonyl oxygens within a tight turn, playing a structural role, but near the protein surface.

In fcc$_3$, the ion is not at the surface of the protein but is apparently performing an important structural role adjacent to the active site. One of the coordinating carbonyls is from Glu534, which is involved in hydrogen bonding to the flavin tail group. The FAD in fcc$_3$ is non-covalently bound and the importance of Glu534 for FAD binding is assessed in this chapter.

The sodium site is closely linked to the active site not only in space but also in sequence. The carbonyl groups of Gly508, Met507 and Thr506 all coordinate to the sodium ion. His505 hydrogen bonds to the water molecule in the sodium coordination sphere. The next residue is His504 which is a completely conserved active site residue, important for Michaelis complex formation. His505 is also investigated by site directed mutagenesis in this chapter. The soluble *Shewanella* fumarate reductases all have a histidine residue, but rest of the family have tyrosine residues at that position in the sequence (Figure 4.3).

```
Fcc3          PGVHHTMGGV

Frda_ecoli    PTAHYTMGGI

frda_wolsu    PMQHYSMGGI

dhsa_ecoli    PTCHYMMGGI

dsha_yeast    PTVHYNMGGI

              *   *:  ***:
```

Figure 4.3: Sequence alignment surrounding residue 505 (S. frigidimarina numbering). His505 (red) is not strictly conserved. The complex II family (shown here are sections of sequence for E. coli and W. succinogenes QFR and also E. coli and yeast SQR) have a tyrosine residue at that position (blue).

Several of the metal sites in the PLP-dependent enzymes may bind different monovalent cations, but fcc₃ is remarkably resistant to removal or replacement of the sodium ion. Extensive dialysis against buffers containing alternative monovalent cations, divalent cations or EDTA (to potentially remove the sodium ion) failed to have any effect. Sodium remains bound to fcc₃ in the electrospray mass spectrometer and the dialysed samples gave the wild-type mass of 63033 Da, which includes sodium.

4.1 Substitution of Glu534

Glu 534 is involved in binding the sodium ion only by a backbone carbonyl which cannot be altered by mutation, but the extent of its importance for FAD binding was assessed by substitution with both alanine and glutamine.

4.1.1 E534A

Initial attempts to purify the mutant were unsuccessful, despite a band at the expected mass on the gel, indicating expression. A small amount of protein was obtained when the protein preparation was carried out in the presence of excess free FAD, but it did not elute in a tight band from DE52, hydroxyapatite or Q-sepharose and remained quite impure. After gel filtration to remove the excess FAD, the content was found to be 30 %. However, the ability of the protein to bind FAD was clearly compromised by the substitution and no kinetic data could accurately be obtained. The inability to purify E534A without excess FAD present suggests that the protein does not fold correctly without FAD bound.

4.1.2 E534Q

Substituting Glu534 with glutamine again caused difficulties in purifying the protein, but a little protein was obtained without the need for excess FAD. The FAD content was determined as only ~15 %. The activity was tested and rates were corrected to

100 % FAD, but the protein deactivated over time so only approximate values for k_{cat} and K_M were obtained; $k_{cat} \approx 4 \text{ s}^{-1}$ and $K_M \approx 50 \text{ }\mu\text{M}$ (pH 7.2).

4.2 Investigating the Role of His505

His505 was substituted by both alanine and tyrosine. The tyrosine mutant was constructed to investigate the possibility of direct ligation to the sodium ion by the tyrosine hydroxyl group replacing water in the sodium coordination sphere.

Electrospray mass spectroscopy was employed both to confirm the mutations and to assess whether sodium remained bound to the protein. Both mutants had mass differences that accounted for the substitution, with sodium present in each case: -67 Da for H505A (expected difference of –66 Da) and +24 Da for H505Y (expected difference of +26 Da).

The FAD contents of H505A and H505Y were slightly lower than the typical wild-type value for wild-type (73 %) at 60 % and 56 % respectively. His505 is 3.3 Å from one of the FAD hydroxyl groups which is bound by Glu534 and may assist in binding the flavin, but is clearly not essential. The percentage of FAD incorporated, although slightly less than wild-type, remained constant. All rates were corrected to 100 % FAD.

4.2.1 Kinetic Characterisation of H505A and H505Y

The Michaelis parameters for the two mutants are in table 4.1, and their pH activity profiles are compared to wild-type in figure 4.2. The mutations have had very little effect on k_{cat} at high pH, but as the pH is lowered the effect on the activity increases. At pH 6, wild-type exhibits its maximal activity. The activity of H505A is 20-fold lower than wild-type and H505Y has half the activity of wild-type at pH 6.

pH	k_{cat} (s^{-1})			K_M (μM)		
	Wild-type	H505A	H505Y	Wild-type	H505A	H505Y
6	658 ± 34	32 ± 1	354 ± 19	43 ± 10	43 ± 6	22 ± 5
7.2	509 ± 15	79 ± 3	377 ± 29	25 ± 2	109 ± 13	25 ± 7
7.5	370 ± 10	101 ± 3	363 ± 29	28 ± 3	129 ± 10	17 ± 6
9	210 ± 13	105 ± 2	240 ± 5	7 ± 2	9 ± 1	21 ± 2

Table 4.1: Comparison of Michaelis parameters for H505A and H505Y with wild-type (Doherty et al, 2000). The effect on k_{cat} for both mutants is greatest at pH 6. The K_M of H505Y appears to have no pH dependence. In H505A an increase in K_M is seen only at pHs 7.2 and 7.5.

The pH dependence of the enzyme has been altered by the substitutions. Wild-type fcc_3 has a straightforward profile with a single pK_a of 7.5 ± 0.1. In contrast, the mutant enzymes have more bell-shaped profiles (Figure 4.4), with maximal activity at pH 6.8 for H505Y and pH 8.1 for H505A. Two pK_a values can be determined for H505A, at 7.1 ± 0.2 and 9.0 ± 0.2. Only one pK_a can be determined for H505Y at 8.2 ± 0.1. The wild-type pKa is attributed to His504 (Figure 4.5). It is thought to enhance the rate of fumarate reduction when protonated, by stabilising the build up of charge in the intermediate after hydride transfer. The pH profiles for H505A and H505Y show that the pK_a is shifted to more basic values, to 8.2 ± 0.1 in H505Y and to 9.0 ± 0.2 in H505A. So substituting a neighbouring residue (His505) has modulated the pK_a of His504.

Some small changes were also seen in the K_M values. The K_M of H505Y is the same for wild-type at pH 7.2 but where the wild-type K_M decreases with increased pH, H505Y appears to have no pH dependence. The K_M of H505A displays a peculiar pH dependence. The values are identical to wild-type at pH 6 and 9, but at 7.2 and 7.5 substrate binding is clearly being affected, with K_M values of 109 μM and 129 μM respectively, a four-fold increase from wild-type.
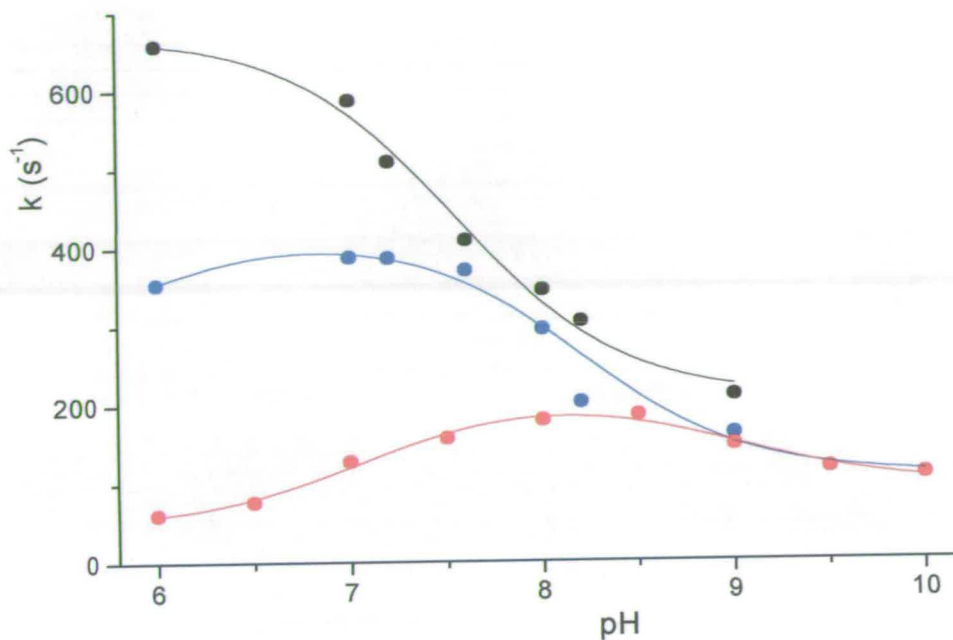
Figure 4.4: pH profiles of wild-type (black), H505Y (blue) and H505A (red). The substitutions appear only to have a significant effect on activity at low pH. The pK_a has shifted from 7.5 ± 0.1 in wild-type to 8.2 ± 0.1 in H505Y and 9.0 ± 0.2 in H505A. A second pK_a at 7.1 ± 0.2 is discernible for H505A.
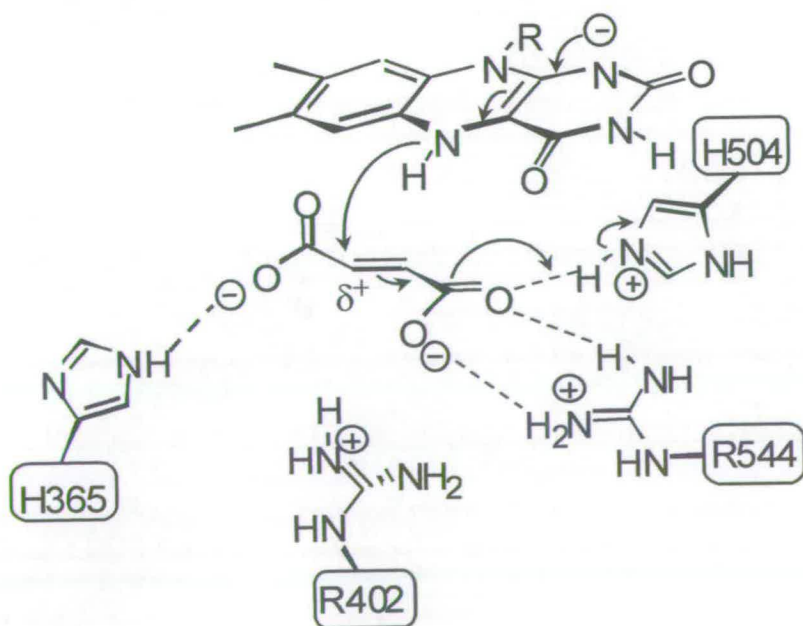
Figure 4.5: The wild-type pK_a of 7.5 is thought to arise from His504 stabilising the build up of negative charge in the intermediate, after hydride transfer.

4.2.2 The Crystal Structures of H505A and H505Y

Substituting a histidine for an alanine been seen to cause structural alterations in the case of H365A (section 1.1.1). Surrounding residues have compensated for the removal of the histidine ring. Slight structural rearrangement of His504, caused by the substitution of His505, could reasonably account for the changes in activity and substrate binding.

The structure of H505A was solved to 1.8 Å resolution and H505Y to 2.0 Å. It was immediately clear that neither substitution had induced significant structural change. The sodium site has not undergone any real changes. Figure 4.6 shows the sodium sites for each mutant compared with wild-type. In H505A there are two water molecules in the cavity left by the imidazole ring, in addition to the one that hydrogen bonds to the sodium ion. In H505Y the tyrosine ring occupies the same position as the histidine ring of wild-type. The hydroxyl group does not directly ligate the sodium ion, but hydrogen bonds to a water molecule at 2.6 Å, which in turn coordinates to the sodium ion at a distance of 2.5 Å.
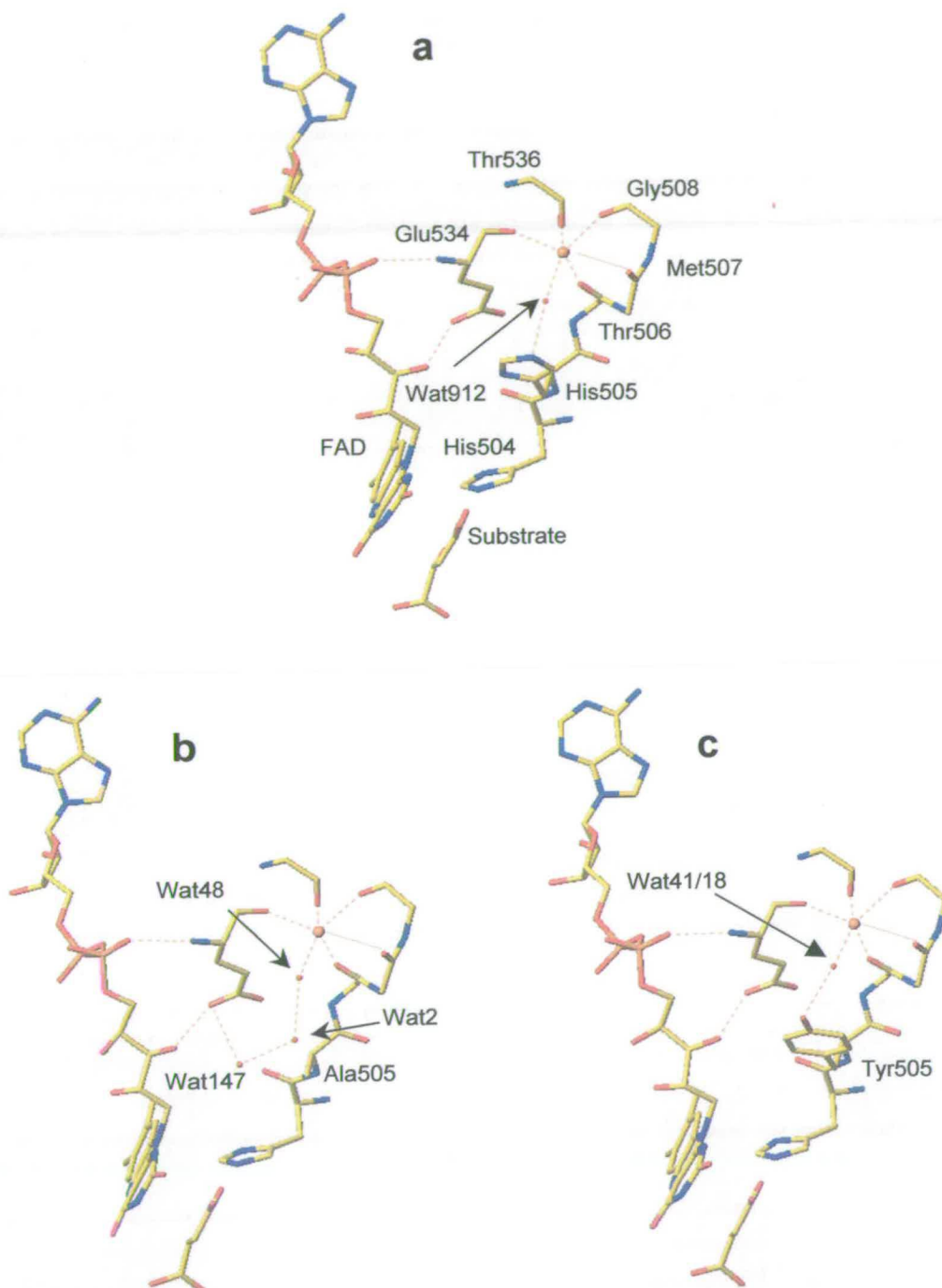
Figure 4.6: The sodium sites of (a) wild-type, (b) H505A and (c) H505Y. The crystals were at pH 6.5. Two water molecules occupy the space vacated by the histidine imidazole ring in H505A. Tyr505 occupies a similar conformation to His505 and hydrogen bonds to a water molecule, it does not directly coordinate the sodium ion.

There have been no real alterations to the active site either. The fumarate molecule is in the twisted conformation and all the interactions important for catalysis, such as proton and hydride transfer, are unaffected. The kinetic data suggest that substitutions to His505 have affected the neighbouring residue His504. The crystal structures show that this is not caused by conformational changes.

Looking at the position of His505 in the structure does give rise to a possible explanation for the pK_a modulation: His505 is located between the active site and the sodium site, or more specifically, between Glu534 and His504 (Figure 4.7). The effect of the Glu negative charge on His504 would be to make it a weaker acid, raising its pK_a. This is observed in the H505A mutant, where the pK_a is shifted from 7.5 to 9.0. So it is likely that His505 minimises the effect of the negative charge of Glu534 on His504. The H505Y substitution has had a less pronounced effect on the pK_a, which is shifted from 7.5 to 8.2. Tyrosine is to some extent able to moderate the effect of the Glu534 charge on His504. It is not surprising to find that H505Y had quite a modest effect, as the equivalent residue in other members of the family is a tyrosine (Figure 4.3).
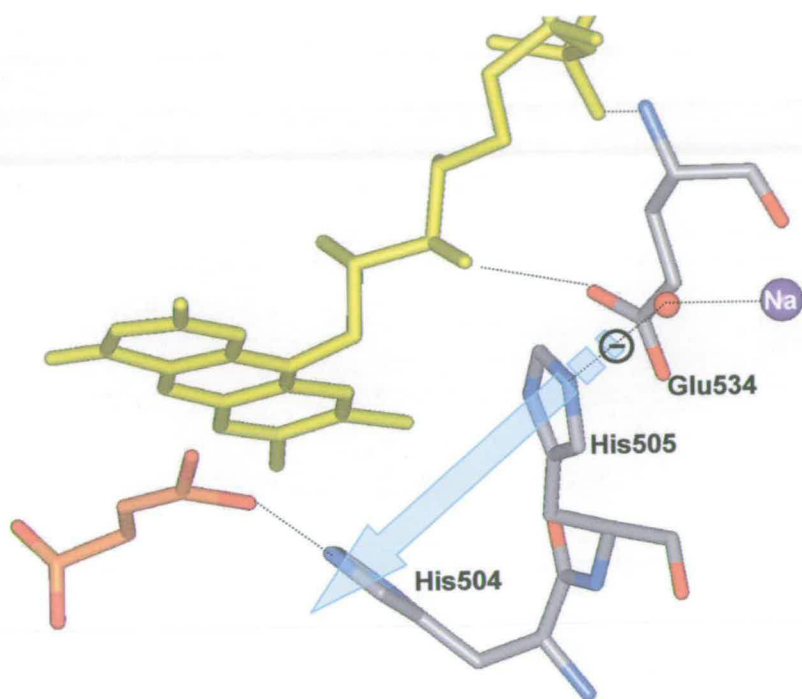
Figure 4.7: Location of His505. His505 is thought to modulate the pKa of His504 by minimising the effect of the Glu534 negative charge.

4.3 Chapter 4 Summary

♦ A structural sodium ion is found adjacent to the active site, bound by five backbone carbonyls Thr506, Met507, Gly508, Thr536 and Glu534) and a water molecule.

♦ Glu534 is vital for FAD binding. Substitution of this residue renders the protein unable to maintain its FAD content.

♦ His505 hydrogen bonds to the water molecule. Substitution of His505 causes loss of activity at low pH but not at high pH.

♦ Wild-type fcc₃ has a pK_a value of 7.5 which is thought to be due to stabilisation of the reaction intermediate by His504. Mutating its neighbour, His505, raises the pK_a.

♦ His505 may moderate the effect of the Glu534 negative charge on His504.

Chapter 5
The Active Site Acid Catalyst

5.0 The Active Site Acid Catalyst

Since the crystal structures of five fumarate reductases were solved in 1999, Arg402 has been the primary candidate for the active site acid. Until recently, however, there remained some controversy, because Lancaster (Lancaster *et al*, 1999) found a water molecule at the active site in the structure of *Wolinella succinogenes* QFR and proposed it to be the active site acid catalyst. There is no water found in the active sites of the other enzymes, so it was thought that the *Wolinella* enzyme was crystallised in an open, inactive form. In 2001 Lancaster published a further crystal structure of *W. succinogenes* QFR. This new crystal form was in a closed conformation, with Arg301 (Arg402 of *S. frigidimarina* fcc₃) overlaying the positions of the acid catalysts of the other fumarate reductases.

Arginine (R)	Alanine (A)	Lysine (K)	Tyrosine (Y)	Glutamine (Q)	Phenylalanine (F)
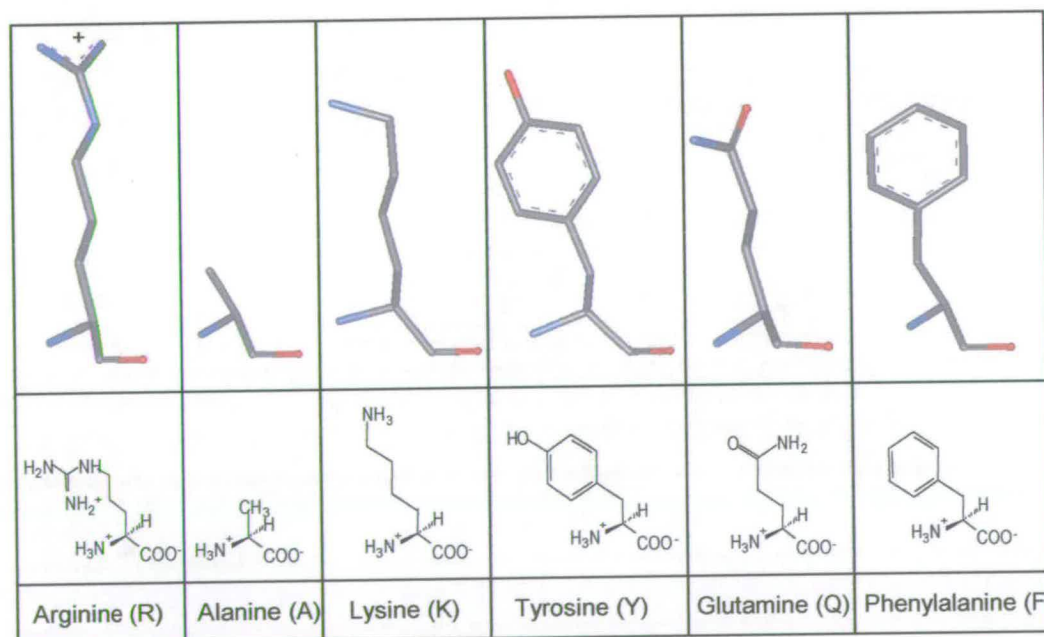
Table 5.1: Substitutions made to Arg402 (left). The active site acid was substituted by five residues with differing abilities to participate in proton transfer.

Arg402 was confirmed as the acid catalyst by mutagenesis studies (Doherty *et al*, 2000). Substitution of the conserved histidine residues at the active site has shown that they are not essential for fumarate reduction. H365A and H504A retain at least 10 % of wild-type activity. In contrast, when Arg402 is substituted by alanine in fcc3, the enzyme is completely inactive (Doherty *et al*, 2000).

Arg402 was then substituted by lysine and tyrosine (Mowat *et al*, 2001). These mutant enzymes retained a detectable level of activity, albeit at a 10^3-10^4-fold lower level than wild-type (Table 5.2).

pH	k_{cat} (s^{-1})		
	Wild-type	R402K	R402Y
6	658 ± 34	0.02 ± 0.01	0.02 ± 0.01
7.2	509 ± 15	0.06 ± 0.01	0.05 ± 0.01
7.5	370 ± 10	-	0.14 ± 0.01
9	210 ± 13	-	-

Table 5.2: Turnover numbers (k_{cat}), for R402K and R402Y compared with wild-type. No rate is detectable above pH 7.2 for R402K or above pH 7.5 for R402Y (Mowat et al, 2001).

5.0.1 A Dual Role for Arg402

The crystal structures of the R402A, K and Y enzymes have each been solved to 2.0 Å resolution and are overlaid with wild-type in Figure 5.1a. R402A has a water molecule in the active site, since this mutant is inactive it must be unable to act as the acid catalyst. The schematic overlay of the three mutant structures with wild-type in Figure 5.1b provides an explanation for the inactivity. The active site contains two separate positions, A and B. Position A contains the proton donating species for the mutants R402K and Y (which do display some fumarate reductase activity) as well as one branch of the arginine guanidinium group in wild-type. Position A is empty in R402A. The other branch of the guanidinium group is in position B where it hydrogen bonds to the fumarate C4 carboxylate and Gln363. R402A and K have water molecules in position B. These observations led to the proposal of a dual role for Arg402. Hydride transfer from the FAD N5 to the fumarate C2 leads to the build up of negative charge at the C4 end of the substrate molecule. The charge is stabilised by the interaction with the NH_2 group of Arg402 at position B. In summary, one amino group of Arg402 acts as a Lewis acid at position B while the other acts as a Brønsted acid in position A, protonating the substrate at C3. Arginine is the only amino acid capable of fulfilling both of these roles simultaneously. Fumarate reduction is detectable if a proton donating species is present in position A, but the lack of a species in B to stabilise the transition state results in extremely low catalytic rates.
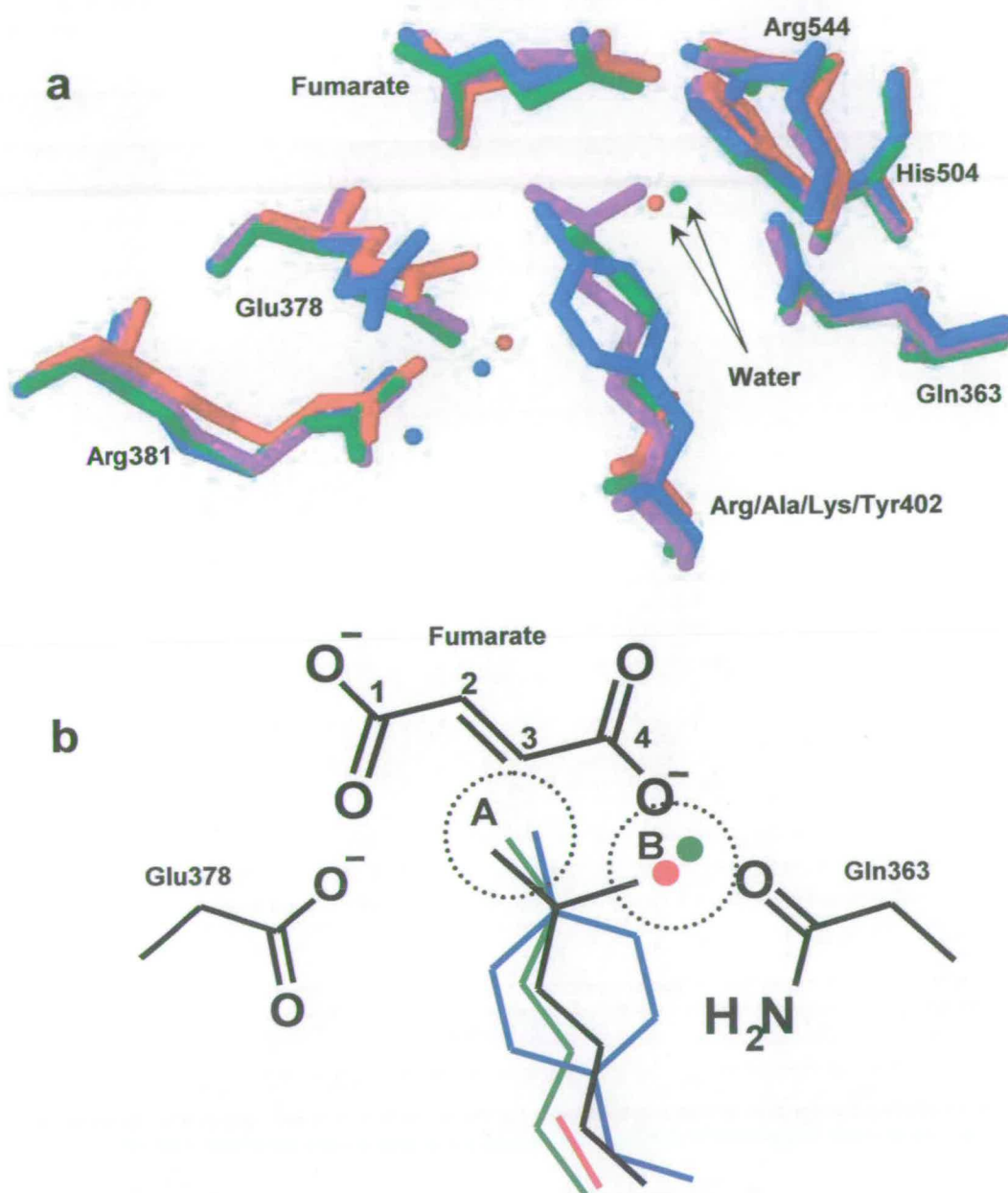
Figure 5.1 (a): Crystal structures of R402A (red), R402K (green) and R402Y (blue) with wild-type (purple). (b) Schematic overlay showing positions A and B within the active site (taken from Mowat et al, 2001).

5.1 Results

5.1.1 R402Q

Arg402 was also substituted with glutamine (Table 5.1). The mass difference was found to be –27 Da (expected difference of –28 Da) and the protein had 87 % FAD incorporation.

At pH 7.2 R402Q had a k_{cat} of 0.010 ± 0.001 s^{-1} and a K_M of 10 ± 2 μM. This mutant displays activity at the extreme lower measurable limit of the assay. A high protein concentration was required to observe any rate, which may introduce errors at low fumarate concentrations because the Michaelis-Menten equation (Appendix) assumes an excess of substrate over protein. The activity of R402Q is 5-fold lower than R402K and Y. The pH profile in Figure 5.2 was obtained under fumarate saturation conditions and shows that R402Q is most active at pH 7. No activity was measurable above pH 9. The rate of fumarate reduction by R402Q is influenced by two ionisible groups with pK$_a$ values of 6.5 ± 0.2 and 7.5 ± 0.2.
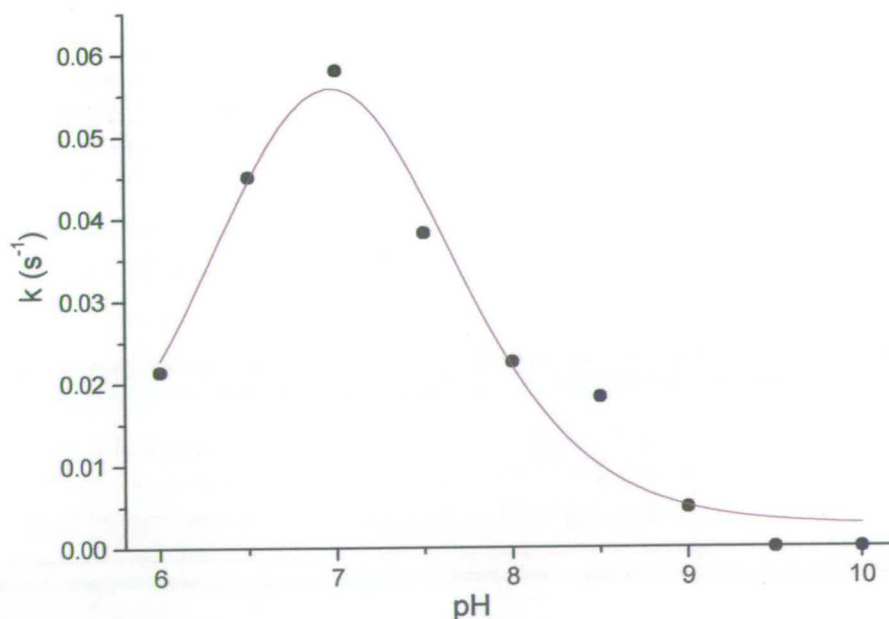
Figure 5.2: The pH profile of R402Q. The mutant has maximal activity at pH 7 and no activity can be detected above pH 9. The profile fits to two pK$_a$ values of 6.5 ± 0.2 and 7.5 ± 0.2.

5.1.1.1 *The Crystal Structure of R402Q*

The crystal structure of R402Q was solved to 1.25 Å, the highest resolution structure available for fcc₃ or any other fumarate reductase. The resolution is sufficient to include hydrogens in the model and to distinguish between the oxygen and amino branches of the Gln402 side chain (Figure 5.3). The amino group of Gln402 is closest to the substrate molecule, essentially in position A. The reason for the minimal activity is immediately clear. The side chain of this residue is shorter than that of arginine, lysine or tyrosine (Table 5.1). The proton transfer distance is 4.5 Å, resulting in the barely detectable catalytic rates. Glutamine is also unable to act as a Lewis acid in position B, the closest distance to the C4 carboxylate is 4.1 Å. The hydride transfer distance is slightly increased from 3.4 Å in wild-type to 3.6 Å in R402Q. The distances along the proton transfer pathway are 3.0 Å from Arg381 to Glu378 and from Glu378 to Gln402, compared with 3.1 Å in the wild-type structure. There are no water molecules in the active site or along the proton pathway.
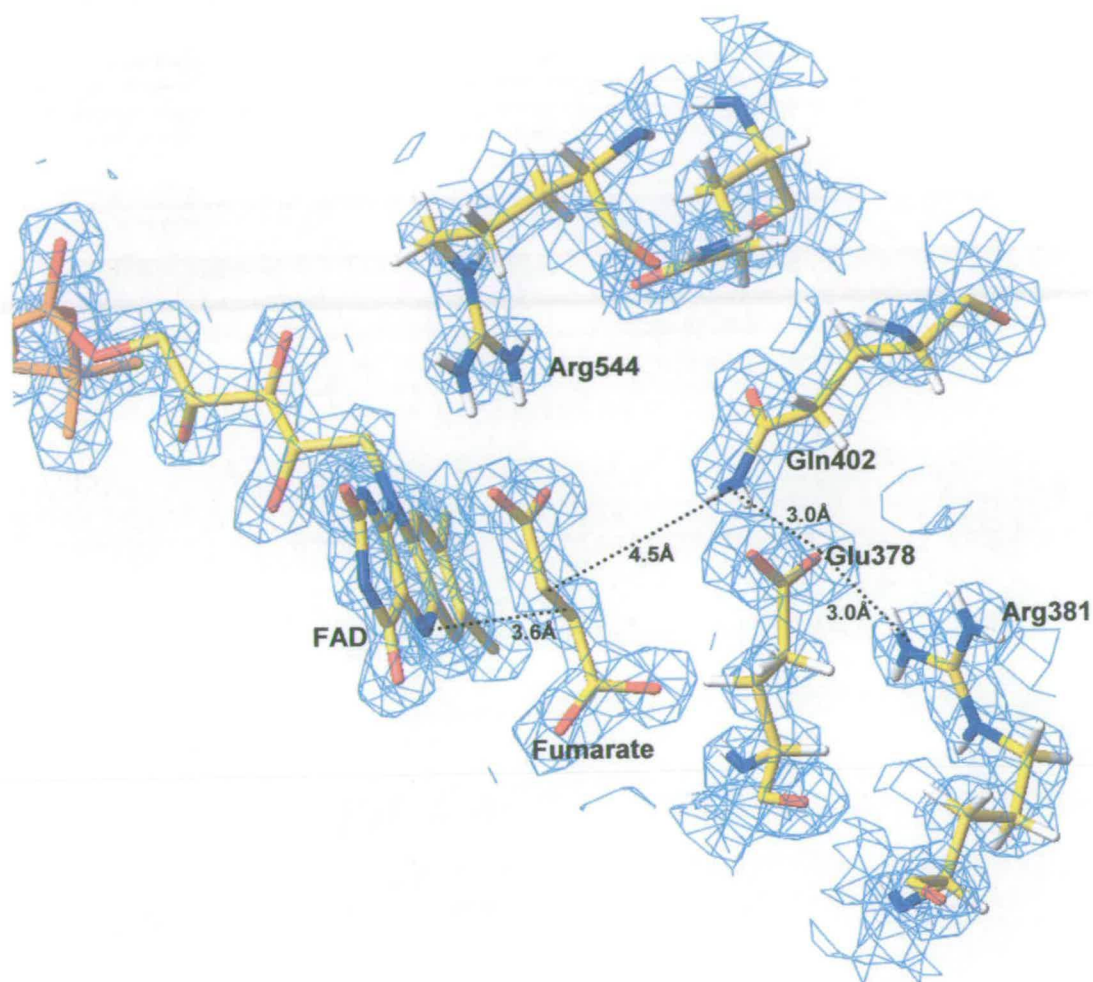
Figure 5.3: The active site in the crystal structure of R402Q. The 1.25 Å resolution allows protons to be modelled in and the amine and carbonyl branches of Gln402 can be distinguished.

5.1.2 R402F

The mutation of Arg402 to phenylalanine was made as a final confirmation of the role of the active site acid. Phenylalanine is an aromatic residue that is unable to act as a proton donor (table 5.1). The mutation was confirmed by mass spectrometry, yielding a mass difference of -10 Da (expected difference of -9 Da). The protein prepared had 64 % FAD bound, but, as predicted, R402F had no detectable fumarate reductase activity.

5.1.3 Addition of Guanidine to R402A

It has previously been observed that some activity, lost by substituting an acid/base catalyst with alanine, can be restored by the addition of an exogenous acid/base. Toney and Kirsch (1989) tested the effect of a variety of free amines on the rate of L-cysteine sulfinate transamination by the K258A mutant of *E.coli* aspartate aminotransferase. Methylamine and ammonia were found to significantly accelerate the rate. Longer chain amines were less effective due to the obligatory steric constraints of the enzyme active site.

Rynkiewicz and Seaton (1996) then used guanidine to restore activity to the R57G mutant of *E.coli* ornithine transcarbamylase (OTCase). This enzyme catalyses the following reaction in the biosynthesis pathway of L-arginine:

$$\text{carbamyl phosphate} + \text{L-ornithine} \rightleftharpoons \text{L-citrulline} + P^i$$

Arg57 was found to be essential for a conformational change induced by the binding of carbamyl phosphate. R57G had a k_{cat} value of only 6 min^{-1}, compared with 1.3×10^5 min^{-1} for wild-type. The addition of guanidine hydrochloride to R57G increased the k_{cat} value to 1.2×10^4 min^{-1}.

The R402A mutant was assayed for fumarate reductase activity under fumarate saturated conditions, with and without the addition of guanidine hydrochloride. No activity was detected in either assay. It is therefore not possible to reactivate the mutant R402A by introducing a guanidinium group externally. If guanidine does occupy the space vacated by Arg402, it may not be correctly oriented to stabilise the transition state, donate protons to C3 and be reprotonated by Glu378 of the proton pathway.

5.1.4 Engineering Water to Act as the Active Site Acid Catalyst

The active site of R402A contains a water molecule, which could act as the active site acid catalyst, but the crystal structure of R402A revealed that it was hydrogen bonded in position B, 4.0 Å from fumarate C3. The hydrogen bonding interactions make it preferable for water to occupy position B rather than position A. Steric constraints prevent double occupation (water molecules in both A and B). This raised the question: if the water molecule in R402A was relocated to position A, could it act as the proton donor?

Gln363 hydrogen bonds to the species occupying position B. The double substitution of Q363F with R402A was constructed, to determine whether a bulky phenylalanine group at position B could sterically block that position, forcing the water molecule to occupy position A (Figure 5.4). If this hypothesis is correct and water is able to take the role of active site acid, then activity should be restored to the inactive mutant R402A by the additional mutation.
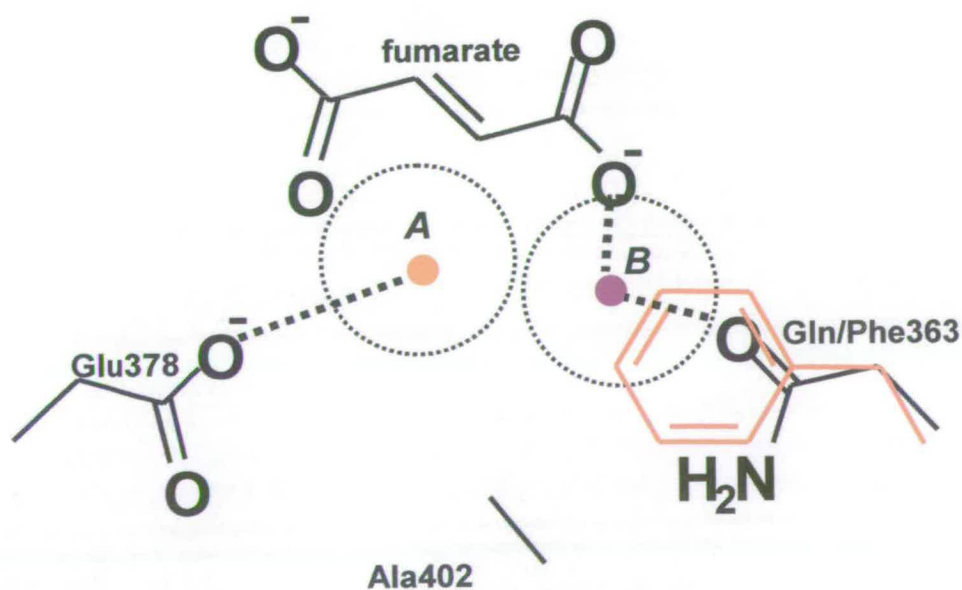
Figure 5.4: Schematic representation of Q363F/R402A. A bulky Phe group was introduced at position B in order to 'push' the water molecule into position A.

5.1.4.1 *Activity of Q363F/R402A*

The double mutant Q363F/R402A had a mass difference from wild-type of –65 Da (expected difference of –66 Da) and the FAD content was 80 %.

The additional mutation of Gln363 to phenylalanine did restore activity to R402A, although k_{cat} is 10^3-10^4-fold lower than wild-type (Table 5.3). The activity levels are, however, approximately 5-fold greater than those of R402K and Y. The K_M is actually 2-5-fold lower than that of wild-type, and increases slightly with increased basicity.

pH	k_{cat} (s⁻¹)		K_M (µM)	
	wild-type	Q363F/R402A	wild-type	Q363F/R402A
6	658 ± 34	0.06 ± 0.001	43 ± 10	6.6 ± 0.6
7.2	509 ± 15	0.33 ± 0.007	25 ± 2	5.0 ± 0.6
7.5	370 ± 10	0.42 ± 0.012	28 ± 3	5.3 ± 0.8
9	210 ± 13	0.28 ± 0.007	7 ± 2	3.3 ± 0.5

Table 5.3: The Michaelis parameters of Q363F/R402A, compared with wild-type (Doherty et al, 2000). The k_{cat} values for Q363F/R402A are 10^3-10^4-fold lower than for wild-type and K_M is 5-fold lower than wild-type.

5.1.4.2 *The Crystal Structure of Q363F/R402A*

The crystal structure was solved to 2.0 Å resolution and confirms that there is now a water molecule in position A (Figure 5.5). The phenyl ring of Phe363 occupies the space around position B that was vacated by the substitution of Arg402 to alanine. The steric bulk of Phe363 has prevented the water molecule from occupying position B. Instead it is in position A, 3.5 Å from fumarate C3 and 2.7 Å from Glu378. The

side chain of Glu378 is, however, rotated ~ 90° from its position in the wild-type proton pathway. This rotation allows Glu378 to occupy a little of the space left by Arg402. The distance between the side chains of the proton pathway residues, Arg381 and Glu378, is now 4.5 Å (compared with 3.1 Å in the wild-type enzyme). So the proton transfer pathway has been compromised, but as a consequence of the change in orientation of Glu378, a water molecule is now included in the pathway (2.9 Å from Arg381 and 3.8 Å from Glu378), which may mediate in proton transfer.
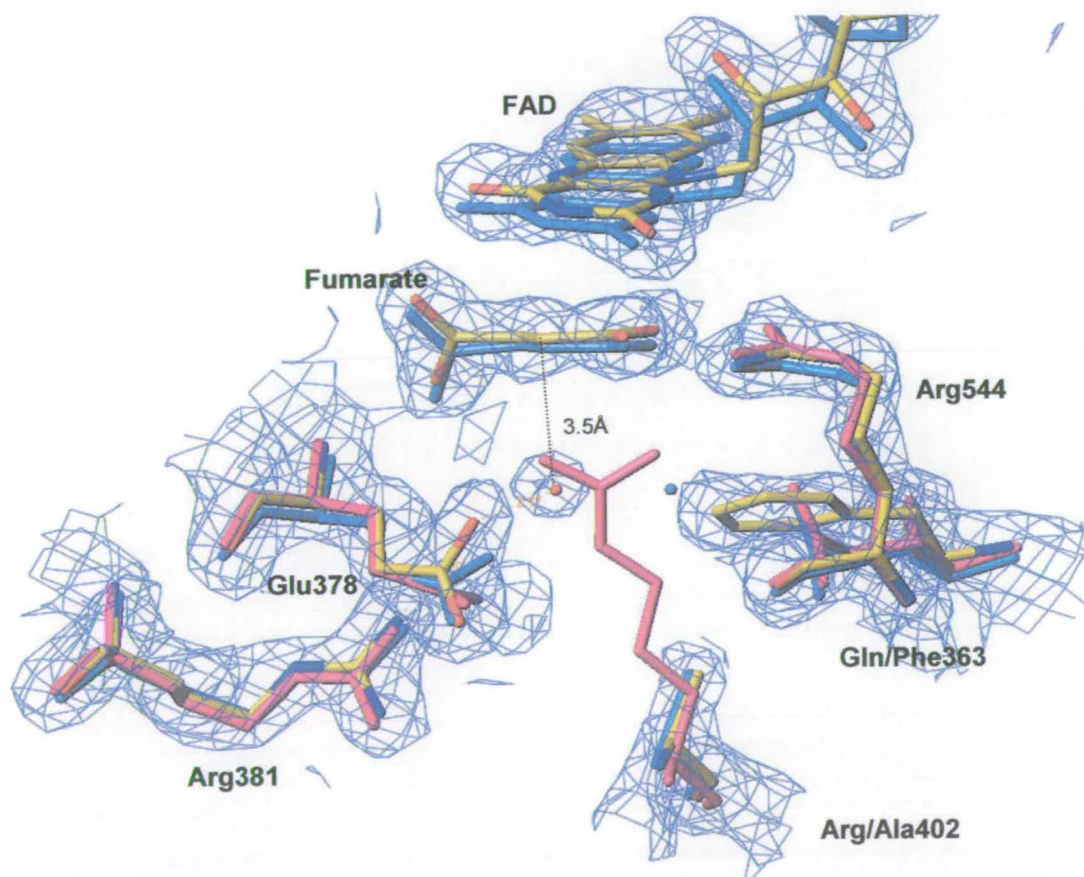
Figure 5.5: The crystal structure of Q363F/R402A. The active site of Q363F/R402A (atom type colours) is overlaid with wild-type (magenta) and R402A (blue), all at pH 6.5. The electron density shown is for Q363F/R402A. The active site of R402A contains a water molecule in position B, where it is incapable of donating a proton to fumarate C3. In Q363F/R402A, density for the water molecule can be seen clearly in position A where it can act as the active site acid catalyst.

5.1.4.3 *Solvent Isotope Effect of Q363F/R402A*

Proton inventories were determined for wild-type and Q363F/R402A by measuring the rates of fumarate reduction in a range of mixed isotope buffers (Figure 5.6). Wild-type fcc_3 has a very large overall solvent isotope effect, k_H/k_D = 8.2 ± 0.4, indicating a complex transition state. The mechanism proposed, which involves reprotonation of the active site acid catalyst by a proton pathway, is consistent with such a large isotope effect.

The overall shape of the proton inventory fits to a model for multiple exchangeable hydrogenic sites in both transition and reactant (Michaelis complex) states (Appendix). With such a fit, it is impossible to draw any conclusions as regards the actual mechanism of fumarate reduction, for example, whether it is a step-wise or concerted process, but it is consistent with the number of residues involved.

Q363F/R402A has an overall solvent isotope effect of 17.0 ± 1.9, double that seen for wild-type. This indicates that proton transfer has been impeded by the mutation. Intriguingly the proton inventory still fits to a model for multiple sites. The water molecule must be trapped in the active site by hydrogen bonds with nearby residues, and requires reprotonation by the proton pathway for it to function as the acid catalyst. If the proton pathway was no longer required one might expect a simplification of the proton inventory. Decreasing the number of exchangeable hydrogenic sites in the transition state manifests itself as a shallower curve. In the extreme case, a single transition state site is seen as a straight line with a negative gradient.

The mechanism for fumarate reduction by Q363F/R402A is shown in Figure 5.7. The kinetic and crystallographic evidence indicates that a water molecule in position A is the proton donating species in the mutant. The proton inventory suggests that the water molecule is bound in the active site and requires reprotonation via the proton pathway.
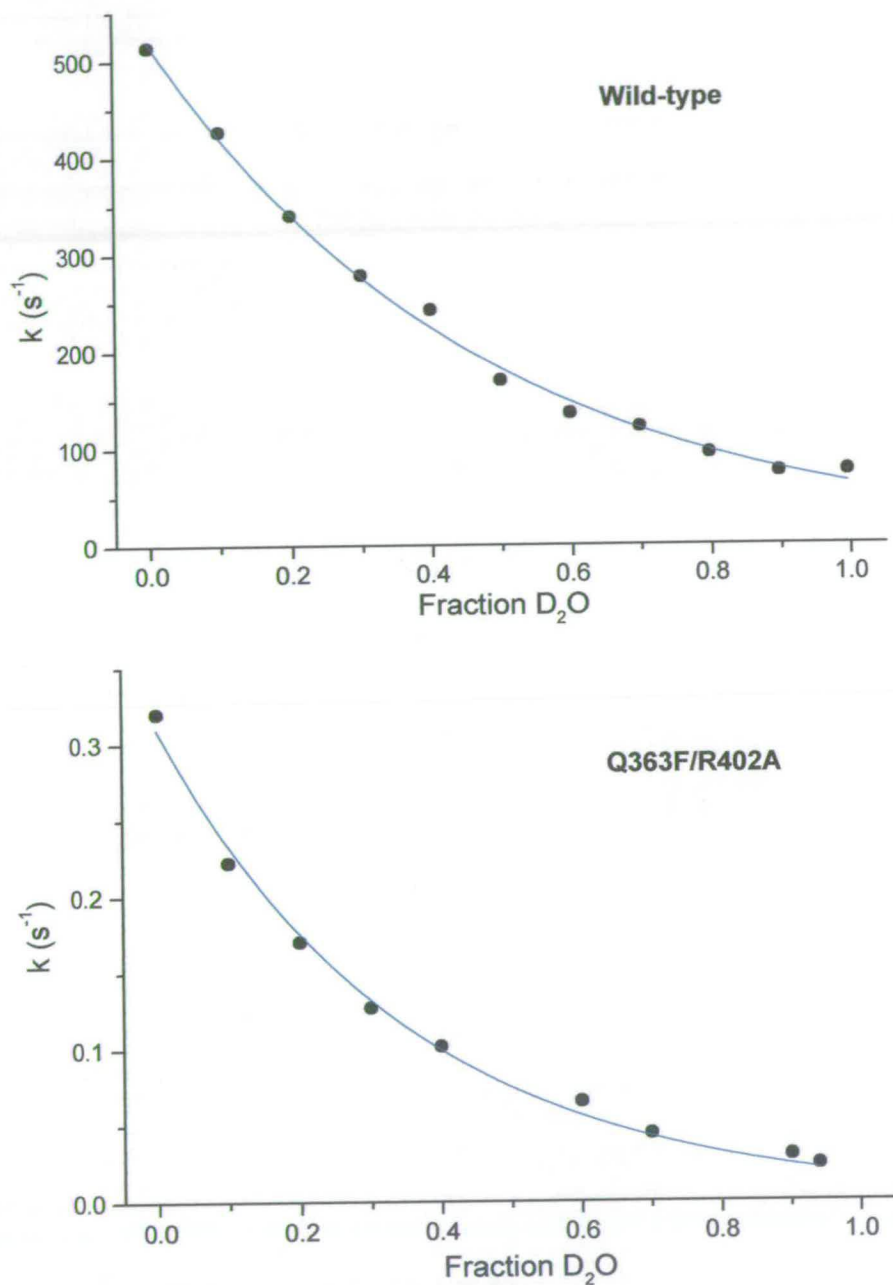
Figure 5.6: *Proton inventories for wild-type (top) and Q363F/R402A (bottom). The two inventories fit to a model for multiple exchangeable hydrogenic sites in both reaction and transition states: $k = k_{cat}(1/n)^x$, where n is the fraction of D_2O (Schowen, 1981). Wild-type has an overall solvent isotope effect, k_H/k_D, of 8.2 ± 0.4 and k_H/k_D for Q363F/R402A is 17.0 ± 1.9.*
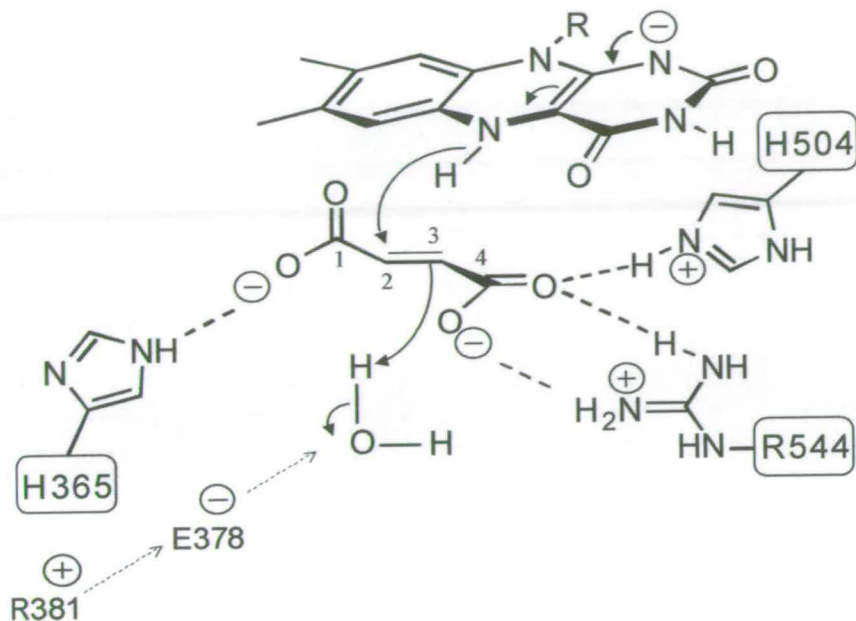
Figure 5.7: Mechanism of fumarate reduction in Q363F/R402A. A water molecule in position A functions as the active site acid catalyst as part of the proton delivery pathway.

5.1.5 Single Substitutions to Gln363

By way of a control, Gln363 was also mutated to alanine and phenylalanine without the R402A substitution. The mutations were, again, confirmed by mass spectrometry. The Q363A mass difference was –54 Da (expected difference of –57 Da) and for Q363F the difference was +19 Da (expected difference of +19 Da). The FAD incorporation for both mutants was the same as the average wild-type content, at 73 %.

5.1.5.1 *The Kinetic Properties of Q363A and Q363F*

The Q363A mutant enzyme retains a third of wild-type activity at pH 7.2, but the value of k_{cat} is dramatically lower at pH 6; decreased 20-fold from wild-type (Table 5.4). The rate of fumarate reduction at pH 7.2 and pH 7.5 is the same. The value of k_{cat} at pH 9 is approximately half that of wild-type. The K_M values for Q363A are generally a little lower than wild-type, decreased 7-fold at pH 6 but the same within error at pH 9.

Q363F has had a much greater effect on both the Michaelis parameters. The enzyme now reduces fumarate with a k_{cat} value of only ~1.5 s⁻¹, a 400-fold decrease from wild-type. The K_M, however, is vastly increased to ≥ 1 mM. These values for k_{cat} and K_M suggest great structural changes at the active site. Particularly when compared to Q363A which had relatively minor effects. The single mutation Q363F has had a greater effect on K_M than substitution of any of the residues directly involved in hydrogen bonding to the fumarate (His365, Thr377, His504 and Arg544). It is equivalent to the double substitutions made to substrate binding residues (chapter 3).

pH	k_{cat} (s⁻¹)			K_M (μM)		
	Wild-type	Q363A	Q363F	Wild-type	Q363A	Q363F
6	658 ± 34	26 ± 1	0.3 ± 0.01	43 ± 10	5.8 ± 1.2	834 ± 102
7.2	509 ± 15	152 ± 2	1.3 ± 0.05	25 ± 2	6.6 ± 0.4	999 ± 132
7.5	370 ± 10	156 ± 3	1.6 ± 0.05	28 ± 3	8.4 ± 0.8	1064 ± 115
9	210 ± 13	131 ± 2	1.6 ± 0.05	7 ± 2	5.7 ± 0.6	1407 ± 160

Table 5.4: The Michaelis parameters of Q363A and Q363F compared with wild-type (Doherty et al, 2000). Q363A has 2-fold to 25-fold less activity than wild-type. The Q363F mutation has had a far more drastic effect, with k_{cat} values decreased 10²-fold and K_M increased 10²-10³ fold.

5.1.5.2 *The Crystal Structure of Q363F*

The crystal structure, at 1.8 Å resolution, revealed the greatest structural change yet seen at the active site of an f*cc₃* mutant (Figure 5.8) and explained the large effects on the values of k_{cat} and K_M. The main difference is the location of Arg402; it is rotated away from the active site by almost 180°, with dislocation of a section of the protein backbone between Ile399 and Ala405. Arg402 is now near the protein surface. This has allowed a water molecule into the active site in position A. It is 3.4 Å from C3 and 2.7 Å from Glu378. As seen in Q363F/R402A, rotation of Glu378 has included a water molecule in the proton pathway which may mediate in proton transfer. In this case it is 3.6 Å from Glu378 and 2.9 Å from Arg381.

The second major alteration is to Arg544, which no longer hydrogen bonds via both branches of the guanidinium group to the fumarate C4 carboxylate, but has moved to occupy some of the space left by Arg 402. In its new orientation Arg544 is 3.4 Å from the C4 carboxylate, below the plane of the fumarate molecule. It now hydrogen bonds to the water molecule in position A at 2.9 Å and participates in a stacking interaction with Phe363. Two water molecules hydrogen bond to the fumarate C4 carboxylate oxygen atoms, in the space vacated by Arg544.
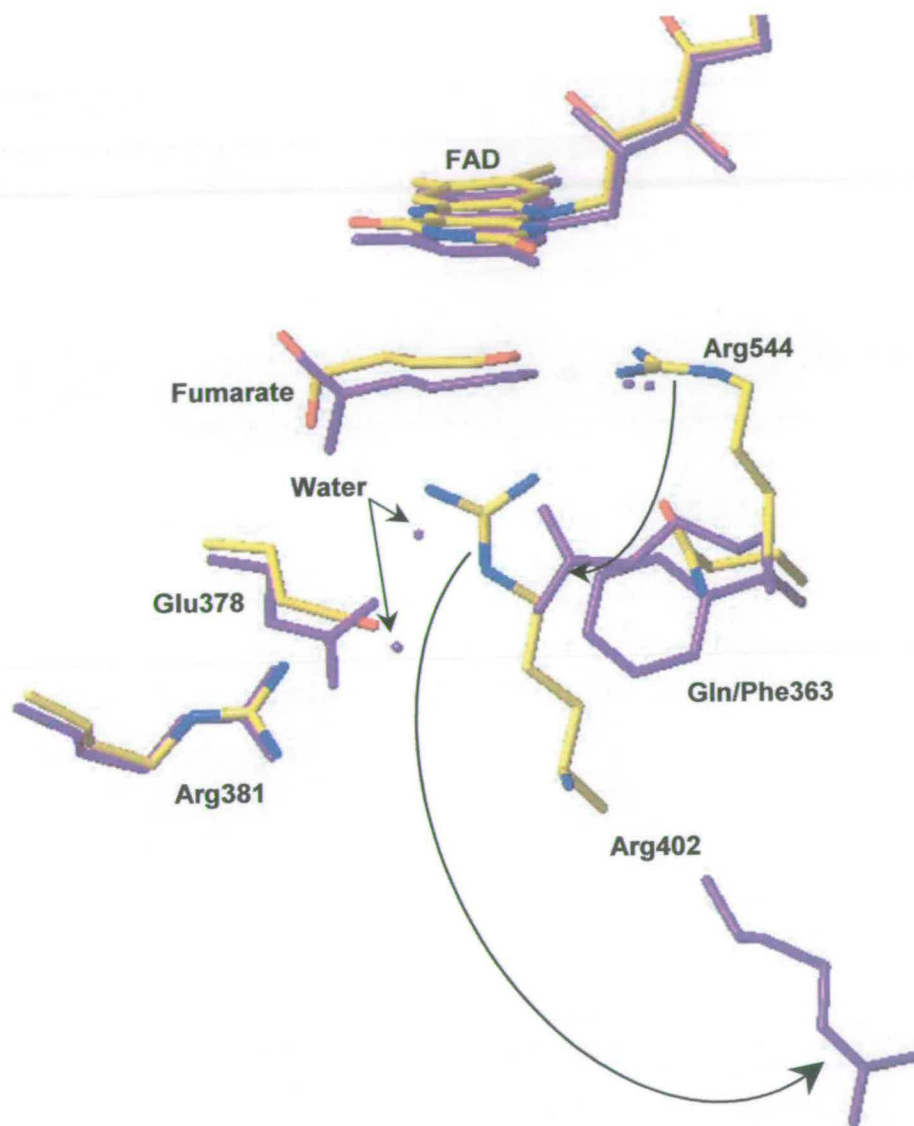
Figure 5.8: Conformational alterations at the active site of Q363F (Wild-type fcc₃ is in atom type colours and Q363F is in purple, both at pH 6.5.). The position of Arg402 has altered by ~180°, now located near the protein surface. Arg544 no longer hydrogen bonds to the fumarate C4 carboxylate. The active site acid is a water molecule, 3.4 Å from C3.

5.1.6 Further Substitutions to Gln363 with R402A

Substituting Gln363 to phenylalanine simultaneously with R402A resulted in a water molecule in position A, giving rise to a small amount of activity (0.35 s^{-1}). Further substitutions of Gln363 to lysine and arginine were made in conjunction with R402A. These double mutants were designed to investigate whether a higher degree of activity could be salvaged by blocking position B to water but maintaining a Lewis acid species in that position.

5.1.6.1 *Activity of Q363K/R402A and Q363R/R402A*

These double mutants do catalyse the reduction of fumarate in substrate saturated assays, but only at levels equivalent to Q363F/R402A. Lysine and arginine are capable of hydrogen bonding, unlike phenylalanine, but are unlikely to be acting as the Lewis acid in position B, as they do not enhance the rate. The crystal structures of the two mutants were solved in order to establish whether Lys363 and Arg363 were conformationally able to hydrogen bond to the C4 carboxylate.

5.1.6.2 *The Crystal Structures of Q363K/R402A and Q363R/R402A*

The structures of both mutants were solved to 1.4 Å resolution. Figures 5.9 and 5.10 show the active sites of Q363K/R402A and Q363R/R402A respectively. Water is present in position A of both mutants to act as the acid catalyst.

In Q363K/R402A the water molecule is 3.5 Å from C3 and only 2.7 Å from Glu378. When Arg402 is substituted by alanine, Glu378 rotates to fill some of the space vacated. This increases the distance between Arg381 and Glu378 and is accompanied by the inclusion of water along the proton pathway. In Q363K/R402A there are two water molecules ideally placed to assist in proton transfer (not shown in Figure 5.9). The water molecule in A is 3.5 Å from C3. The reason that the rate is not accelerated by having a lysine in position B, rather than phenylalanine is because the distance to

the C4 carboxylate is just a little too far to be a hydrogen bond (3.6 Å), so it cannot be stabilising the charge build up in the intermediate.

In Q363R/R402A the water molecule is slightly further away from the substrate, 3.8 Å. The proton pathway is again assisted by two water molecules (not shown in Figure 5.11). In this structure it is immediately apparent that Arg363 is not acting as the Lewis acid because the side chain is folded away from the active site, far from the C4 carboxylate.

The electron density observed for these two mutants (Figures 5.9a and 5.10a) shows that the molecule bound at the active site is not fumarate. In the wild-type structure hydroxylation was seen to have occurred at the substrate C2 during crystallisation/diffraction. Figure 1.20b proposed a mechanism for attack by water at C2. By binding with the C1 carboxylate twisted out of the plane of the molecule and the polarisation of the double bond by the positive environment around the C4 end of the molecule, C2 is the carbon rendered susceptible to attack. Despite this, Q363K/R402A and Q363R/R402A are hydroxylated at C3. This must be due to the location of water molecules and the time spent on a particularly high energy beam to collect data to 1.4 Å resolution.
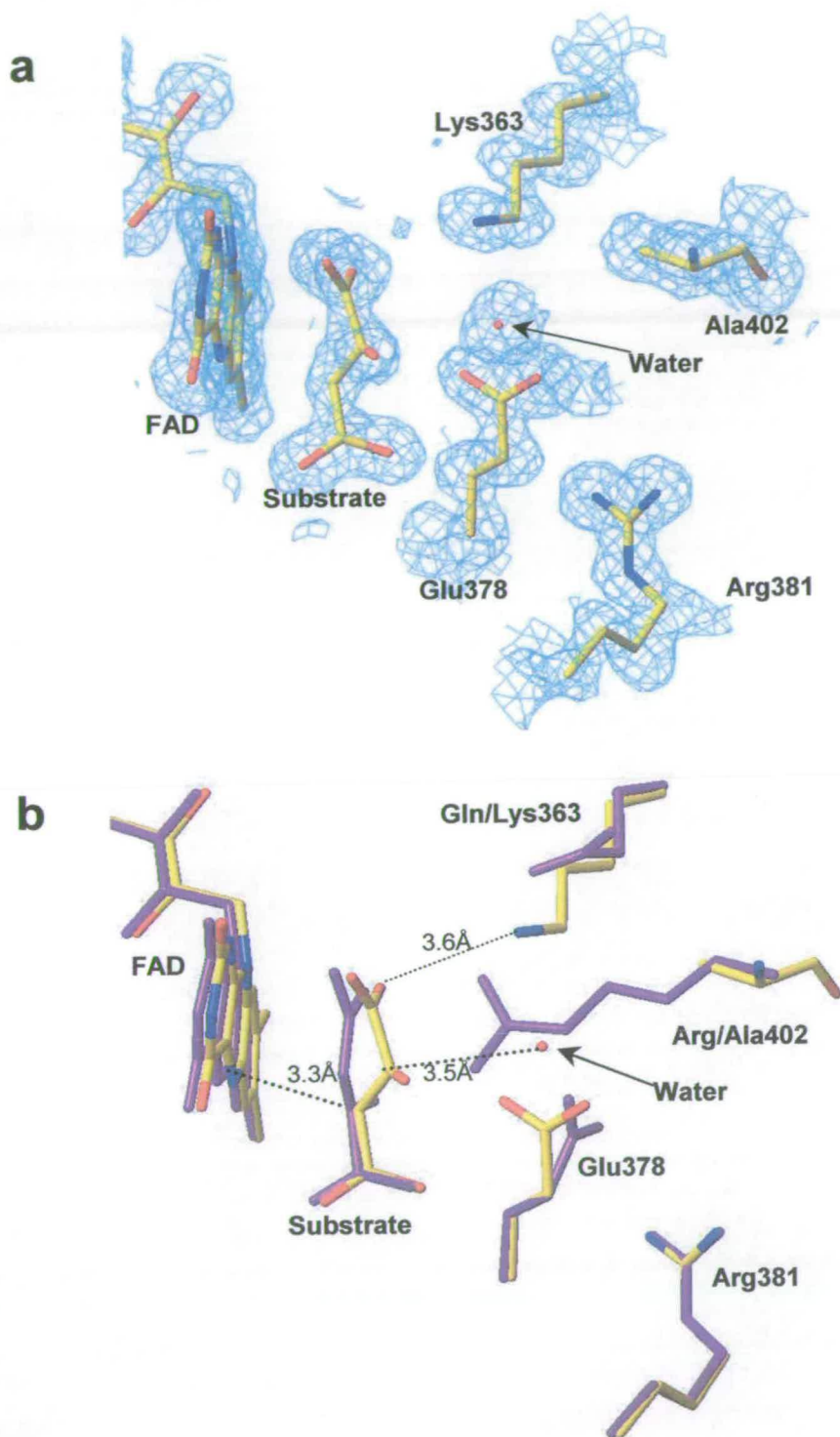
Figure 5.9: The crystal structure of Q363K/R402A (pH 6.5). (a) Electron density around the active site. The substrate molecule is hydroxylated at C3. (b) Q363K/R402A (atom type colours) overlaid with wild-type (purple). The distances shown are for Q363K/R402A.
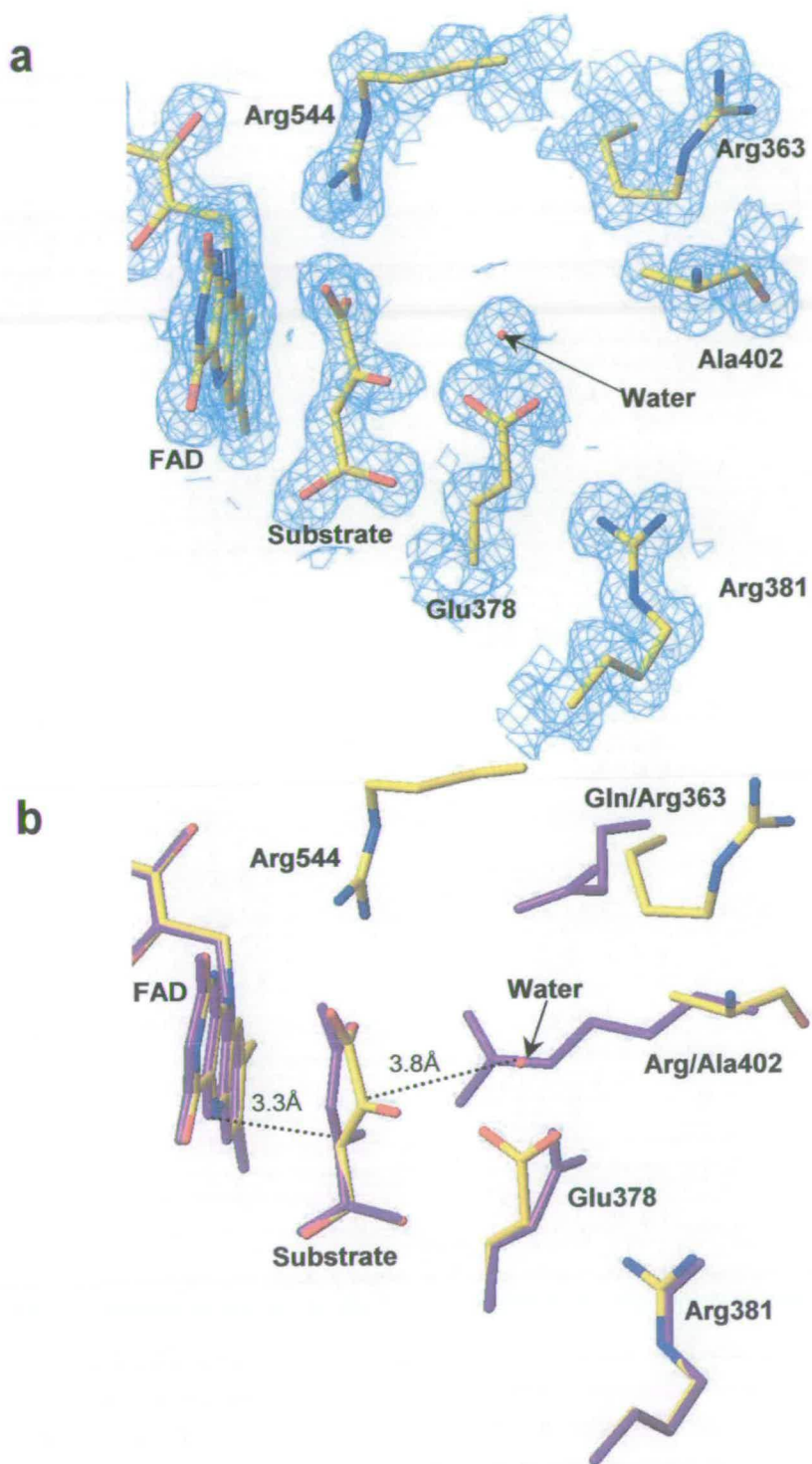
Figure 5.10: The crystal structure of Q363R/R402A (pH 6.5). (a) Electron density around the active site. (b) Q363R/R402A (atom type colours) overlaid with wild-type (purple). The distances shown are for Q363R/R402A. Arg363 is unable to hydrogen bond to the C4 carboxylate.

5.2 Chapter 5 Summary

- Arg402 is the active site acid catalyst. The crystal structure shows Arg402 ideally placed for proton transfer at 3.0 Å from the fumarate C3. The substitution of Arg402 to alanine renders the enzyme completely inactive.

- Arginine fulfils a dual role within the active site: as a Brønsted acid in position A and as a Lewis acid in position B, stabilising the intermediate.

- R402Q is able to catalyse fumarate reduction but only at the lower limit of detection by the assay (a 10^4-fold decrease from wild-type). The crystal structure shows that this is because the shorter side chain of glutamine results in a proton transfer distance of 4.5 Å.

- Substituting phenylalanine for Arg402 inactivates the enzyme.

- R402A has a water molecule in position B of the active site, which is too distant to act as the acid catalyst. Water can be engineered to act as the acid (in position A) by blocking position B with the additional mutation of Gln363 to phenylalanine (Q363F/R402A).

- The double mutants Q363K/R402A and Q363R/R402A are no more active than Q363F/R402A, despite their potential to act as the Lewis acid in position B. The crystal structures reveal that this is because the Lys and Arg side chains are conformationally unable to hydrogen bond to the C4 carboxylate.

- The single mutation Q363F disrupts the active site architecture, with Arg402 rotated away ~180° towards the protein surface.

Chapter 6

The Proton Pathway

6.0 The Proton Pathway

In its active conformation, the substrate binding site of fcc$_3$ excludes water, but for turnover the active site acid, Arg402 must be reprotonated. Analysis of the crystal structure suggested that the residues Glu378 and Arg381 provided an ideal pathway for reprotonating the active site acid catalyst. These residues are completely conserved throughout the family of fumarate reductases and succinate dehydrogenases (Figure 6.1).

```
Fcc3          VMVTEAVRGNGAILV      EITTRDKASAAIL

frda_ecoli    ILMTEGCRGEGGILV      ELGPRDKVSQAFW

frda_wolsu    ILLTEGCRGDGGILR      ELASRDVVSRRMI

dhsa_ecoli    VLVTEGCRGEGGYLL      DLAGRDVVARSIM

dsha_yeast    CLITEGARGEGGFLV      DLACRDVVSRAIT

              : :**. **:*. *       ::. ** :. :
```

Figure 6.1: Conservation of the proton transfer residues. A section of the amino acid sequence from S. frigidimarina fcc₃ is aligned with the analogous sequences from E. coli and W. succinogenes fumarate reductases as well as those from E. coli and yeast succinate dehydrogenases. Arg402 (blue), Glu378 (red), and Arg381 (green) are all strictly conserved throughout the family of fumarate reductases and succinate dehydrogenases.

Figure 6.2 shows the proton delivery pathway and includes distances for hydride and proton transfer. Arg402 is 3.0 Å from the fumarate C3. The Glu378 carboxylate is approximately perpendicular to the guanidinium groups of both Arg402 and Arg381, which are 3.3 Å and 3.1 Å, respectively, from the same branch of the Glu378 carboxylate.
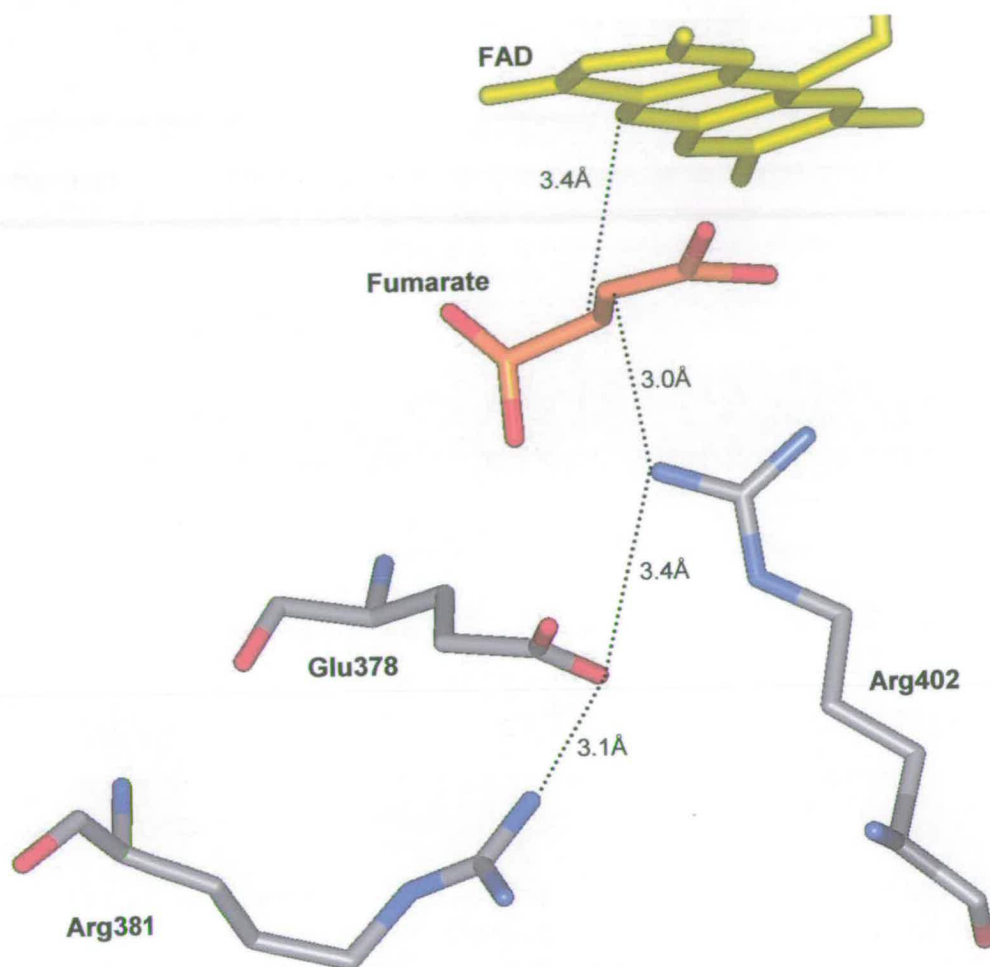
Figure 6.2: The proton pathway of fcc₃. Arg402, the active site acid catalyst, is reprotonated through the protein via the residues Arg381 and Glu378. Arg381 is close to the protein surface and may pick up a proton from solvent.

Arg381 is near the surface of the protein and can receive a proton from solution. The structure reveals that there is no water within the proton pathway itself, proton transfer must proceed purely via the residues. This is unusual, but not unique, as other known proton pathways normally involve hydrogen bonding networks of water molecules and residue side chains.

Perhaps the most extensively studied proton pathway is that of the reaction centre from the photosynthetic bacterium *Rhodobacter sphaeroides*. The reaction centre uses light energy to reduce quinone to quinol. The two protons for this reaction are supplied by a hydrogen bonding network consisting of both amino acid side chains and water molecules. The proton entry point has been identified from crystal structures of the reaction centre with the proton transfer inhibitors Cd^{2+} and Zn^{2+} bound (Axelrod *et al*, 2000; Paddock *et al*, 1999). The metal binds to Asp-H124, His-H126 and His-H128 on the protein surface. Protons travel from there to the quinone binding site via Asp-M17, Asp-L210, Asp-L213, Glu-L212 and Ser-L223 which are interspersed with water molecules (Figure 6.3a). In this pathway there are parallel branches for the uptake of protons, one via Asp-M17 and the other by Asp-L210 (Paddock *et al*, 2001). Proton uptake is coupled to electron transfer. The first electron transfer, forming a semiquinone, is coupled to the protonation of Glu-L212, close to the quinone binding site. During the second electron transfer another proton is taken up and performs the first protonation of the semiquinone. Finally quinol is formed by transfer of the proton from Glu-L212.

Shimizu *et al* (2000) identified a hydrogen boding network for proton delivery in cytochrome P450nor from the denitrifying fungus *Fusarium oxysporum*. The enzyme catalyses the reduction of NO to N_2O. In a cryotemperature structure they located a water molecule (Wat99) hydrogen bonded to the heme-iron bound water molecule (Wat1). The network of hydrogen bonds continues via Ser286, Wat39 and Asp393 to the solvent. This pathway differs from that of fcc₃, both by the involvement of hydrogen bonded water molecules and also by the fact that this pathway is one of several alternative and interlinking networks (Figure 6.3b).
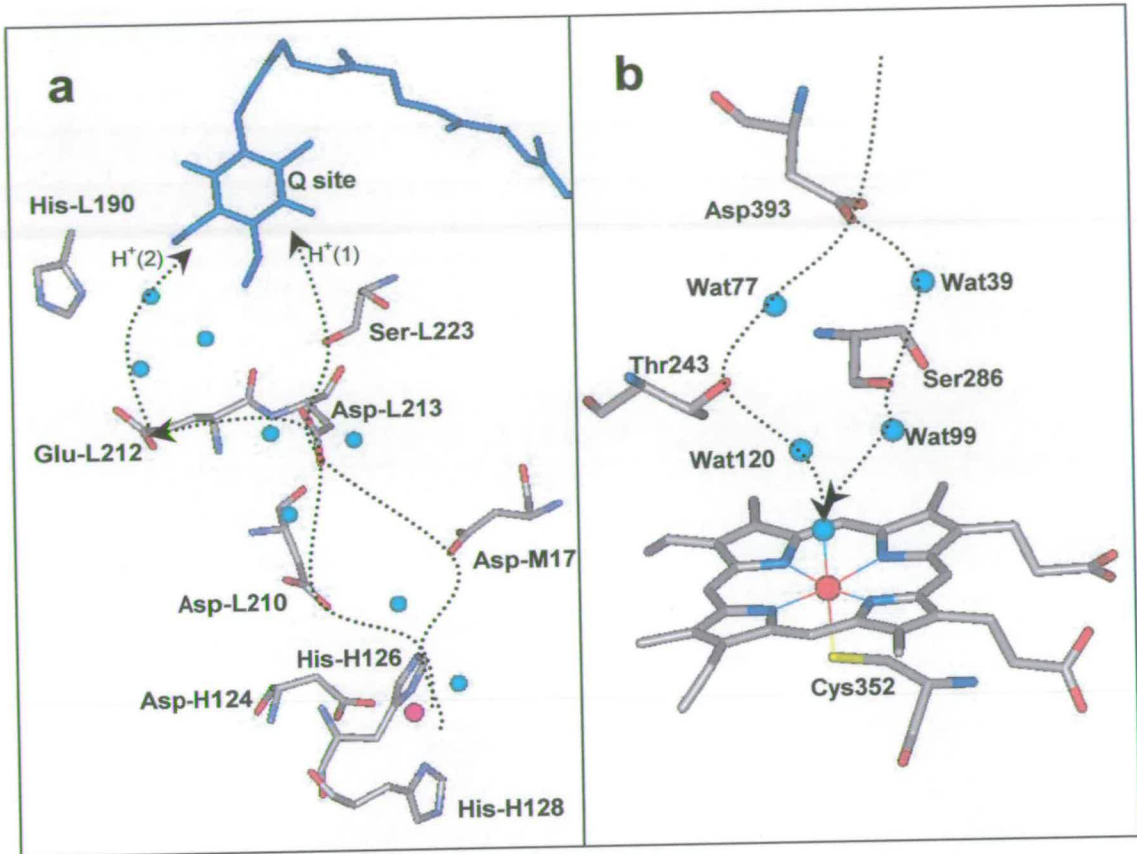
Figure 6.3: (a) The proton pathway from the Rhodobacter sphaeroides reaction centre (Axelrod et al, 2000). Proton transfer is coupled to electron transfer. Zn^{2+} (magenta) is bound at the proton entry point. The first proton to be taken up from the solvent protonated Glu-L212 initially and is then used in the second protonation step at the quinol binding site. (b) Part of the hydrogen bonding network for proton transfer from Fusarium oxysporum P450nor (Shimizu et al, 2000). Several hydrogen bonding pathways of amino acid side chains and water molecules combine to form a larger network to provide protons for the reaction: $2NO + 2H^+ \rightarrow N_2O + H_2O$.

6.1 Substitutions Made to the Proton Pathway Residues

In order to investigate the roles of Glu378 and Arg381, substitutions were made to both residues (Table 6.1). Glu378 was substituted with alanine to remove all functionality, but also to aspartate, which has the same functional group as glutamate but a shorter sidechain length and to glutamine, which maintains the chain length but removes the negative charge of the residue. Arg381 was substituted by lysine; replacing a guanidinium group with an amine. Arg381 was also substituted by methionine, which is unable to participate in proton transfer.

The mass differences confirming the mutations and the average percentage of FAD incorporated are shown in Table 6.2.

Glutamate (E)	Alanine (A)	Aspartate (D)	Glutamine (Q)	Arginine (R)	Lysine (K)	Methionine (M)
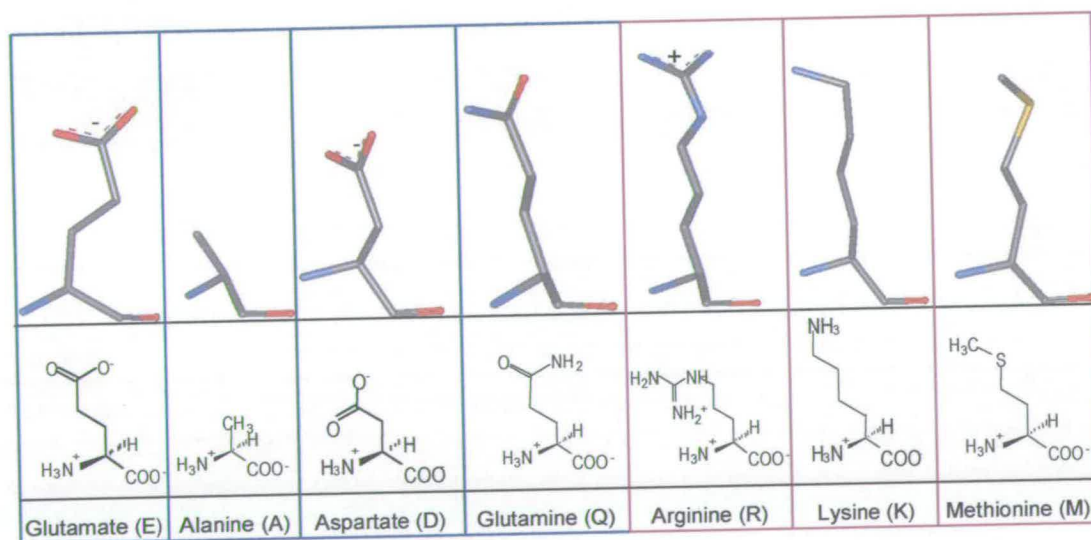
Table 6.1: Substitutions made to the proton pathway residues. Glu378 was substituted with alanine, aspartate and glutamine. Arg381 was substituted with lysine and methionine.

	Mass (Da)	Mass Difference (Da)	Expected Difference (Da)	%FAD
Wild-type	63033	N/A	N/A	73
E378A	62973	-60	-58	65
E378D	63017	-16	-14	69
E378Q	63036	+3	-1	75
R381K	63004	-29	-28	78
R381M	63013	-20	-25	60

Table 6.2: Mass differences caused by substitution of the proton pathway residues and the average FAD percentages determined for the mutants. The error for the mass data is ± 5 Da.

6.2 Kinetic Analysis

6.2.1 The Kinetic Properties of E378A, D and Q.

The kinetic parameters determined for the mutants are shown in Table 6.3. E378A was found to be completely inactive within the limits of the assay. Clearly, alanine is incapable of functioning in the proton pathway and the substitution has prevented the reprotonation of Arg402. The inactivity of this mutant emphasises the importance of the proton pathway in fumarate reduction.

Both E378D and E378Q have measurable fumarate reductase activity but both substitutions have greatly decreased the activity of the enzyme. Substitution with aspartate has lowered the k_{cat} value by approximately 500-fold. The pH dependence of k_{cat} has also been reversed; wild-type is most active at pH 6 whereas E378D is most active at pH 9. Replacing a glutamate with an aspartate may appear to be a conservative mutation, but it has had a significant effect on the rate of fumarate reduction by fcc₃. E378Q is even less active, the k_{cat} values are decreased 10^3-fold.

The glutamine substitution can barely maintain the proton pathway and reprotonation of Arg402.

A secondary effect of these mutations is apparent from the K_M values for E378D and E378Q. Alterations at residue 378 affect substrate binding. The substrate is described as being tightly held by 11 hydrogen bonds (Taylor *et al*, 1999). The major contributors at either end of the molecule are those residues investigated in chapter 3, but Glu378 is also involved, via a hydrogen bond from the backbone amide to the C1 carboxylate. Glu378 hydrogen bonds to the same oxygen of the carboxylate as His365, its neighbour, Thr377, hydrogen bonds to the other carboxylate oxygen. Substitution of Glu378 should not affect the hydrogen bond from the amide, but the K_M values for the mutants suggest that this may not be the case.

pH	k_{cat} (s⁻¹)			K_M (μM)		
	Wild-type	E378D	E378Q	Wild-type	E378D	E378Q
6	658 ± 34	1.27 ± 0.05	0.08 ± 0.01	43 ± 10	72 ± 13	90 ± 31
7.2	509 ± 15	2.05 ± 0.11	0.38 ± 0.01	25 ± 2	319 ± 63	204 ± 34
7.5	370 ± 10	2.43 ± 0.07	0.33 ± 0.02	28 ± 3	549 ± 54	207 ± 54
9	210 ± 13	5.92 ± 0.14	0.29 ± 0.02	7 ± 2	1487 ± 123	620 ± 128

Table 6.3: Michaelis parameters for E378D and E378Q compared with wild-type (Doherty et al, 2000). The k_{cat} values for E378D and Q are increased from wild-type ~500-fold and 10³-fold respectively. The increased K_M values indicate that substitution of Glu378 has also compromised substrate binding.

6.2.2 Substitution of Arg381

Arginine 381 is at the surface of the protein, but substitution results in a great loss of catalytic activity. The R381K mutation has decreased the k_{cat} 40-200-fold, but

maintains the general pH trend of wild-type, most active at pH 6 (Table 6.4). R381M, however, is least active at pH 6 and activity is lowered 10^2-10^3-fold.

K_M values for R381K and R381M are not significantly altered from wild-type. Arg381 is clearly important for catalytic activity but it has no direct role in substrate binding.

pH	k_{cat} (s^{-1})			K_M (μM)		
	Wild-type	R381K	R381M	Wild-type	R381K	R381M
6	658 ± 34	16 ± 0.4	0.49 ± 0.01	43 ± 10	99 ± 7	6.6 ± 0.9
7.2	509 ± 15	8 ± 0.5	2.20 ± 0.12	25 ± 2	35 ± 5	8.7 ± 2.8
7.5	370 ± 10	5 ± 0.4	2.80 ± 0.12	28 ± 3	33 ± 7	4.7 ± 1.1
9	210 ± 13	1.2 ± 0.1	2.29 ± 0.11	7 ± 2	5 ± 1	13.9 ± 3.0

Table 6.4: Michaelis parameters for R381K and R381M compared with wild-type (Doherty et al, 2000). The k_{cat} values are 10-10^2-fold and 10^2-10^3-fold lower than wild-type for R381K and R381M respectively. The K_M values are not significantly different to the wild-type values.

6.3 Solvent Isotope Studies

The proton inventory for wild-type fcc_3 is reported in chapter 5. Proton inventories were also constructed for the proton pathway mutants, at pL 6, 7.2 and 9 (where L = H or D, Figure 6.4 and Table 6.5). All the inventories fit to a model for multiple exchangeable hydrogenic sites (Appendix), as does wild-type. So none of the substitutions made have simplified the transition state. The overall solvent isotope effect for each mutant is greatest at pL 6, decreasing with pL which is logical as there is a higher degree of protonation/deuteration at low pL.
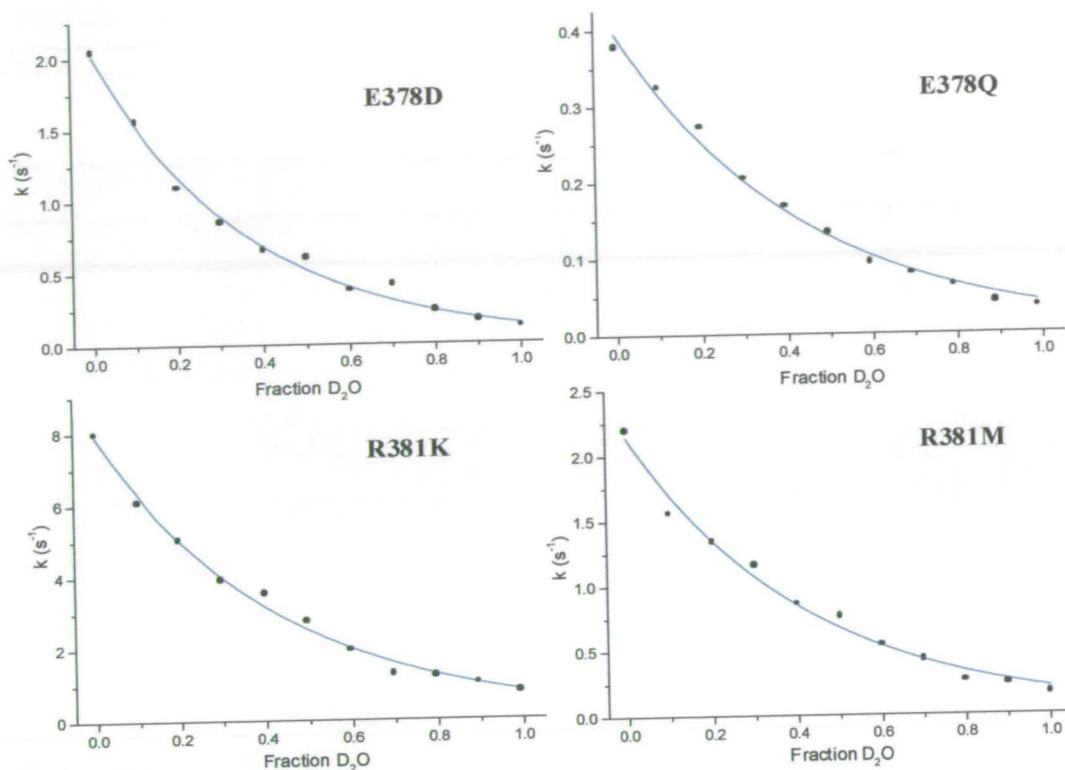
Figure 6.4: *Proton inventories for the proton pathway mutants. All fit to a model for multiple exchangeable hydrogenic sites (k = k$_{cat}$(1/n)^x where n is the fraction of D$_2$O).*

pL	Wild-type	E378D	E378Q	R381K	R381M
6	13 ± 2	24 ± 5	12 ± 1	11 ± 1	15 ± 2
7.2	8.2 ± 0.4	15 ± 1.6	9.6 ± 0.8	9.9 ± 0.8	10.3 ± 1.1
9	4.0 ± 0.3	9 ± 1	6 ± 1	4 ± 0.1	8 ± 1

Table 6.5: *Solvent isotope effects (k$_H$/k$_D$) for the proton pathway mutants. Values of k$_H$/k$_D$ are greater at low pL where there is a higher degree of protonation/deuteration.*

Too close an analysis of these figures is, at present, impossible. All of these substitutions decrease the activity to well below the minimum activity of wild-type fcc₃. At high pH, His504 is deprotonated and unable to stabilise the intermediate, but the intermediate does still form and the enzyme can maintain a turnover rate of 200 s⁻¹. All the proton pathway mutants are well below this rate so pH profiles are not necessarily comparing the same ionisable groups. The same is true of comparing pL profiles in H_2O and D_2O. The overall solvent isotope effects for wild-type and the mutants are so large that you are not necessarily detecting a shift in one pK_a upon deuteration, but perhaps the emergence of different groups influencing the activity. For example, Figure 6.5 shows the pL-activity profile for E378Q in both H_2O and D_2O. The rate in H_2O does not fall below 0.075 s⁻¹, whereas in the D_2O plot remains well below 0.05 s⁻¹. Schowen (1981) described 'normal' behaviour for an enzyme in D_2O as a pK_a shift of +0.5 to +0.6 units. The higher pK_a value E378Q is essentially unchanged (within error) and the lower pK_a in D_2O is extrapolated to 5.1 ± 0.4 which is a negative shift.

So looking purely at trends in the solvent isotope effects, there is a slight increase for R381K, R381M and E378Q. At pL 7.2, for example, $k_H/k_D = 10$, compared to 8 in wild-type. k_H/k_D for E378D, however, is double that of wild-type at all values of pL. This substitution has surely hindered proton transfer.
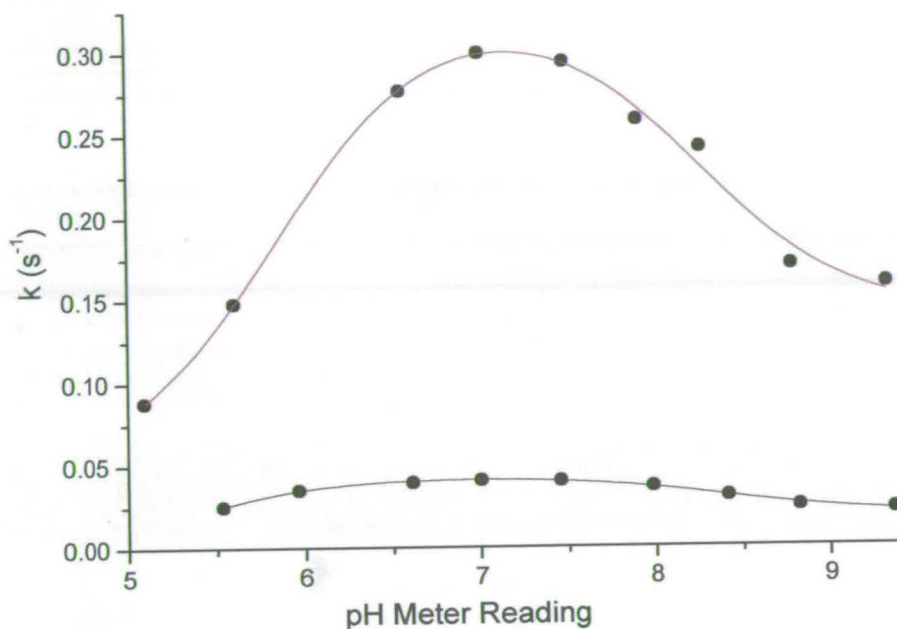
Figure 6.5: Activity profiles for E378Q in H₂O (purple) and D₂O (black). The maximal rate of fumarate reduction in D₂O by E378Q is lower than the minimum rate in H₂O, so the pK_a values (5.8 ± 0.1 and 8.2 ± 0.1 in H₂O, 5.1 ± 0.4 and 8.4 ± 0.1 in D₂O) may not be directly comparable.

6.4 The Crystal Structures of E378D and R381K

6.4.1 E378D

The solvent isotope results appear counter-intuitive. E378D could be expected to have less effect on proton transfer, due to the similar functionalities of aspartate and glutamate. To attempt an explanation, the crystal structure of E378D was solved to 1.7 Å resolution.

An overlay of the proton pathways in E378D and wild-type in is shown in Figure 6.6. Unfortunately it does little to explain why E378D has such a large solvent isotope effect. There have been no major structural alterations to the proton pathway. The hydride transfer distance, from FAD N5 to fumarate C2, is unchanged at 3.4 Å and

the proton transfer distance from Arg402 to fumarate C3 is only increased from 3.0 Å to 3.1 Å. The Asp378 carboxylate group does not overlay that of Glu378 in wild-type, but one branch does occupy almost the same position, 3.2 Å to Arg402 (3.1 Å in wild-type) and 3.5 Å to Arg381 (3.1 Å in wild-type). These changes in distance are not very large, but even small alterations in proton transfer distance may lead to large changes in proton transfer rate.
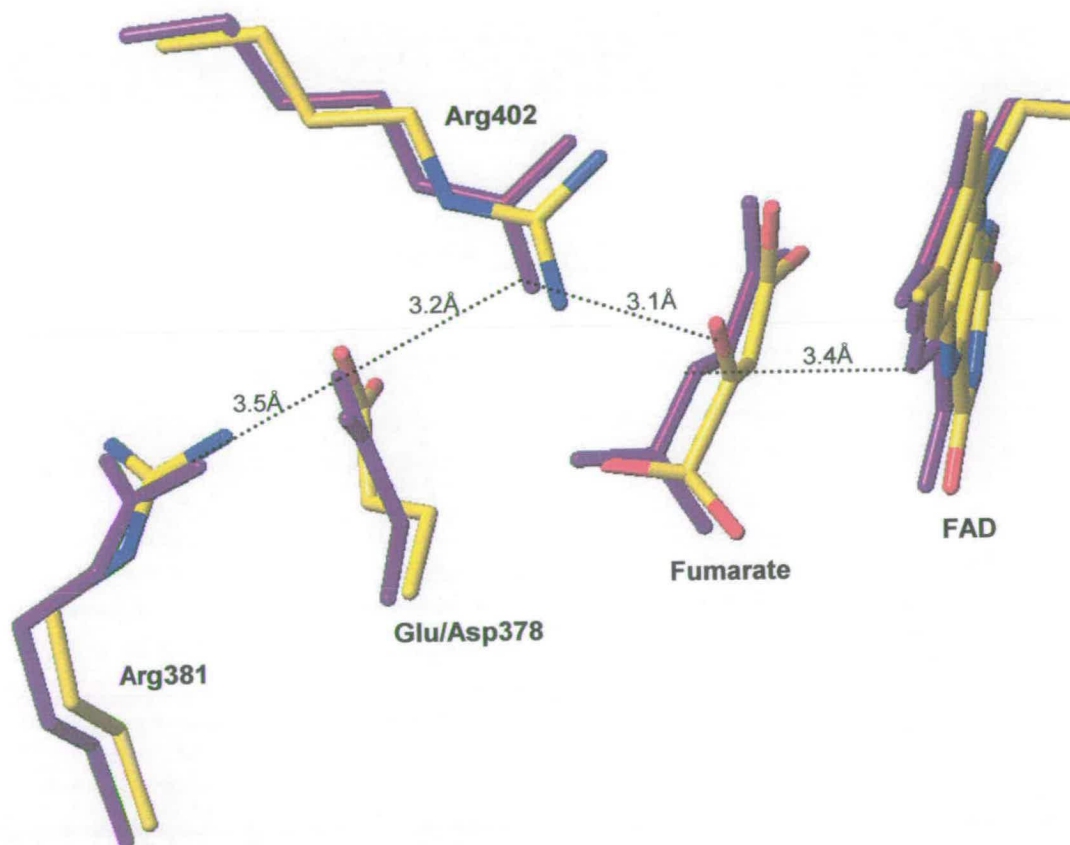
Figure 6.6: The crystal structure of E378D. The proton pathway of E378D (purple) is overlaid with that of wild-type (atom type colours), both at pH 6.5. The distances shown are for E378D and are little altered by the substitution.

6.4.2 R381K

The crystal structure of R381K was solved to 2.1 Å resolution. This substitution has actually had a greater effect structurally, on the proton pathway (Figure 6.7). The proton transfer distance from Arg402 to fumarate C3 is unchanged at 3.0 Å. Glu378 has altered its conformation, rotated ~ 90° and is now 3.0 Å from Arg402. The distance between Glu378 and Lys381 is now large, 6.1 Å, however the substitution has allowed two water molecules into the pathway. These are likely to mediate proton transfer between Lys381 and Glu378.
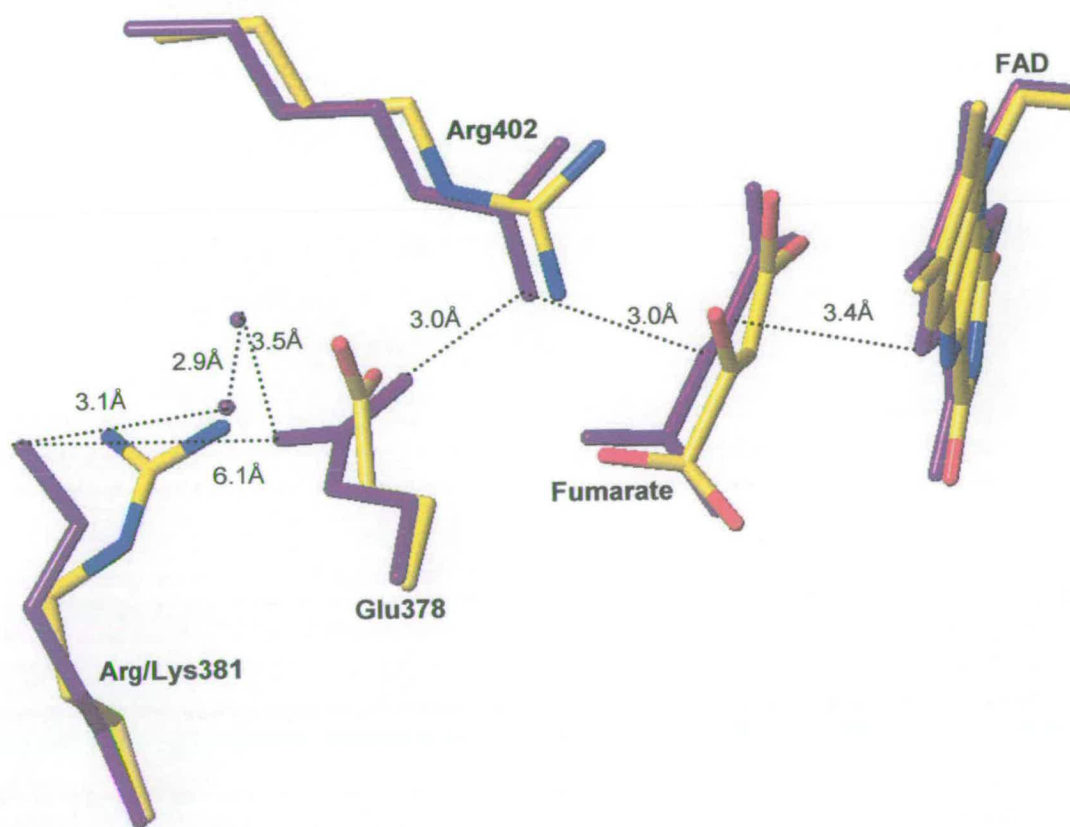
Figure 6.7: The crystal structure of R381K. The proton pathway of R381K (purple) is overlaid with that of wild-type (atom type colours), both at pH 6.5. Two water molecules are now included in the pathway and may mediate proton transfer. The distances shown are for R381K and include the two water molecules between Lys381 and Glu378.

6.4.3 Water in the Proton Pathway

Water molecules participating in the proton pathway may be the key to understanding why the relatively conservative mutation of Glu378 to aspartate has a far greater effect on proton transfer than Glu378 to glutamine. R381K, R381M and E378Q have all had a minimal effect on proton transfer (as seen in the solvent isotope effects). It is possible that the difference in these situations is the inclusion of water, mediating in proton transfer along the pathway, thus compensating for the effects of the substitutions.

Substituting the branched arginine group for a linear amine in R381K, so close to the protein surface, has had the effect of including two water molecules. It is likely that this also occurs in R381M. The conservative nature of the E378D substitution may in fact be the key to its comparatively large solvent isotope effect. The charge remains the same and Arg381 does not alter its conformation, so no water is allowed into the pathway to mediate proton transfer. No water is seen within the wild-type proton pathway either. No crystal structure is yet available for E378Q but the effect of removing the negative charge between the two arginine residues may result in repulsion between Arg381 and Arg402, altering the position of Arg381 and allowing water into the pathway.

This is at present merely speculation, the structures of E378Q and R381M must be solved to confirm the theory. If it is the case, then E378D is the only mutant for which we see the direct effect of the substitution on proton transfer, unmediated by water.

6.4.4 An Interesting Aside

The electron density at the active site of E378D suggests that the FAD is covalently linked to the protein (Figure 6.8). The nature of the linkage is in itself novel, Met375 to the FAD C6. Previously observed cases of covalent flavin linkages involve cysteine, histidine or tyrosine residues (Figure 1.3d). It is known that the FAD is not covalently bound in solution because the FAD content can be determined as usual by precipitating the protein to leave FAD in solution. The electrospray mass spectroscopy analysis of wild-type and E378D shows that neither has covalently bound FAD. If the FAD was always covalently attached then it would precipitate/ionise with the protein. So the apparent covalent linkage is an artefact of crystallography. The resolution of the structure is high (1.7 Å) and no alternative configuration of Met375 fits the electron density.

In order to try and confirm the presence of a covalently bound FAD, four protein samples were irradiated either for two hours or overnight on the X-ray beam. The solution conditions mirrored those of the crystal and two samples were frozen in imitation of crystal freezing. To determine whether the irradiation had caused a covalent bond to form, the mass of the samples were determined by LCMS. All four samples had the expected mass for E378D and there was no evidence of a second population with mass increased by 829 Da. Further crystals are currently being grown in an attempt to reproduce the structure with covalent FAD.
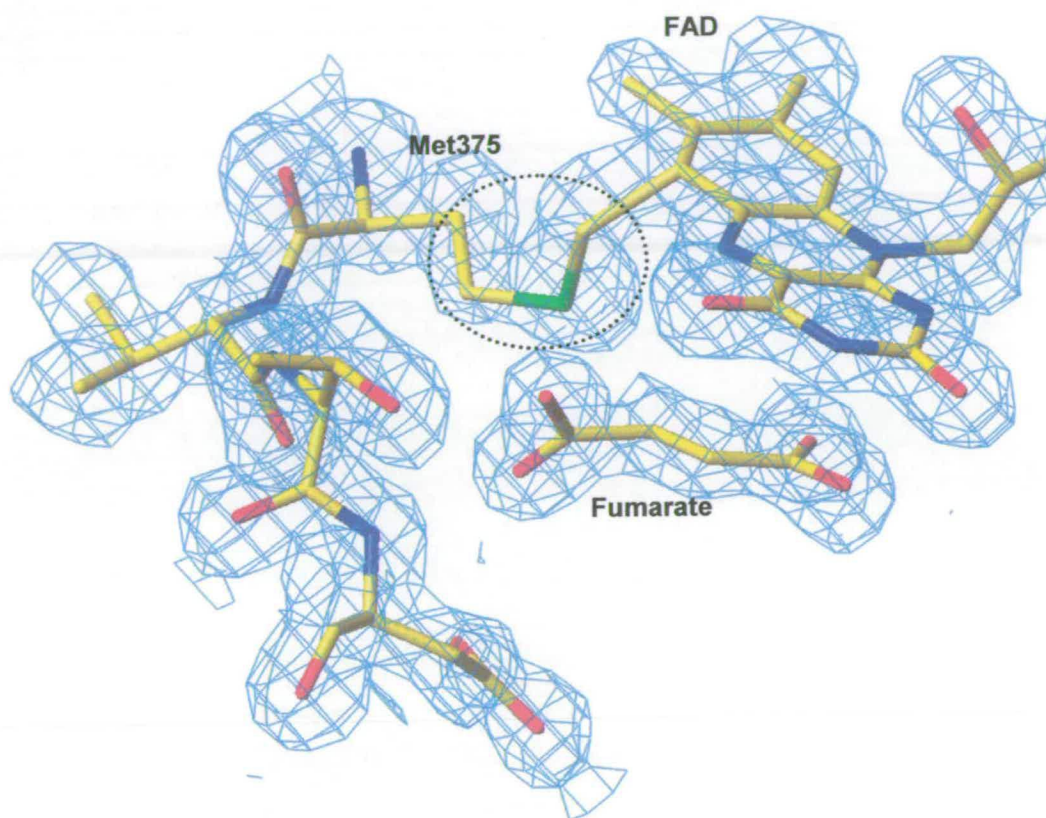
Figure 6.8: The covalent linkage of FAD and Met375 in E378D. The electron density around the FAD clearly shows that the FAD is covalently linked to the protein via Met375 in this mutant.

6.5 A Link Between Proton Transfer and Electron Transfer?

R402A, E378A and R381M were analysed by protein film voltammetry (A. Jones and E. Rothery personal communication, Jones, 2002). In this technique the protein is immobilised on an electrode surface, so electrons entering/exiting the protein can be exactly controlled. A typical non-turnover signal is shown in figure 6.9a. The sharp feature is the two-electron FAD peak and the shoulder is the envelope of four one-electron heme peaks. The rate of electron transfer in the protein can be investigated by varying the scan rate. Very high scan rates may exceed the protein

internal electron transfer rate and this is seen by a splitting between the oxidative and reductive peaks (Figure 6.9b, Jones *et al*, 2000). If the peak separations are plotted as a 'trumpet' plot (Figure 6.9c), they can be fitted to the Butler-Volmer equations (6.2a and b) to give a rate of electron transfer (Hirst and Armstrong, 1998).

$$k_{ox} = k_0 \exp(-\alpha nF(E-E^0)/RT) \qquad\qquad 6.2a$$

$$k_{red} = k_0 \exp((1-\alpha)nF(E-E^0)/RT) \qquad\qquad 6.2b$$

Where k_0 is the standard electrochemical rate constant, E is the applied potential and E^0 is the reduction potential. The number of electrons transferred is n and α is the Butler-Volmer transfer coefficient. Trumpet plots for wild-type, E378D and R381M are in Figure 6.9c. The peak separation occurs at a lower scan rate in the mutants than in wild-type, indicating that electron transfer has been impeded. The value of k_0 for wild-type is 456 ± 23 s^{-1}. For E378D, k_0 is 104 ± 10 s^{-1}, for R381M it is 70 ± 20 s^{-1} and for R402A it is 42 ± 2 s^{-1}. So substituting the residues involved in proton transfer appears to affect the electron transfer rates within the protein. This is not the case for all substitutions made at catalytically important residues. For the substrate binding mutant H365A, k_0 was unchanged from wild-type (Jones, 2002).

There is also evidence for the reverse occurring. Substitution of one of the axial histidine ligands (His61) of heme four (closest to the FAD), to an alanine results in a loss of electron transfer cooperativity at the FAD, but also results in an increased solvent isotope effect. The magnitude of the k_H/k_D is 16, which is the same as that for the proton pathway mutant E378D (E. Rothery, personal communication).

So results are emerging to suggest that proton transfer and electron transfer are closely linked in fcc_3. If electron transfer were somehow gated by proton transfer then the solvent isotope effect of H61A suggests that the reverse is true also. The nature of such a relationship is as yet unresolved.
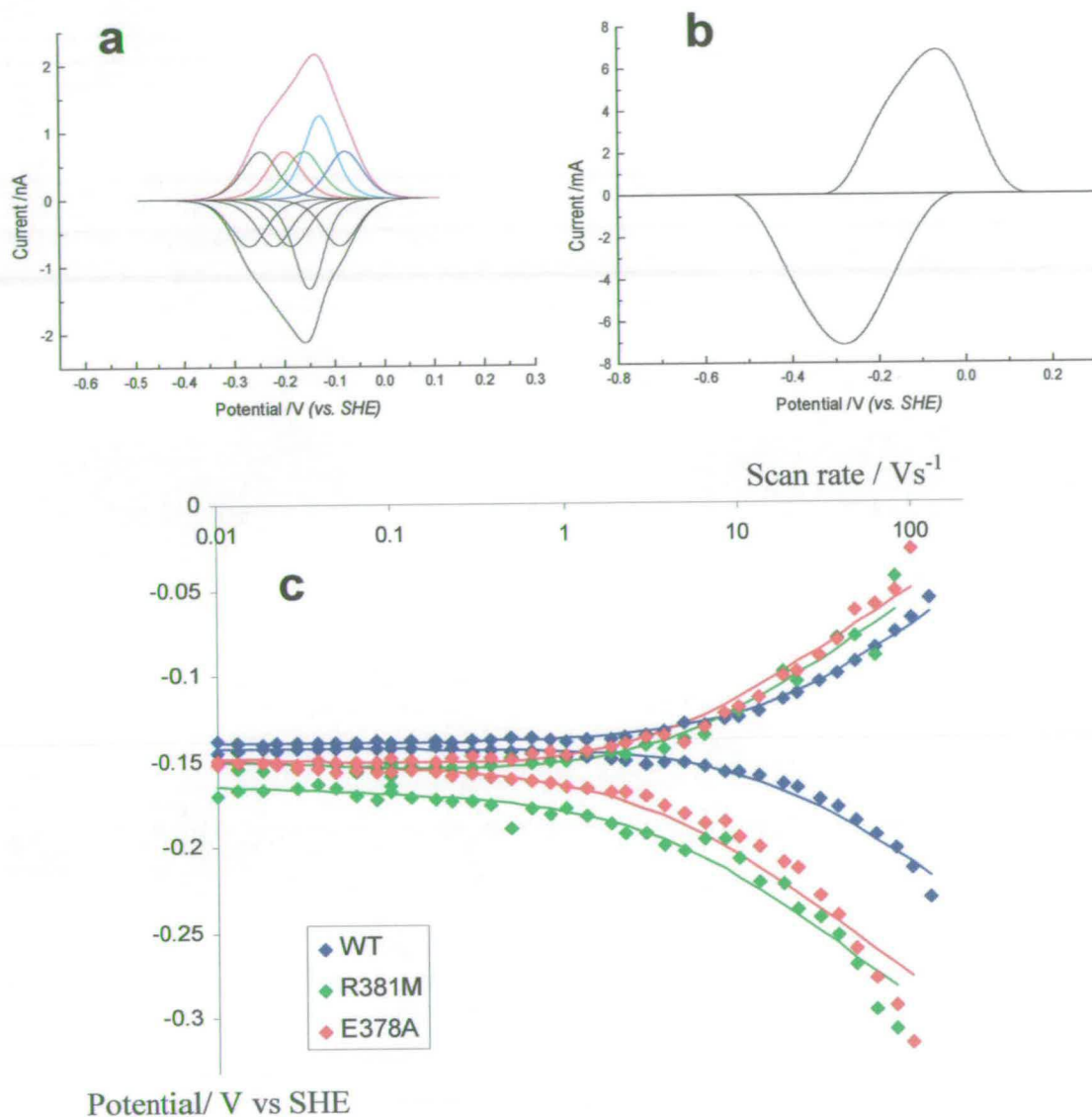
Figure 6.9: (a) A typical non-catalytic PFV signal for fcc₃. The signal can be deconvoluted into a sharp 2e⁻ FAD peak (cyan) and four broader 1e⁻ heme peaks (red, green, blue and black). The scan rate is 10 mVs⁻¹. (b) At higher scan rates (in this case 100 mVs⁻¹) the internal electron transfer rate is exceeded and splitting is seen between the oxidative and reductive peaks. (c) Trumpet plots for E378A and R381M compared with wild-type. A plot of the peak separation as a function of scan rate is called a trumpet plot. Peak separation occurs at a lower scan rate for the proton transfer mutants, suggesting that electron transfer has also been affected.

6.6 Chapter 6 Summary

- The active site acid, Arg402, requires reprotonation through the protein, by the proton pathway of residues Glu378 and Arg381.

- Substituting Glu378 or Arg381 showed both residues to be vital for catalysis.

- The solvent isotope effects for all proton pathway mutants are slightly increased. For E378D the value of k_H/k_D is doubled, so this substitution has clearly hindered proton transfer.

- Water molecules, allowed into the proton pathway by some of the mutations, are likely to mediate in proton transfer and so E378D (which has no water in the pathway) may have the only isotope effect that truly reflects the mutation made.

- The crystallisation/diffraction process for E378D has resulted in a novel Met-C6 FAD covalent linkage.

- There is evidence to suggest that proton and electron transfer are coupled in fcc_3. Substitutions to the proton pathway residues also result in a reduced rate of electron transfer. Substitutions to a heme axial ligand increase the solvent isotope effect.

Appendices

7.0 Appendices

7.1 References

Ackrell, B. A. C., Cochran, B., and Cecchini, G., (1989) *Arch. Biochem. Biophys*, **268**, 26-34.

Axelrod, H.L., Abresch, E.C., Paddock, M.L., Okamura, M.Y., Feher, G. (2000) *PNAS*, **97**, 1542-1547.

Bamford, V., Dobbin, P.S., Richardson, D. J., and Hemmings, A. M. (1999) *Nat. Struct. Biol*, **6**, 12, 1104-1107.

Beliaev, A.S., Saffarini, A.D. (1998) *J. Bacteriology*, **180**, 6292.

Blaut, M. , Whittaker, K., Valdovinos,A., Ackrell, B.A.C., Gunsalus, R.P., Cecchini, G. (1989) *J. Biol. Chem*, **264**, 13599-13604.

Bossi, R.T., Negri, A., Tedeschi, G., Mattevi, A. (2002) *Biochemistry*, **41**, 3018-3024.

Boyer, P.D. (1993) *Biochim. Biophys. Acta*, **1140**, 215-250.

Bowman, J.P., McCammon, S.A., Nichols, D.S., Skerratt, J.H., Rea, S.M., Nichols, P.D., McMeekin, T.A. (1997) *Int. J. Syst. Bacteriol*, **47**, 1040-1047.

Cecchini, G., Thompson, C.R., Ackrell, B.A.C., Westenberg, D.J., Dean, N., Gunsalus, R.P. (1986) *PNAS*, **83**, 8898-8902.

Cecchini, G., Ackrell, B.A.C., Deshler, J.O., Gunsalus, R.P. (1986) *J. Biol. Chem*, **261**, 1808-1814.

Cecchini, G., Schröder, I., Gunsalus, R.P., Maklashina, E. (2002) *Biochim. Biophys. Acta*, **1553**, 140-157.

Cole, S.T., Condon, C., Lemire, B.D., Weiner, J.H. (1985) *Biochimica et Biophysica Acta*, **811**, 381-403.

Dichristina, T.J., DeLong, E.F. (1994) *J. Bacteriology*, **176**, 1468.

Dobbin, P. S., Butt, J. N., Powell, A.K., Reid, G.A., and Richardson, D. J. (1999) *Biochem. J*, **342**, 439-448.

Doherty, M. K. (1999) PhD Thesis, University of Edinburgh, UK.

Doherty, M. K., Pealing, S. L., Miles, C. S., Moysey, R., Taylor, P., Walkinshaw, M. D., Reid, G. A., and Chapman, S. K. (2000) *Biochemistry*, **39**, 10695-10701.

Fergusen-Miller, S., Babcock, G.T. (1996) *Chem. Rev*, **96**, 2889-2907.

Garcin, E., Venede, X., Hatchikian, E.C., Volbeda, A., Frey, M., Fontella-Camps, J.C. (1999) *Structure with Folding and Design*, **7**, 557-566.

Gibbons, C., Montgomery, M.G., Leslie, A.G.W., Walker, J.E. (2000) *Nat. Struct. Biol*, **7**, 1055-1061.

Glascoe, P.K., Long, F.A. (1960) *J. Phys. Chem*, **64**, 188-191.

Gordon, E.H.J., Pealing, S.L., Chapman, S.K., Ward, F.B., Reid, G.A. (1998) *Microbiology*, **144**, 937-945.

Gordon, E.H.J., Pike, A.D., Hill, A.E., Cuthbertson, P.M., Chapman, S.K., Reid, G.A. (2000) *Biochem. J*, **349**, 153-158.

Groß, R., Simon, J., Lancaster, C.R.D., Kröger, A. (1998) *Mol. Microbiol*, **30**, 639-646.

Heering, H.A., Weiner, J.H., Armstrong, F.A. (1997) *J.A.C.S*, **119**, 11628-11638.

Higuchi, Y., Yagi, T., Yasuoka, N. (1997) *Structure*, **5**, 1671-1680.

Hirst, J., Armstrong, F.A. (1998) *Anal.Chem*, **70**, 5062-5071.

Hohenester, E., Keller, J.W., Jansonius, J.N. (1994) *Biochemistry*, **33**, 13561-13570.

Iverson, T. M., Luna-Chavez, C., Cecchini, G., and Rees, D. C. (1999) *Science*, **284** 1960-1966.

Iverson, T. M., Luna-Chavez, C., Croal, L.R., Cecchini, G., and Rees, D. C. (2002) *J. Biol. Chem*, **277**, 16124-16130.

Iwata, S., Ostermeier, C., Ludwig, B., Michel, H. (1995) *Nature*, **376**, 660-669.

Iwata, S., Lee, J.W., Okada, K., Kyongwon Lee, J., Iwata, M., Rasmussen, B., Link, T.A., Ramaswamy, S., Jap, B.K. (1998) *Science*, **281**, 64-71.

Jones, A.K., Camba, R., Reid, G.A., Chapman, S.K., Armstrong, F.A. (2000) *J.A.C.S*, **122**, 6494-6495.

Jones, A.K. (2002) D.Phil Thesis, St. John's College, University of Oxford, UK.

Jormakka, M., Törnroth, S., Byrne, B., Iwata, S. (2002) *Science*, **295**, 1863-1868.

Käck, H., Sandmark, J., Gibson, K., Schneider, G., Lindqvist, Y. (1999) *J. Mol. Biol*, **291**, 857-876.

Kröger, A., Biel, S., Simon, J., Gross, R., Unden, G., Lancaster, C.R.D. (2002) *Biochim. Biophys. Acta*, **1553**, 23-38.

Lancaster, C.R.D., Kröger, A., Auer, M., Michel, H. (1999) *Nature*, **402**, 377-385.

Lancaster, C.R.D., Groß, R., Haas, A., Ritter, M., Mäntele, W., Simon, J., Kröger, A. (2000) *PNAS*, **97**, 13051-13056.

Lancaster, C.R.D., Groß, R., Simon, J. (2001) *Eur. J. Biochem*, **268**, 1820-1827.

Lancaster, C.R.D. (2002) *Biochim. Biophys. Acta*, **1553**, 1-6.

Lange, C., Hunte, C. (2002) *PNAS*, **99**, 2800-2805.

Léger, C., Heffron, K., Pershad, H.R., Maklashina, E., Luna-Chavez, C, Cecchini, G., Ackrell, B.A., Armstrong, F.A. (2001) *Biochemistry*, **40**, 11234-11245.

Levin, R.E. (1972) *Antonie van Leeuwenhoek*, **38**, 3962-3972.

Leys, D., Tsapin, A.S., Nealson, K.H., Meyer, T.E., Cusanovich, M.A., Van Beeuman, J.J. (1999) *Nat. Struct. Biol*, **6**, 1113-1117.

Leys, D., Meyer, T.E., Tsapin, A.S., Nealson, K.H., Cusanovich, M.A., Van Beeuman, J.J. (2002) *J. Biol. Chem*, **277**, 35703-35711.

Lorenzen, J.P., Kröger, A., Unden, G. (1993) *Arch. Microbiol*, **159**, 477-483.

Macheroux, P., *Methods in Molecular Biology,***131** in 'Flavoprotein Protocols' (Ed. Chapman, S. K., and Reid, G. A.) 1-7.

Maklashina, E., Berthold, D.A., Cecchini, G. (1998) *J. Bact.* **180**, 5989-5996.

Malashkevich, V.N., Strop, P., Keller, J.W., Jansonius, J.N., Toney, M.D. (1999) *J. Mol. Biol*, **294**, 193-200.

Matias, P.M., Soares, C.M., Saraiva, L.M., Coelho, R., Morris, J., Le Gall, J., Carrondo, M.A. (2001) *J. Biol. Chem*, **6**, 63-81.

Mattevi, A, Tedeschi, G., Bacchella, L., Coda, A., Negri, A., Ronchi, S. (1999) *Structure*, 7, 745-756.

Messias, A.C., Kastrau, D.H., LeGall, J., Turner, D. (1998) *J. Mol. Biol*, **281**, 719-739.

Morris, C.J., Gibson, D.M., Ward, F.B. (1990) *FEMS Microbiology Letters*, **69**, 259-262.

Morris, C.J., Black, A.C., Pealing, S.L., Manson, F.D.C., Chapman, S.K., Reid, G.A., Gibson, D.M., Ward, F.B. (1994) *Biochem. J*, **302**, 587-593.

Mowat, C.G., Moysey, R., Miles, C.S., Leys, D., Doherty, M.K., Taylor, P., Walkinshaw, M.D., Reid, G.A., Chapman, S. K. (2001) *Biochemistry*, **40**, 12292-12298.

Moysey, R.K. (2001) PhD Thesis, University of Edinburgh, UK.

Myers, C.R., Nealson, K.H. (1990) *J. Bacteriology*, **172**, 6232-6238.

Myers, C.R., Myers, J.M. (1997) *J. Bacteriology*, **179**, 1143-1152.

Myers, J. M., and Myers, C. R., (2000), *J. Bacteriology*, **182**, 67-75

Nicholls, D.G., Ferguson, S.J. (1992) Bioenergetics 2, (London: Academic Press).

Odagami, T., Morita, J., Takama, K., Suzuki, S. (1994) *Letters in Applied Microbiology*, **18**, 50-52.

Ohnishi, T., Moser, C.C., Page, C.C., Dutton, P.L., Yano, T. (2000) *Structure*, **8**, R23-R32.

Paddock, M.L., Graige, M.S., Feher, G., Okamura, M.Y. (1999) *PNAS*, **96**, 6183-6188.

Paddock, M.L., Ädelroth, P., Chang, C., Abresch, E.C., Feher, G., Okamura, M.Y. (2001) *Biochemistry*, **40**, 6893-6902.

Page, C.C., Moser, C.C., Chen, X., Dutton, P,L. (1999) *Nature*, **402**, 47-52.

Passanha, M., Brennan, L., Xavier, A.V., Cuthbertson, P.M., Reid, G.A., Chapman, S.K., Turner, D.L., Salgueiro. (2001) *FEBS Letters*, **489**, 8-13.

Pealing, S.L., Black, A.C., Manson, F.B.C., Ward, F.B., Chapman, S.K., Reid, G.A. (1992) *Biochemistry*, **31**, 12132-12140.

Pealing, S.L., Cheesman, M.R., Reid, G.A., Thomson, A.J., Ward, F.B., Chapman, S.K. (1995*) Biochemistry*, **34**, 6153-6158.

Picarra-Pereira, M.A., Turner, D.L., LeGall, J., Xavier, A.V. (1993) *Biochem. J*, **294**, 909-915.

Pickard, C., Foght, J.M., Pickard, M.A., Westlake, D.W.S. (1993) *Can. J. Microbiol*, **39**, 715-717.

Reid, G.A., Gordon, E.H.J., Hill, A.E., Doherty, M.K., Turner, K.L., Holt, R., Chapman, S.K. (1998) *Biochem. Soc. Trans*, **26**, 418-421.

Reid, G.A. & Gordon, E.H.J. (1999) *Int. J. Syst. Bacteriol*, **49**, 189-191.

Rhee, S., Parris, K.D., Ahmed, S.A., Miles, E.W., Davies, D.R. (1996) *Biochemistry*, **35**, 4211-4221.

Rothery, R.A., Weiner, J.H (1998) *Eur. J. Biochem*, **254**, 588-595.

Rousset, M., Motet, Y., Guiliarelli, B., Forget, N., Asso, M., Bertrand, P., Fontecilla-Camps, J.C., Hatchikian, E.C. (1998) *PNAS*, **95**, 11625-11630.

Rynkiewicz, M.J., Seaton, B.A. (1996) *Biochemistry*, **35**, 16174-16179.

Saffarini, D.A., Nealson, K.H. (1993) *J. Bacteriology*, **175**, 7938-7944.

Saffarini, D.A., DiChristina, T.J., Bermudes, D., Nealson, K.H. (1994) *FEMS Microbiology Letters*, **119**, 271-278.

Sawers, G. (1994) *Antonie Van Leeuwenhoek*, **66**, 57-88.

Schäfer, G., Anemüller, S., Moll, R. (2002) *Biochim. Biophys. Acta*, **1553**, 57-73.

Schöwen, K. B., and Showen, R. L., (1982), *Methods in Enzymology*, **87**, 651-606

Schöwen, R. L., (1981) in 'Isotope Effects on Enzyme-catalysed Reactions' P. 64 University Park Press, Baltimore, Maryland.

Schröder, I., Gunsalus, R.P., Ackrell, B.A.C., Cecchini, G. (1991) *J. Biol. Chem*, **266**, 13572-13579.

Schwalb, C.; Chapman, S. K.; Reid, G. A. (2002) *Biochem. Soc. Trans*, **30**, 658-662.

Scrutton, N.S. (1999) *Methods in Molecular Biology*, **131**: Flavoprotein protocols (Ed: Chapman, S.K. and Reid, G.A.) 181-193.

Senior, A.E., Nadanaciva, S., Weber, J. (2002) *Biochim. Biophys. Acta*, **1553**, 188-211.

Shimizu, H., Park, S-Y., Lee, D-S., Shoun, H., Shiro, Y. (2000) *J. Inorg. Biochem*, **81**, 191-205.

Simon, J., Gross, R., Ringel, M., Schimdt, E., and Kröger, A., (1998) *Eur. J. Biochem.*, **251**, 418-426.

Simon, J., Gross, R., Einsle, O., Kroneck, P.M.H., Kröger, A., Klimmek, O. (2000) *Mol. Microbiol*, **35**, 686-696.

Stock, D., Leslie, A.G.W., Walker, J.E. (1999) *Science*, **286**, 1700-1705.

Sucheta, A., Cammack, R., Weiner, J., and Armstrong, F. A. (1993) *Biochemistry*, **32**, 5455-5465.

Suzuki, T., Ueno, H., Mitome, N., Suzuki, J., Yoshida, M. (2002) *J. Biol. Chem*, **277**, 13281-13285.

Taylor, P., Pealing, S. L., Reid, G. A., Chapman, S. K., and Walkinshaw, M. D. (1999) *Nature Structural Biology*, **6**, 12, 1108-1112.

Tedeschi, G., Ronchi, S., Simonic, T., Treu, C., Mattevi, A., Negri, A. (2001) *Biochemistry*, **40**, 4738-4744.

Thorneley, R.N.F. (1974) *Biochim. Biophys. Acta*, **333**, 487-496.

Toney, M. D., and Kirsch, J. F. (1993), *Biochemistry*, **32**, 1471-1479.

Toney, M.D., Hohenester, E., Cowan, S.W., Jansonius, J.N. (1993) *Science*, **261**, 756-759.

Toney, M.D., Hohenester, E., Keller, J.W., Jansonius, J.N. (1995) *J. Mol. Biol*, **245**, 151-179.

Tornroth, S., Yankovskaya, V., Cecchini, G., Iwata, S. (2002) *Biochimica et Biophysica Acta* **1553**, 171-176.

Trumpower, B.L. (1990) *Microbiological Reviews*, **54**, 101-129.

Tsapin, A.I., Burbaev, D.S., Nealson, K.H., Keppen, O.I. (1995) *Applied Magnetic Resonance*, **9**, 509-516.

Tsukihara, T., Aoyama, H., Yamashita, E., Tomizaki, T., Yamaguchi, H., Shinzawa-Itoh, K., Nakashima, R., Yaono, R., Yoshikawa, S. (1996) *Science*, **272**, 1136-1144.

Turner, K. L., Doherty, M. K., Heering, H. A., Armstrong, F. A., Reid, G. A., and Chapman, S. K. (1999) *Biochemistry*, **38**, 3302-3309,

Turner, D.L., Salgueiro, C.A., Catarino, T., LeGall, J., Xavier, A.V. (1996) *Eur. J. Biochem*, **241**, 723-731.

van Hellemond, J.J., Tielens, A.G.M. (1994) *Biochemical Journal*, **304**, 321-331.

Venkataswaran, K., Dollhopf, M.E., Aller, R., Stackebrandt, E., Nealson, K.H. (1998) *Int. J. Syst. Bacteriol*, **48**, 965-972.

Volbeda, A., Garcin, E., Piras, C., de Lacey, A.L., Fernandez, V.M., Hatchikian, E.C., Frey, M., Fontecilla-Camps, J.C. (1996) *J.A.C.S*, **118**, 12989-12996.

Weiss, H., Friedrich, T., Hofhaus, G., Preis, D. (1990) *Eur. J. Biochem*, **90**, 563-576.

Werth, M. T., Cecchini, G., Manodori, A., Ackrell, B. A. C., Schroder, I., Gunsalus, R. P., and Johnson, M. K., (1990) *PNAS*, **87**, 8965-8969.

Westenberg, D.J., Gunsalus, R. P., Ackrell, B. A. C., Sices, H., Cecchini, G. (1990) *J. Biol. Chem*, **265**, 815-822.

Zhang, Z., Huang, L., Shulmeister, V.M., Chi, Y-I., Kim, K.K., Hung, L-W., Crofts, A.R., Berry, E.A., Kim, S-H. (1998) *Nature*, **392**, 677-684.

7.2 Abbreviations

Abs	Absorbance
ADP	Adenosine diphosphate
ATP	Adenosine triphosphate
D_2O	deuterated water
DMSO	Dimethyl Sulphoxide
DNP	2-[1-(p-chlorophenyl)ethyl] 4, 6-dinitrophenol
E. coli	*Eschericia coli*
EDTA	Ethylene diamine tetraacetic acid
FAD	Flavin Adenine Dinucleotide
Fdh	Formate dehydrogenase
FMN	Flavin Mononucleotide
FPLC	Fast protein liquid chromatography
Frd	Fumarate reductase
HQNO	2-heptyl 4-hydroxy quinoline N-oxide
Hyd	Hydrogenase
I	Ionic strength
IPTG	Isopropyl-β-thiogalactoside
ISP	Iron sulfur protein
Laspo	L-aspartate oxidase
LB	Luria broth
MK	Menaquinone
NAD^+/NADH	Nicotinamide adenine dinucleotide
NMR	Nuclear magnetic resonance
ox	Oxidised
PAGE	Polyacrylamide gel electrophoresis
P^i	Inorganic phoshate
PFV	Protein film voltammetry
QFR	Quinol:Fumarate Reductase
red	Reduced
Sdh	Succinate Dehydrogenase
SDS	Sodium dodecyl sulfate
SQR	Succinate:Quinone Oxidoreductase
Tris	Tris(hydroxymethyl) aminomethane
UQ	Ubiquinone
UV	Ultra-violet

7.2.1 Amino Acids

Alanine	Ala	A
Arginine	Arg	R
Asparagine	Asn	N
Aspartic acid	Asp	D
Cysteine	Cys	C
Glutamic acid	Glu	E
Glutamine	Gln	Q
Glycine	Gly	G
Histidine	His	H
Isoleucine	Ile	I
Leucine	Leu	L
Lysine	Lys	K
Methionine	Met	M
Phenylalanine	Phe	F
Proline	Pro	P
Serine	Ser	S
Threonine	Thr	T
Tryptophan	Trp	W
Tyrosine	Tyr	Y
Valine	Val	V

7.2.2 Kinetic parameters

k_{cat}	Rate constant under saturating conditions
k_{obs}	Observed rate
K_M	Michaelis constant
K_D	Binding constant

7.2.3 Standard units

m	metre	°C	degrees Celsius
g	gram	M	molar
s	second	Da	Dalton units
l	litre	Å	Angstrom

7.3 Derivation of the Michaelis-Menten Equation

$$E + S \underset{k_{-1}}{\overset{k_1}{\rightleftharpoons}} ES \xrightarrow{k_{cat}} E + P \qquad (7.3.1)$$

Where E = enzyme, S = substrate, ES = enzyme-substrate complex (Michaelis complex) and P = product.

For the enzyme catalysed reaction above, the catalytic rate, $V = k_{cat} [ES]$ (7.3.2)

At steady state it is assumed that the concentration of the intermediate remains constant while the concentrations of substrate and product are changing. So the rate of formation of ES is the same as the rate of dissociation of ES (either back to E + S or on to E + P).

$$k_1 [E][S] = k_{cat} [ES] + k_{-1} [ES]$$

$$\Rightarrow \qquad [ES] = \frac{k_1[E][S]}{k_{cat} + k_{-1}} \qquad (7.3.3)$$

The Michaelis constant, K_M:

$$K_M = \frac{k_{-1} + k_{cat}}{k_1}$$

Compared with the dissociation constant, K_D:

$$K_D = \frac{k_{-1}}{k_1}$$

So, substituting into expression 7.3.3:

$$[ES] = \frac{[E]\,[S]}{K_M} \qquad (7.3.4)$$

The substrate is in excess over enzyme so [S], the concentration of free substrate is assumed to be the same as the total concentration of substrate. Only a small amount of enzyme is added, however so:

$$[E] = [E]_0 - [ES] \qquad (7.3.5)$$

Where [E] is the concentration of free enzyme and $[E]_0$ is the total concentration of enzyme.

Substituting into expression 7.3.4:

$$[ES] = \frac{([E]_0 - [ES])\,[S]}{K_M} \qquad (7.3.6)$$

And rearranging:

$$[ES] = \frac{[E]_0[S]}{K_M = [S]} \qquad (7.3.7)$$

Finally, substituting into expression 7.3.2 gives the Michaelis-Menten equation:

$$\boxed{V = \frac{k_{cat}\,[E]_0[S]}{K_M + [S]}} \qquad (7.3.8)$$

7.4 Solvent Isotope Effects

Isotope effects arise from differences in the free energies of the ground and transition states in D_2O compared to H_2O. The different masses of D and H give rise to different specific bond vibrational energy levels. For example, the ground state for C-D is ~ 4.8 kJmol^{-1} lower in energy than that of C-H. So more energy is required to break a bond involving D than H. A primary isotope effect is the result of a D bond being broken during the rate determining step of a reaction.

In a mixed isotopic solution any exchangeable hydrogenic sites will contain a mixture of D and H at equilibrium. The ratio of occupation at a hydrogenic site 'i' is called the isotopic fractionation factor, φ_i:

$$\varphi_i = \frac{[D]_i \, / \, [H]_i}{[n \, / \, (1-n)]}$$

Where n is the atom fraction of deuteration in mixed isotope solvent.

$\varphi = 1$ only if the strength of binding is the same as an average site in the bulk solvent.

$\varphi < 1$ when binding is weaker than an average solvent site. Protium will accumulate at these sites.

$\varphi > 1$ when binding is stronger than an average solvent site. Deuterium will accumulate at these sites.

Some typical fractionation factors (Schöwen and Schöwen, 1982):

Group	φ
OL	1.0
NL	0.92
N^+L	0.97
COOL	1.23-1.28
SL	0.40-0.46

Where L = H or D.

$$LOD + RH \xrightarrow{k_H} [LOD + TH] \longrightarrow$$
$$\varphi^R \updownarrow \qquad\qquad \updownarrow \varphi^T$$
$$LOH + RD \xrightarrow{k_D} [LOH + TD] \longrightarrow$$
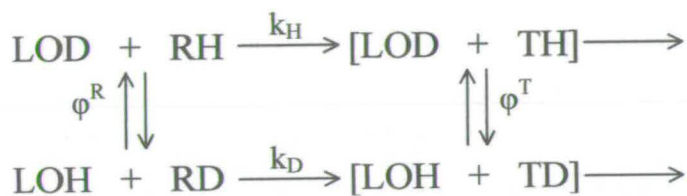
The scheme above applies to a reactant with one exchangeable hydrogenic site (RH), in mixed isotopic solvent. TH is the activated complex which also has one exchangeable site.

k_H is the rate of formation of TH

k_D is the rate of formation of TD

φ^R is the equilibrium constant of exchange in the reactant state.

φ^T is the equilibrium constant of exchange in the transition state.

Since the cycle is closed thermodinamically:

$$k_H \varphi^T = k_D \varphi^R$$

Rearranging this expression gives the solvent isotope effect in terms of fractionation factors:

$$\frac{k_H}{k_D} = \frac{(\varphi^T)^{-1}}{(\varphi^R)^{-1}}$$

For more than one exchangeable site:

$$\frac{k_H}{k_D} = \frac{\prod_i^v \varphi_i^T}{\prod_j^v \varphi_j^R}$$

7.4.1 Proton Inventories

The rates in mixtures of H_2O and D_2O can sometimes allow the breakdown of the overall isotope effect into its component φ^R and φ^T contributions. The rate constant in mixed isotopic solvent is k_n which is given by k_0 (the rate in pure H_2O) corrected for each contributing hydrogenic site:

$$\frac{k_D}{k_H} = \frac{\prod_i^v (1 - n + n\,\varphi_i^T)}{\prod_j^v (1 - n + n\,\varphi_j^R)}$$

The numerator is the sum of the transition state contributions and the denominator is the sum of the reactant state contributions. So if the isotope effect arises from a single hydrogenic site in the transition state (for example, the abstraction of a proton from a hydroxyl group in the rate determining step):

$$k_n = k_0 \prod_i^v (1 - n + n\,\varphi_i^T)$$

The proton inventory will be linear as shown by the dark blue line in Figure 7.1. Increasing the number of sites in the transition state increases the curvature, as shown by the increasingly pale blue lines in Figure 7.1.

For a single exchangeable site in the reactant state:

$$k_n = k_0 \left[1 \left/ \prod_j^v (1 - n + n\, \varphi_i^{T}) \right. \right]$$

This is the deepest bowl-shaped curve, the dark red line in Figure 7.1. Increasing the number of reactant state sites decreases the curvature (red to yellow lines in Figure 7.1).

Both transition state and reactant state models eventually converge on the black line in Figure 7.1, for multiple sites in both reactant and transition states. It is not possible to attribute sites to a particular state, so the equation for this line is:

$$k_n = k_0 \, (k_D/k_H)^n$$
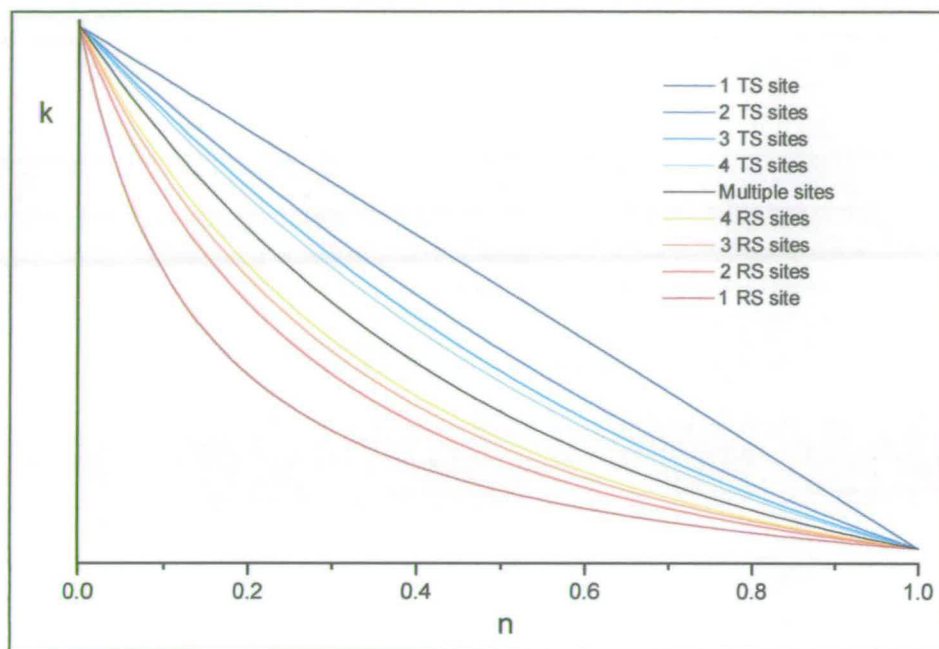
Figure 7.1: Example curves generated for proton inventories. A straight line is obtained if a single exchangeable hydrogenic site in the transition state is responsible for the solvent isotope effect. The deepest curve is obtained when a single site in the reactant state is responsible for the effect.

7.5 Conferences and Courses Attended

- 14th International Symposium on Flavins and Flavoproteins, Cambridge, 14th-18th July 2002. (poster presented)

- 10th International Conference on Bioinorganic Chemistry, Florence, 26th-31st August 2001. (poster presented)

- 34th International Conference on Coordination Chemistry, Edinburgh, 9th-14th July 2000. (poster presented)

- 4th Firbush Redox Enzymes Meeting, University of Edinburgh, 7-9th June 2000.

- 5th Firbush Redox Enzymes Meeting, University of Edinburgh, 6-8th June 2001. (speaker)

- 6th Firbush Redox Enzymes Meeting, University of Edinburgh, 5-7th June 2002.

- Inorganic Chemistry Group Meeting, University of Edinburgh, Firbush field centre, 25th-27th April 2001. (poster presented)

- Inorganic Chemistry Group Meeting, University of Edinburgh, Firbush field centre, 25th-27th April 2002. (speaker)

- Department of Chemistry Colloquia.

- Inorganic Chemistry Group Seminars.

7.6 Publications

Pankhurst, K.L., Mowat, C.G., Miles, C.S., Leys, D., Walkinshaw, M.D., Reid, G.A., Chapman, S.K. (2002) "The role of His505 in the soluble fumarate reductase from *Shewanella frigidimarina*," *Biochemistry,* **41**, 8551-8556.

Mowat, C.G., Pankhurst, K.L., Miles, C.S., Leys, D., Walkinshaw, M.D., Reid, G.A., Chapman, S.K. (2002) "Engineering water to act as an active-site acid catalyst in a soluble fumarate reductase." *Biochemistry,* **41**, 11990-11996.

Katherine L. Pankhurst, Christopher G. Mowat, Caroline S. Miles, Emma L. Rothery, Mary K. Doherty, Graeme A.Reid and Stephen K. Chapman. (2002) "Investigating the Proton Pathway in Flavocytochrome *c₃* from *Shewanella frigidimarina* by Site Directed Mutagenesis." *Flavins and Flavoproteins,* 779-784.

C.G. Mowat, K.L. Pankhurst, C.S. Miles, D. Leys, G.A. Reid, M.D. Walkinshaw and S.K. Chapman. (2002) "A Universal Mechanism for the Fumarate Reductase and Succinate Dehydrogenase Family." *Flavins and Flavoproteins,* 739-747.

Reid, G. A., Miles, C. S., Moysey, R., Pankhurst, K. L., and Chapman, S. K., (2000) "Catalysis in fumarate reductase". *Biochimica et Biophysica Acta*, **1459**, 310-315.

Role of His505 in the Soluble Fumarate Reductase from *Shewanella frigidimarina*[†]

Katherine L. Pankhurst,[‡] Christopher G. Mowat,[‡,§] Caroline S. Miles,[§] David Leys,[#] Malcolm D. Walkinshaw,[§] Graeme A. Reid,[§] and Stephen K. Chapman*[‡]

Department of Chemistry, University of Edinburgh, West Mains Road, Edinburgh EH9 3JJ, United Kingdom, Institute of Cell and Molecular Biology, University of Edinburgh, Mayfield Road, Edinburgh EH9 3JR, United Kingdom, and Department of Biochemistry, Adrian Building, University of Leicester, University Road, Leicester LE1 7RH, United Kingdom

Received February 21, 2002; Revised Manuscript Received April 4, 2002

ABSTRACT: The X-ray structure of the soluble fumarate reductase from *Shewanella frigidimarina* [Taylor, P., Pealing, S. L., Reid, G. A., Chapman, S. K., and Walkinshaw, M. D. (1999) *Nat. Struct. Biol. 6*, 1108−1112] clearly shows the presence of an internally bound sodium ion. This sodium ion is coordinated by one solvent water molecule (Wat912) and five backbone carbonyl oxygens from Thr506, Met507, Gly508, Glu534, and Thr536 in what is best described as octahedral geometry (despite the rather long distance from the sodium ion to the backbone oxygen of Met507 (3.1 Å)). The water ligand (Wat912) is, in turn, hydrogen bonded to the imidazole ring of His505. This histidine residue is adjacent to His504, a key active-site residue thought to be responsible for the observed pK_a of the enzyme. Thus, it is possible that His505 may be important in both maintaining the sodium site and in influencing the active site. Here we describe the crystallographic and kinetic characterization of the H505A and H505Y mutant forms of the *Shewanella* fumarate reductase. The crystal structures of both mutant forms of the enzyme have been solved to 1.8 and 2.0 Å resolution, respectively. Both show the presence of the sodium ion in the equivalent position to that found in the wild-type enzyme. The structure of the H505A mutant shows the presence of two water molecules in place of the His505 side-chain which form part of a hydrogen-bonding network with Wat48, a ligand to the sodium ion. The structure of the H505Y mutant shows the hydroxyl group of the tyrosine side-chain hydrogen-bonding to a water molecule which is also a ligand to the sodium ion. Apart from these features, there are no significant structural alterations as a result of either substitution. Both the mutant enzymes are catalytically active but show markedly different pH profiles compared to the wild-type enzyme. At high pH (above 8.5), the wild type and mutant enzymes have very similar activities. However, at low pH (6.0), the H505A mutant enzyme is some 20-fold less active than wild-type. The combined crystallographic and kinetic results suggest that His505 is not essential for sodium binding but does affect catalytic activity perhaps by influencing the pK_a of the adjacent His504.

In the absence of oxygen, many bacteria are able to use fumarate as a terminal electron acceptor for respiration. In the majority of organisms, these fumarate reductases (which are closely related to succinate dehydrogenase) are bound to the inner face of the cytoplasmic membrane and contain both iron−sulfur centers and FAD[1] (*1, 2*). However, in

* To whom correspondence should be addressed. Prof. S. K. Chapman, Department of Chemistry, University of Edinburgh, West Mains Road, Edinburgh EH9 3JJ, U.K. E-mail: S.K.Chapman@ed.ac.uk. Fax/phone (44) 131 650 4760.
[‡] Department of Chemistry, University of Edinburgh.
[§] Institute of Cell and Molecular Biology, University of Edinburgh.
[#] University of Leicester.
[1] Abbreviations: Fcc₃, flavocytochrome c_3; H505A, histidine505 → alanine mutation; H505Y, histidine505 → tyrosine mutation; FAD, flavin adenine dinucleotide

Shewanella species a soluble, periplasmic fumarate reductase is produced. The presence of four *c*-type heme groups and one FAD has led to this enzyme being designated as flavocytochrome c_3 (Fcc₃) (*3*). Examination of the crystal structures of the fumarate reductases from *Escherichia coli* (PDB entry 1FUM (*1*)), *Wolinella succinogenes* (1QLA, 1QLB (*4*), 1E7P (*5*)) and *Shewanella* species (1QJD (*6*), 1D4E (*7*), 1QO8 (*8*)) shows a clear conservation of the active site architecture. This is consistent with a universal mechanism for fumarate reduction in all the enzymes (*6, 9−11*).

The highest resolution (1.8 Å) fumarate reductase structure is that for Fcc₃ from *Shewanella frigidimarina* (1QJD) (*6*). Close examination of this structure reveals the presence of an internally bound sodium ion (*6, 12*). This sodium ion is tightly held and is clearly seen in electrospray mass spectrometry of wild-type and mutant forms of Fcc₃ (*9, 11*). In the Fcc₃ structure (1QJD), the sodium ion is coordinated by five backbone carbonyl oxygen atoms (from T506, M507, G508, E534, and T536) and one solvent water molecule (Wat912) (Figure 1) in a geometry close to octahedral. These observations, together with the fact that the sodium ion lies close to both the FAD and the active site, led to the

FIGURE 1: Panel (a) shows the region surrounding the internal bound sodium ion in flavocytochrome c_3. The sodium is shown in orange. Interactions with ligating oxygen atoms are shown as dotted lines, as are some hydrogen-bonding interactions. All sodium to ligand distances are 2.4 Å, except for that involving Met507, which is 3.1 Å. Panels (b) and (c) show the electron density surrounding the region of the internal bound sodium ion in the crystal structures of the H505A and H505Y mutant forms of flavocytochrome c_3, respectively. The sodium ion is shown in orange. Interactions between the sodium and the ligating oxygen atoms are shown as orange dotted lines. Electron density maps were calculated using Fourier coefficients $2F_o - F_c$. Where F_o and F_c are the observed and calculated structure factors, respectively, the latter based on the final model. The contour level is 1σ, where σ is the rms electron density. The figure was generated using TURBO–FRODO (21).

suggestion that it might play an important structural or regulatory role in the enzyme (12). An interesting feature of the sodium ion site is that the water ligand (Wat912) is

hydrogen-bonded to His505, which is, in turn, next to a key substrate-binding residue, His504. In the present paper, we report an investigation into the importance of His505 in terms

of maintaining the integrity of the sodium site and affecting catalysis. We describe the kinetic characterization of the H505A and H505Y mutant enzymes together with their high-resolution X-ray crystal structures.

MATERIALS AND METHODS

DNA Manipulation, Strains, Media, and Growth. The mutant enzymes H505A-Fcc₃ and H505Y-Fcc₃ were generated by site-directed mutagenesis using the method of Kunkel and Roberts (*13*) as described previously (*3, 9*).

Mutagenic oligonucleotides CCTGGTGTTCACGCTAC-TATGGGTGGC (which substitutes histidine 505 with alanine) and GGTGTTCACTACACTATGGG (which substitutes histidine 505 with tyrosine) were used. Mismatched bases are underlined. Screening for the H505A and H505Y mutations was carried out by sequencing of single stranded DNA. Dideoxy chain termination sequencing (*14*) using the Sequenase version 2.0 kit (United States Biochemicals) was carried out for the former and automated sequencing on a Perkin-Elmer ABI Prism 377 instrument for the latter. Both mutated *fccA* coding sequences were fully sequenced from single stranded DNA to check that no secondary mutations had been introduced.

The modified coding sequences were cloned into the broad-host range expression plasmid pMMB503EH (*15*) on an ~1.8 kbp *Eco*RI−*Hind*III fragment to generate pCM89 (H505A *fccA*/pMMB503EH) and pCM93 (H505Y *fccA*/pMMB503EH). Expression in the Δ*fccA S. frigidimarina* strain EG301 (*3*) was carried out as described previously (*9*).

Protein Purification and Kinetic Analysis. Wild-type and mutant forms of Fcc₃ were purified as previously reported (*16*). Protein samples for crystallization and mass spectrometry were subjected to an additional purification step using FPLC with a 1-mL Resource Q column (Pharmacia) as described by Pealing et al. (*17*). Protein concentrations were determined using the Soret band absorption coefficient for the reduced enzyme (752.8 mM^{-1} cm^{-1} at 419 nm) (*16*).

The FAD content of Fcc₃ mutants was determined using the method of Macheroux (*18*), and all steady-state rate constants were corrected for the percentage of FAD present.

Mass spectrometry of proteins was carried out using a Micromass Platform II Electrospray mass spectrometer. Samples were prepared in 0.1% formic acid and introduced to the spectrometer via direct infusion. The spectrometer was standardized using horse heart myoglobin.

The steady-state kinetics of fumarate reduction were followed at 25.0 °C as described by Turner et al. (*19*). The fumarate-dependent reoxidation of reduced methyl viologen was monitored at 600 nm using a Shimadzu UV−PC 1501 spectrophotometer. To ensure anaerobicity, the spectrophotometer was housed in a Belle Technology glovebox under a nitrogen atmosphere with the O₂ level maintained well below 2 ppm. Assay buffers contained 0.45 M NaCl and 0.2 mM methyl viologen and were adjusted to the appropriate pH values using 0.05 M HCl or NaOH as follows: Tris/HCl (pH 7.0−9.0); MES/NaOH (pH 5.4−6.8); and CHES/NaOH (pH 8.6−10). The viologen was reduced by addition of sodium dithionite until a reading of around 1 absorbance unit was obtained (corresponding to around 80 μM reduced methyl viologen). The concentration of reduced methyl viologen could be varied between 100 and 20 μM with no effect on the rate of reaction. A known concentration of enzyme was added, and the reaction was initiated by addition of fumarate (0−1 mM).

Kinetic parameters K_m and k_{cat} were determined from the steady-state results using nonlinear regression analysis (Microcal Origin software). Profiles of pH versus maximum rate-constant were constructed by activity measurement under saturating substrate conditions at a range of pH values.

Crystallization and Refinement. Crystallization of H505A and H505Y flavocytochromes c_3 was carried out by hanging drop vapor diffusion at 4 °C in Linbro plates. Crystals were obtained with well solutions comprising 100 mM Tris-HCl buffer (pH 7.4−8.2) (measured at 25 °C), 80 mM NaCl, 16−19% PEG 8000, and 10 mM fumarate. Hanging drops of 4 μL were prepared by adding 2 μL of 6 mg/mL protein (in 10 mM TrisHCl, pH 8.5) to 2 μL of well solution. After approximately 10 days, needles of up to 1 × 0.2 × 0.2 mm and plates of up to 0.5 × 0.5 × 0.2 mm were formed. Crystals were immersed in a solution of 100 mM sodium acetate buffer, pH 6.5, 20% PEG 8000, 10 mM fumarate, and 80 mM NaCl, containing 23% glycerol as cryoprotectant, prior to mounting in nylon loops and flash-cooling in liquid nitrogen. For H505A flavocytochrome c_3, a data set was collected to 1.8 Å resolution at Daresbury synchrotron radiation source (Station 9.6, $\lambda = 0.979$ Å) using an ADSC Quantum 4 detector, and for H505Y flavocytochrome c_3, a data set was collected to 2.0 Å resolution at DESY in Hamburg (Station BW7B, $\lambda = 0.8459$ Å) using a Mar Research mar345 image plate detector. Crystals of both mutant forms were found to belong to space group $P2_1$. The H505A flavocytochrome c_3 crystal was found to have cell dimensions $a = 45.632$ Å, $b = 92.798$ Å, $c = 79.056$ Å, and $\beta = 91.02°$, while the H505Y flavocytochrome c_3 crystal was found to have cell dimensions $a = 76.989$ Å, $b = 87.274$ Å, $c = 89.366$ Å, and $\beta = 104.43°$.

Data processing was carried out using the HKL package (*20*). The wild-type Fcc₃ structure (1QJD), stripped of water, was used as the initial model for molecular replacement. Electron density fitting was carried out using the program Turbofrodo (*21*). Restraints for the FAD were calculated from two small molecule crystal structures (Cambridge Crystallographic Database codes HAMADPH and VEFHUJ10). Structure refinement was carried out using Refmac (*22*).

The atomic coordinates have been deposited in the Protein Data Bank [entries 1KSS (H505A) and 1KSU (H505Y)].

RESULTS

Characterization of Mutant Enzymes. The molecular masses of the mutant enzymes were determined by electrospray mass spectroscopy. In comparison to wild-type (63 033 Da, which includes the bound sodium ion), the mass difference was found to be −67 Da for H505A (expected difference of −66 Da) and +24 Da for H505Y (expected difference of +26 Da). These mass differences indicate that the sodium remains bound in both mutant enzymes. All the mutations were further verified by DNA sequencing. The average FAD content of the mutant enzymes was found to be 60%, H505A and 56%, H505Y. This is slightly lower than typical values for the recombinant wild-type enzyme of around 73%. All catalytic rates were corrected for the variation in FAD content.

Table 1: Comparison of k_{cat} and K_m Values for Wild-Type, H505A, and H505Y Forms of Fcc₃ (25 °C, I = 0.45 M)

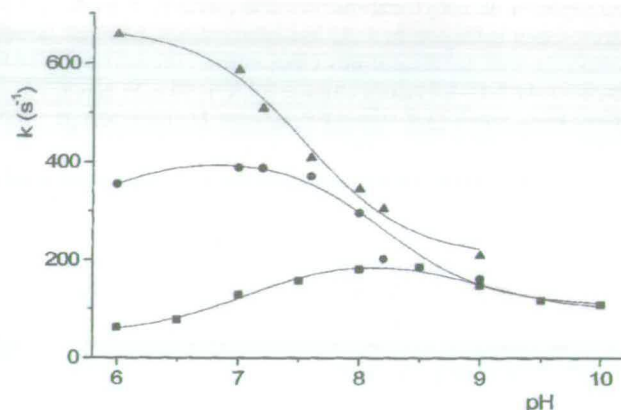|	k_{cat} (s^{-1})			K_m (μM)		
pH	wild-type[a]	H505A	H505Y	wild-type[a]	H505A	H505Y
6.0	658 ± 34	32 ± 1	354 ± 19	43 ± 10	43 ± 6	22 ± 5
7.2	509 ± 15	79 ± 3	377 ± 29	25 ± 2	109 ± 13	25 ± 7
7.5	370 ± 10	101 ± 3	363 ± 29	28 ± 3	129 ± 10	17 ± 6
9.0	210 ± 13	105 ± 2	240 ± 5	7 ± 2	9 ± 1	21 ± 2

[a] Values for wild-type taken from ref 9.

FIGURE 2: pH dependence of fumarate reductase activity (under saturating substrate conditions at 25 °C, I = 0.45 M: wild-type Fcc₃ (triangles); H505A Fcc₃ (squares); H505Y Fcc₃ (circles).

Table 2: Data Collection and Refinement Statistics

	H505A	H505Y
resolution (Å)	20.0−1.8	20.0−2.0
total no. of reflections	318233	536347
no. of unique reflections	58239	77608
completeness (%)	95.4	99.2
$(I)/[\sigma(I)]$	18.5	11.3
R_{merge} (%)[a]	7.5	7.2
R_{merge} in outer shell (%)	18.5 (1.86−1.80 Å)	22.3 (2.07−2.00 Å)
R_{cryst} (%)[b]	15.64	16.70
R_{free} (%)[b]	20.61	23.86
rmsd from ideal values		
bond lengths (Å)	0.011	0.012
bond angles (deg)	2.2	2.4
Ramachandran analysis		
most favored (%)	87.9	89.0
additionally allowed (%)	12.1	10.8

[a] $R_{merge} = \sum_h \sum_i |I(h) - I_i(h)|/\sum_h \sum_i I_i(h)$, where $I_i(h)$ and $I(h)$ are the ith and mean measurement of reflection h, respectively. [b] $R_{cryst} = \sum_h |F_o - F_c|/\sum_h F_o$, where F_o and F_c are the observed and calculated structure factor amplitudes of reflection h, respectively. R_{free} is the test reflection data set, 5% selected randomly for cross validation during crystallographic refinement.

The ability of H505-substituted forms of Fcc₃ to catalyze fumarate reduction was determined over a range of pH values. The resulting k_{cat} and K_m parameters for wild-type and mutant forms of Fcc₃ are compared in Table 1. The pH profiles shown in Figure 2 show that the mutations have little effect on activity at high pH. However, as the pH is lowered, there is an increasing effect on activity. In fact, at pH 6.0 the k_{cat} value for the wild-type enzyme is some 20-fold higher than that for the H505A mutant. The wild-type enzyme exhibits a straightforward pH profile with a single pK_a of 7.5 ± 0.1 and with optimum activity below pH 6.0. In contrast, the two mutant enzymes show more bell-shaped pH profiles with two pK_a values of 7.1 ± 0.2 and 9.0 ± 0.2 determinable for H505A and one pK_a of 8.2 ± 0.1 for H505Y.

The Crystal Structures of the Mutant Flavocytochromes c_3. Data sets to a resolution of 1.8 Å (H505A) and 2.0 Å (H505Y) were used to refine the structures to final R factors of 15.64% (H505A, R_{free} = 20.61%) and 16.70% (H505Y, R_{free} = 23.86%) (Table 2). For the H505A mutant enzyme, the final model consists of one protein molecule comprised of residues 1−568, four hemes, the FAD, one substrate molecule (fumarate), and one sodium ion. In addition, the H505A model contains 1096 water molecules. In the case of the H505Y mutant enzyme, there are two molecules in the asymmetric unit so the final model consists of two protein molecules (with composition as described above) and a total of 1866 water molecules. For each protein molecule, three residues at the C-terminus (569−571) could not be located in the electron density maps. The rmsd fit of all backbone atoms for the wild-type and H505A mutant flavocytochromes c_3 is 0.3 Å, and for the wild-type and H505Y mutant enzyme the fit is also 0.3 Å, indicating no major differences between the structures. Because the H505Y crystal structure has two

molecules in the asymmetric unit, the rmsd fit value stated is the average over both molecules (A and B).

The crystal structures of the H505A and H505Y mutant enzymes do not show any unexpected structural changes compared to the wild-type structure (Figure 1). In the wild-type structure, His505 is seen to form a hydrogen bond with a water molecule (Wat912) at a distance of 2.9 Å, which in turn is part of the coordination sphere of the bound sodium ion, some 2.4 Å from the sodium. In the H505A mutant enzyme, the space vacated by the removal of the imidazole moiety is occupied by two water molecules, Wat2 and Wat147, which are 3.4 and 3.9 Å from the Ala505 side chain carbon, respectively (Figure 1). One of these water molecules, Wat2, is 3.1 Å from Wat48, which is in the equivalent position to that taken by Wat912 in the wild-type structure. Wat48 also ligates to the bound sodium ion at a distance of 2.5 Å. In the structure of the H505Y mutant Fcc₃, the tyrosine side-chain occupies the same position as that taken by the His505 side-chain in the wild-type structure (Figure 3). The hydroxyl group of the tyrosine is hydrogen-bonded to a water molecule (Wat41 in molecule A, Wat18 in molecule B) at 2.6 Å. These water molecules are shown to coordinate to the sodium ion at a distance of 2.5 Å. In all structures mentioned, the sodium ion is found in the same position.

The replacement of the histidine at position 505 has little structural effect at the active site even though it is adjacent to His504, a residue thought to be involved in both Michaelis complex formation and transition state stabilization. The bound fumarate assumes the same twisted conformation as observed for the hydroxylated, malate-like, molecule in the wild-type active site, and the important interactions required
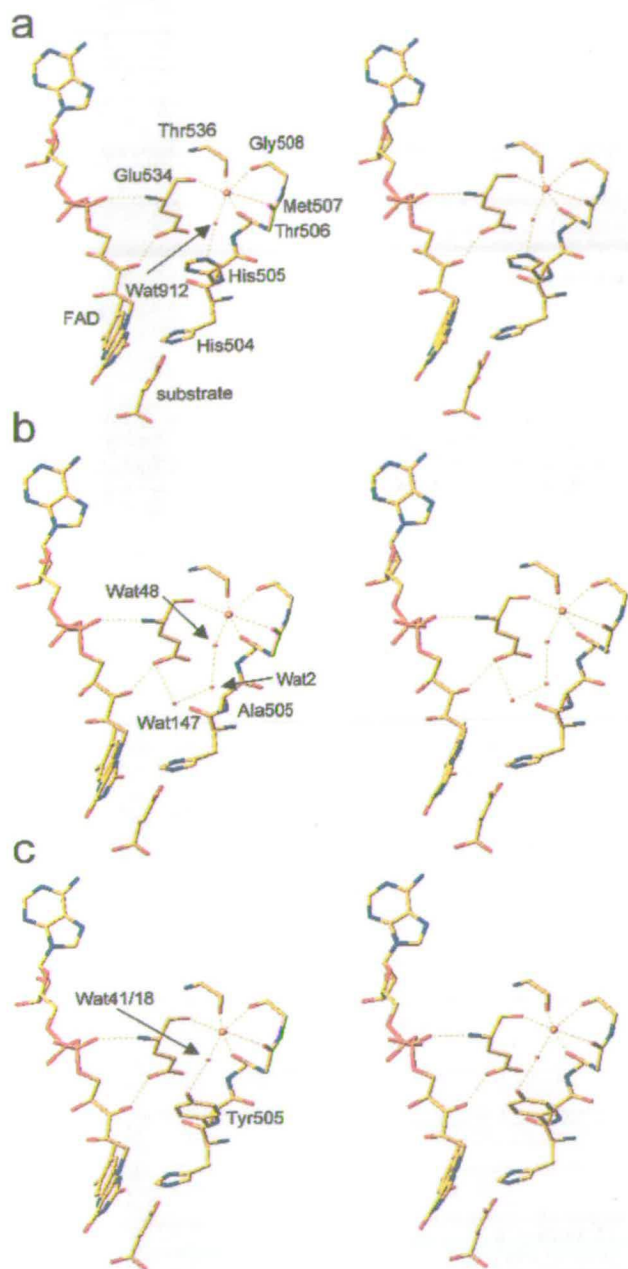
FIGURE 3: Stereoview of the region surrounding the sodium and the FAD in (a) wild-type, (b) H505A, and (c) H505Y flavocyto-chromes c_3. In each case, the sodium ion is shown as an orange sphere. The orange dotted lines indicate the coordination sphere of the sodium in each form of the enzyme, as well as some important hydrogen-bonding interactions. This diagram was generated using TURBO–FRODO (21).

FIGURE 4: The reaction mechanism for fumarate reduction by Fcc₃ as originally proposed by Taylor et al. (6). Catalysis is initiated by the twisting out of plane of the C1 carboxylate group (on the left) of fumarate. The substrate is polarized by interactions with charged residues facilitating hydride transfer from N5 of reduced FAD to the substrate C2. The role of His504 is to stabilize the build up of negative charge on the substrate prior to protonation. Arg402 (3.0 Å from C3) is ideally positioned to donate a proton to substrate C3 resulting in the formation of succinate. Arg402 is immediately reprotonated via a proton pathway involving Arg381 and Glu378. The relative positions of His505 and Glu534 show schematically how His505 decreases the effect that the negative charge of Glu534 has on His504.

for catalysis (hydride transfer distance, proton delivery distance) are unaffected by the mutations.

DISCUSSION

The mechanism for the fumarate reductase (Fcc₃) catalyzed reaction, as originally proposed by Taylor et al. (6), is shown in Figure 4. In this mechanism His504 of Fcc₃ is shown protonating the C4 carboxylate to facilitate the transient formation of a carbanion at C3. Previous mutagenesis and pH studies indicated that a protonated His504 could enhance the rate of reaction but was not essential for it (9). This led

to the suggestion that it was the imidazole of His504 that was responsible for the observed pK_a of around 7.5 seen in the wild-type enzyme. We have now shown that substitution of the adjacent residue, His505, can have significant effects on the pH dependence of Fcc₃. These are fairly modest for the H505Y mutation, with the largest effects on k_{cat} and K_m being less than 2-fold at pH 6.0, Table 1. However, in the case of the H505A mutation the effects are quite large with a 20-fold fall in the value of k_{cat} at pH 6.0.

It is clear that for both mutant enzymes there has been a shift in the pK_a value for enzyme activity. The most likely explanation is that substitution at position 505 has had an effect on the pK_a of the active site residue His504. Thus, the H505Y mutation appears to shift this pK_a from 7.5 to 8.2 and the H505A mutation from 7.5 to 9.0. The key question is, how do the substitutions at His505 modulate the pK_a of His504? The answer may lie in an examination of the three-dimensional structure of Fcc$_3$ in the region around His505. The imidazole ring of His505 lies between His504 and Glu534, and it is likely therefore that His505 helps to minimize the effect of the negative charge of Glu534 on His504. Removing the ring of His505, as is the case in the H505A mutant, would allow the charge on Glu534 to affect His504 making it a weaker acid. This is what seems to have happened since the pK_a shifts from 7.5 to 9.0 in the H505A mutant. The less pronounced effect seen for the H505Y mutation, on the other hand, is consistent with the phenol ring of the tyrosine being able to modulate the effect of the charge of Glu534 on His504. Indeed, it is not surprising that the H505Y mutation has a fairly modest effect, since the equivalent residue to His505 in most fumarate reductases (including the *E. coli* and *W. succinogenes* enzymes) is in fact a tyrosine.

In the wild-type Fcc$_3$ structure (*6*), His505 hydrogen bonds to a water molecule (Wat912) which is in the coordination sphere of the bound sodium ion. It is clear from the structures of the H505A and H505Y mutant enzymes that the replacement of the histidine does not significantly alter the inner-coordination sphere of the sodium ion (Figure 1). Two water molecules occupy the space vacated by the removal of the imidazole ring in the H505A. These form a hydrogen-bonding network to a water molecule which is in the equivalent position to that taken by Wat912 in the wild-type structure, and which ligates the sodium ion at a distance of 2.5 Å. In the H505Y structure, the tyrosine side-chain occupies approximately the same position as that taken by the imidazole ring of His505 in the wild-type structure (Figure 3). In this case, the hydroxyl group of the tyrosine hydrogen bonds to the water ligand. Thus, the sodium ion is found in essentially the same position in the wild-type and mutant structures of Fcc$_3$. An interesting question is how the sodium site in Fcc$_3$ compares to that seen in the other known fumarate reductase structures.

The structures of the fumarate reductases from *Shewanella oneidensis* MR1 (2.5 Å resolution) (*7*) and *E. coli* (3.3 Å resolution) (*1*) do not show any sodium ions assigned in the PDB files (1D4E and 1FUM, respectively). However, the arrangement of the protein backbone around the putative "sodium" site in these two enzymes is the same as in the wild-type Fcc$_3$ structure (1QJD, 1.8 Å resolution) (*6*). Clearly, the assignment of sodium would be difficult in these two lower resolution structures. Overall, however, the similarities between the structures of these enzymes would lead us to suggest that this sodium site is conserved throughout the fumarate reductase family.

In conclusion, we have demonstrated that His505 is not essential for sodium ion binding but may play a role in modulating the pK_a of a key active site residue, His504.

ACKNOWLEDGMENT

REFERENCES

1. Iverson, T. M., Luna-Chavez, C., Cecchini, G., and Rees, D. C. (1999) *Science 284*, 1961–1966.
2. Körtner C., Lauterbach F., Tripier D., Unden G., and Kröger, A. (1990) *Mol. Microbiol. 4*, 855–860.
3. Gordon, E. H. J., Pealing, S. L., Chapman, S. K., Ward, F. B., and Reid, G. A. (1998) *Microbiology 4*, 937–945.
4. Lancaster, C. R. D., Kröger, A., Auer, M., and Michel, H. (1999) *Nature 402*, 377–385.
5. Lancaster, C. R. D., Groβ, R., and Simon, J. (2001) *Eur. J. Biochem. 268*, 1820–1827.
6. Taylor P., Pealing, S. L., Reid, G. A, Chapman, S. K., and Walkinshaw, M. D. (1999) *Nat. Struct. Biol. 6*, 1108–1112.
7. Leys, D., Tsapin, A. S., Nealson, K. H., Meyer, T. E., Cusanovich, M. A., and Van Beeumen, J. J. (1999) *Nat. Struct. Biol. 6*, 1113–1117.
8. Bamford, V., Dobbin, P. S., Richardson, D. J., and Hemmings. A. M. (1999) *Nat. Struct. Biol. 6*, 1104–1107.
9. Doherty, M. K., Pealing, S. L., Miles, C. S., Moysey, R., Taylor, P., Walkinshaw, M. D., Reid, G. A., and Chapman, S. K. (2000) *Biochemistry 39*, 10695–10701.
10. Reid, G. A., Miles, C. S., Moysey, R. K., Pankhurst, K. L., and Chapman, S. K. (2000) *Biochim. Biophys. Acta 1459*, 310–315.
11. Mowat, C. G., Moysey, R., Miles, C. S., Leys, D., Doherty, M. K., Taylor, P., Walkinshaw, M. D., Reid, G. A., and Chapman S. K. (2001) *Biochemistry 40*, 12292–12298.
12. Chapman, S. K., Morrison, C. A., Reid, G. A., Pealing, S. L., Taylor, P., and Walkinshaw M. D. (1999) in *Flavins and Flavoproteins 1999* (Ghisla, S., Kroneck, P., Macheroux, P., and Sund, H., Eds.) pp 105–113, Rudolf Weber, Agency for Scientific Publications, Berlin.
13. Kunkel, T. A., and Roberts, J. D. (1987) *Methods Enzymol. 154*, 367–382.
14. Sanger, F., Nicklen, S., and Coulson, A. R. (1977) *Proc. Natl. Acad. Sci. U.S.A. 74*, 5463–5467.
15. Michel, L. O., Sandkvist, M., and Bagdasarian, M. (1995) *Gene 152*, 41–45.
16. Pealing, S. L., Cheesman, M. R., Reid, G. A., Thomson, A. J., Ward, F. B., and Chapman, S. K. (1995) *Biochemistry 34*, 6153–6158.
17. Pealing, S. L., Lysek, D. A., Taylor, P., Alexeev, D., Reid, G. A., Chapman, S. K., and Walkinshaw, M. D. (1999*) J. Struct. Biol. 127*, 76–78.
18. Macheroux, P. (1999) in *Flavoprotein Protocols: Methods in Molecular Biology* (Chapman, S. K., and Reid, G. A., Eds.) Vol. 131, pp 1–7, Humana Press, Totowa, New Jersey.
19. Turner K. L., Doherty M. K., Heering H. A., Armstrong F. A., Reid G. A., and Chapman S. K. (1999) *Biochemistry 38*, 3302–3309.
20. Otwinowski, Z., and Minor, W. (1997) *Methods Enzymol. 276*, 307–326.
21. Roussel, A., and Cambillau, C. (1991) TURBO–FRODO, in *Silicon Graphics Geometry Partners Directory 86*, Silicon Graphics, Mountain View, CA.
22. Murshudov, G. N., Vagin, A. A., and Dodson, E. J. (1997) *Acta Crystallogr. D53*, 240–255.

BI020155E

Engineering Water To Act as an Active Site Acid Catalyst in a Soluble Fumarate Reductase[†]

Christopher G. Mowat,[‡,§] Katherine L. Pankhurst,[‡] Caroline S. Miles,[§] David Leys,[ǁ] Malcolm D. Walkinshaw,[§] Graeme A. Reid,[§] and Stephen K. Chapman*,[‡]

Department of Chemistry, University of Edinburgh, West Mains Road, Edinburgh EH9 3JJ, U.K., Institute of Cell and Molecular Biology, University of Edinburgh, Mayfield Road, Edinburgh EH9 3JR, U.K., and Department of Biochemistry, Adrian Building, University of Leicester, University Road, Leicester LE1 7RH, U.K.

ABSTRACT: The ability of an arginine residue to function as the active site acid catalyst in the fumarate reductase family of enzymes is now well-established. Recently, a dual role for the arginine during fumarate reduction has been proposed [Mowat, C. G., Moysey, R., Miles, C. S., Leys, D., Doherty, M. K., Taylor, P., Walkinshaw, M. D., Reid, G. A., and Chapman, S. K. (2001) *Biochemistry 40*, 12292−12298] in which it acts both as a Lewis acid in transition-state stabilization and as a Brønsted acid in proton delivery. This proposal has led to the prediction that, if appropriately positioned, a water molecule would be capable of functioning as the active site Brønsted acid. In this paper, we describe the construction and kinetic and crystallographic analysis of the Q363F single mutant and Q363F/R402A double mutant forms of flavocytochrome c_3, the soluble fumarate reductase from *Shewanella frigidimarina*. Although replacement of the active site acid, Arg402, with alanine has been shown to eliminate fumarate reductase activity, this phenomenon is partially reversed by the additional substitution of Gln363 with phenylalanine. This Gln → Phe substitution in the inactive R402A mutant enzyme was designed to "push" a water molecule close enough to the substrate C3 atom to allow it to act as a Brønsted acid. The 2.0 Å resolution crystal structure of the Q363F/R402A mutant enzyme does indeed reveal the introduction of a water molecule at the correct position in the active site to allow it to act as the catalytic proton donor. The 1.8 Å resolution crystal structure of the Q363F mutant enzyme shows a water molecule similarly positioned, which can account for its measured fumarate reductase activity. However, in this mutant enzyme Michaelis complex formation is impaired due to significant and unpredicted structural changes at the active site.

Bacterial fumarate reductases allow the use of fumarate as a terminal electron acceptor in anaerobic respiration. Within this enzyme family, there are essentially two types of fumarate reductase. The majority of organisms utilize a membrane-bound complex that is closely related to succinate dehydrogenase and uses iron−sulfur centers and FAD[1] as cofactors (*1, 2*). However, in *Shewanella* species a soluble periplasmic, tetraheme, FAD-containing enzyme (flavocytochrome c_3) is produced (*3*). Despite these differences, the crystal structures of fumarate reductases from *Escherichia coli* [PDB entry 1FUM (*1*)], *Wolinella succinogenes* [1QLA, 1QLB (*4*), and 1E7P (*5*)], and *Shewanella* species [1QJD (*6*), 1D4E (*7*), and 1QO8 (*8*)] show a clear conservation of the active site architecture. This conservation of the active site around the FAD is consistent with a common mechanism for fumarate reduction. Indeed, there is now a considerable body of evidence for the operation of a universal mechanism for fumarate reduction throughout this family of enzymes (*6, 9, 10*).

The structure of the enzyme from *Shewanella frigidimarina* [1QJD (*6*)] is at 1.8 Å resolution, the highest-resolution structure available for any of the fumarate reductases. On the basis of this structure, a mechanism was proposed involving the use of an arginine residue (Arg402) as the active site acid catalyst (*6*). Arg402 transfers protons to the substrate as part of a proton delivery pathway involving Arg381 and Glu378 (*9*). More recently, the role of Arg402 has been investigated further by site-directed mutagenesis, and a dual role has been proposed which takes advantage of the unique ability of the residue to act as both a Lewis acid (stabilizing the build-up of negative charge in the transition state) and a Brønsted acid (delivering a proton to the substrate) (*10*). Using this mechanism, we have proposed the existence of two separate positions at the active site of

* To whom correspondence should be addressed: Department of Chemistry, University of Edinburgh, West Mains Road, Edinburgh EH9 3JJ, U.K. E-mail: S.K.Chapman@ed.ac.uk. Fax and phone: (44) 131 650 4760.
‡ Department of Chemistry, University of Edinburgh.
§ Institute of Cell and Molecular Biology, University of Edinburgh.
ǁ University of Leicester.

¹ Abbreviations: Fcc₃, flavocytochrome c_3; Q363F/R402A, glutamine 363 → phenylalanine, arginine 402 → alanine double mutation; Q363F, glutamine 363 → phenylalanine single mutation; FAD, flavin adenine dinucleotide.
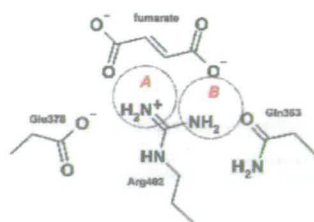
FIGURE 1: Schematic representation of positions A and B in the active site of flavocytochrome c_3. It can be seen that the bifurcated side chain of Arg402 results in the occupation of position A and position B by Brønsted acid and Lewis acid groups, respectively, thus explaining its efficiency as the acid catalyst in fumarate reductase.

fumarate reductase (Figure 1): position A, which when occupied by a species capable of Brønsted acid function may act as the proton donor during succinate formation, and position B, which if occupied by a Lewis acid species can stabilize the transition state and consequently increase the rate of catalysis (*10*). This conclusion was reached as a result of kinetic and structural studies on three Arg402-substituted forms of flavocytochrome c_3. Replacement of Arg402 with lysine or tyrosine was shown to introduce a Brønsted acid function at position A of the active site leading to active enzymes, albeit with greatly decreased activity. However, replacement of Arg402 with alanine produced an enzyme with no measurable catalytic activity. The structure of the R402A mutant enzyme reveals the existence of a water molecule at position B but no ordered entity at position A. This explained the lack of fumarate reductase activity in the R402A mutant (*10*). Our "two-position" model led us to propose that if the R402A enzyme could be re-engineered to place a water molecule in position A (with conservation of the arrangement of the remainder of the proton delivery pathway), then fumarate reductase activity would be restored. To achieve this aim, we have re-engineered the R402A enzyme so that access of water to position B is sterically prohibited, with the intention of forcing a water molecule into position A. In this paper, we report the construction and kinetic and crystallographic characterization of the Q363F single-mutant and Q363F/R402A double-mutant flavocytochromes c_3. The structure of the Q363F/R402A enzyme reveals the existence of a water molecule at the active site of the enzyme which is indeed capable of assuming the role of an active site acid catalyst, while the structure of the Q363F single-mutant enzyme reveals the origin of its unexpected kinetic characteristics.

MATERIALS AND METHODS

DNA Manipulation, Strains, Media, and Growth. The mutant enzymes Q363F and Q363F/R402A Fcc₃ were generated using the QuikChange XL Site-Directed Mutagenesis Kit (Stratagene). In the case of the Q363F mutation, the template for the reaction was pEGX1 (WT *fccA*/pMMB503EH) (*3*), while for the Q363F/R402A mutation, the template was pCM68 (R402A *fccA*/pMMB503EH) (*9*).

Oligonucleotides were designed to incorporate the glutamine 363 to phenylalanine change and were complementary to the same sequence on both strands of the plasmid: GA-AAGACATGCAGTATATCTTCGCTCACCCAACACTAT-CTG (complementary to the antisense strand) and CAGAT-

AGTGTTGGGTGAGCGAAGATATACTGCATGTCTTTC (complementary to the sense strand). Mismatched bases are underlined. Temperature cycling, product digestion with *Dpn*I, and transformation of *E. coli* XL-10 Gold ultracompetent cells were carried out as per the Stratagene protocol. Plasmid DNA (Q363F *fccA*/pMMB503EH, pCM138; Q363F+ R402A *fccA*/pMMB503EH, pCM139) was screened for the required mutation using an ABI Prism 3100 genetic analyzer, and the mutated *fccA* coding sequence was similarly sequenced to verify that no secondary mutations had been introduced. Expression in Δ*fccA S. frigidimarina* strain EG301 (*3*) was carried out as described previously (*9*).

Protein Purification and Kinetic Analysis. Wild-type and mutant forms of flavocytochrome c_3 were purified as previously reported (*11*). Protein samples for crystallization and mass spectrometry were subjected to an additional purification step using FPLC with a 1 mL Resource Q column (Pharmacia) as described by Pealing et al. (*12*). Protein concentrations were determined using the Soret band absorption coefficient for the reduced enzyme (752.8 mM⁻¹ cm⁻¹ at 419 nm) (*11*).

The FAD content of Fcc₃ mutants was determined using the method of Macheroux (*13*), and all steady-state rate constants were corrected for the percentage of FAD present.

Mass spectrometry of proteins was carried out using a Micromass Platform II Electrospray mass spectrometer. Samples were prepared in 0.1% formic acid and introduced into the spectrometer via direct infusion. The spectrometer was standardized using horse heart myoglobin.

The steady-state kinetics of fumarate reduction were followed at 25 °C as described by Turner et al. (*14*). The fumarate-dependent reoxidation of reduced methyl viologen was monitored at 600 nm using a Shimadzu UV-PC 1501 spectrophotometer. To ensure anaerobicity, the spectrophotometer was housed in a Belle Technology glovebox under a nitrogen atmosphere with the O_2 level maintained well below 2 ppm. Assay buffers contained 0.45 M NaCl and 0.2 mM methyl viologen and were adjusted to the appropriate pH values using 0.05 M HCl or NaOH as follows: Tris-HCl (pH 7.0−9.0), MES/NaOH (pH 5.4−6.8), and CHES/NaOH (pH 8.6−10). The viologen was reduced by addition of sodium dithionite until a reading of ~1 absorbance unit was obtained (corresponding to ~80 μM reduced methyl viologen). The concentration of reduced methyl viologen could be varied between 100 and 20 μM with no effect on the rate of reaction. A known concentration of enzyme was added and the reaction initiated by addition of fumarate.

Kinetic parameters K_M and k_{cat} were determined from the steady-state results using nonlinear regression analysis (Microcal Origin software).

Crystallization and Refinement. Crystallization of Q363F and Q363F/R402A flavocytochrome c_3 was carried out by hanging drop vapor diffusion at 4 °C in Linbro plates. Crystals were obtained with well solutions comprising 100 mM Tris-HCl buffer (pH 7.8−8.5) (measured at 25 °C), 80 mM NaCl, 16−19% PEG 8000, and 10 mM fumarate. Hanging drops 4 μL in volume were prepared by adding 2 μL of 6 mg/mL protein [in 10 mM Tris-HCl (pH 8.5)] to 2 μL of well solution. After approximately 10 days, needles of up to 1 mm × 0.2 mm × 0.2 mm and plates of up to 0.5 mm × 0.5 mm × 0.2 mm were formed. Crystals were immersed in a solution of 100 mM sodium acetate buffer

Table 1: Kinetic Parameters for Fumarate Reduction in Wild-Type, Q363F, and Q363F/R402A Flavocytochromes c_3

pH	k_{cat} (s^{-1}) wild type[a]	k_{cat} Q363F/R402A	k_{cat} Q363F	K_M (μM) wild type[a]	K_M Q363F/R402A	K_M Q363F
6.0	658 ± 34	0.064 ± 0.001	0.26 ± 0.01	43 ± 10	6.6 ± 0.6	843 ± 102
7.2	509 ± 15	0.332 ± 0.007	1.34 ± 0.05	25 ± 2	5.0 ± 0.6	999 ± 132
7.5	370 ± 10	0.420 ± 0.012	1.64 ± 0.05	28 ± 3	5.3 ± 0.8	1064 ± 115
9.0	210 ± 13	0.278 ± 0.007	1.61 ± 0.06	7 ± 2	3.3 ± 0.5	1407 ± 160

[a] Values for the wild-type enzyme taken from ref 9.

(pH 6.5), 20% PEG 8000, 10 mM fumarate, and 80 mM NaCl, containing 23% glycerol as a cryoprotectant, prior to mounting in nylon loops and flash-cooling in liquid nitrogen. For the Q363F mutant enzyme, crystal data were collected to 1.8 Å resolution at SRS Daresbury (station 9.6, λ = 0.87 Å) using an ADSC Quantum 4 ccd detector, and for Q363F/R402A, crystal data were collected to 2.0 Å resolution at DESY in Hamburg, Germany (station BW7B, λ = 0.8459 Å), using a Mar Research mar345 image plate detector. Crystals of both enzymes were found to belong to space group $P2_1$. The Q363F single mutant was found to have the following cell dimensions: a = 78.520 Å, b = 88.886 Å, c = 91.194 Å, and β = 104.42°; the Q363F/R402A double mutant was found to have the following cell dimensions: a = 77.971 Å, b = 88.280 Å, c = 90.087 Å, and β = 103.89°.

Data processing was carried out using the HKL package (15). The wild-type Fcc$_3$ structure (1QJD), stripped of water, was used as the initial model for molecular replacement. Electron density fitting was carried out using the program TURBO-FRODO (16). Restraints for the FAD were calculated from two small molecule crystal structures (Cambridge Crystallographic Database codes HAMADPH and VEF-HUJ10). Structure refinement was carried out using Refmac (17).

The atomic coordinates have been deposited in the Protein Data Bank [entries 1LJ1 (Q363F/R402A) and 1M64 (Q363F)].

RESULTS

Characterization of the Mutant Enzyme. The molecular masses of the Q363F and Q363F/R402A mutant enzymes were determined by electrospray mass spectrometry. In comparison to the wild type (63 033 Da), the mass difference was found to be −65 Da for the Q363F/R402A enzyme (expected difference of −66 Da) and 19 Da for the Q363F enzyme (expected difference of 19 Da). Both mutations were further verified by DNA sequencing. The average FAD contents of the Q363F and Q363F/R402A mutant enzymes were found to be 73 and 80%, respectively. This is equivalent to the typical values for the recombinant wild-type enzyme of ~73%. All catalytic rates were corrected for the variation in FAD content.

The ability of the two mutant flavocytochromes c_3 to catalyze fumarate reduction was determined over a range of pH values. The resulting k_{cat} and K_M parameters for the wild-type and mutant forms of Fcc$_3$ are compared in Table 1. Unlike the R402A single mutant, the Q363F/R402A enzyme does exhibit measurable fumarate reductase activity, albeit with a k_{cat} some 10^3–10^4-fold lower (depending on pH) than that seen for the wild-type enzyme. In terms of K_M, values for the Q363F/R402A enzyme are ~5-fold lower than those of the wild type, decreasing slightly with increasing pH. In the case of the Q363F single-mutant enzyme, values of k_{cat}

Table 2: Data Collection and Refinement Statistics

	Q363F/R402A	Q363F
resolution (Å)	15.0–2.0	15.0–1.8
total no. of reflections	412535	604721
no. of unique reflections	75611	108491
completeness (%)	94.5	96.6
$I/[\sigma(I)]$	9.2	15.8
R_{merge} (%)[a]	7.2	6.2
R_{merge} in outer shell (%)	22.6 (2.07–2.00)	17.6 (1.86–1.80)
R_{cryst} (%)[b]	16.08	16.30
R_{free} (%)[b]	23.47	22.37
rmsd from ideal values		
bond lengths (Å)	0.013	0.012
bond angles (deg)	2.7	2.3
Ramachandran analysis		
most favored (%)	88.6	88.4
additionally allowed (%)	11.3	11.4

[a] $R_{merge} = \sum_h \sum_i |I(h) - I_i(h)|/\sum_h \sum_i I_i(h)$, where $I_i(h)$ and $I(h)$ are the ith and mean measurements of reflection h, respectively. [b] $R_{cryst} = \sum_h |F_o - F_c|/\sum_h F_o$, where F_o and F_c are the observed and calculated structure factor amplitudes of reflection h, respectively. R_{free} is the test reflection data set, 5% selected randomly for cross validation during crystallographic refinement.

are ~10^3-fold lower than in the wild-type enzyme, but with hugely elevated K_M values in the millimolar region that would indicate significant impairment of Michaelis complex formation.

Crystal Structure of Q363F and Q363F/R402A Mutant Flavocytochrome c_3. For the Q363F and Q363F/R402A mutant enzymes, data sets to resolutions of 1.8 and 2.0 Å, respectively, were used to refine the structures to final R-factors of 16.30% (R_{free} = 22.37% for Q363F) and 16.08% (R_{free} = 23.47% for Q363F/R402A) (see Table 2). For each mutant enzyme, there are two independent molecules in the asymmetric unit and the final model consists of two protein molecules, each comprised of residues 1–568, four hemes, the FAD, one substrate molecule (fumarate), and one sodium ion. In addition, the Q363F model contains 2111 water molecules and the Q363F/R402A model 1630 water molecules. For each protein molecule, three residues at the C-terminus (569–571) could not be located in the electron density maps. The rmsd fit of all backbone atoms for the wild-type and Q363F/R402A mutant flavocytochromes c_3 is 0.3 Å, indicating no major differences between the structures, while the rmsd fit for all backbone atoms for the wild-type and Q363F mutant enzymes is 0.6 Å, indicating greater differences as a result of the single Q363F substitution. Due to the fact that there are two molecules in the asymmetric unit for each structure, the stated rmsd fit value is the average over both molecules (A and B). The rmsd fit of all backbone atoms between molecules A and B within each model is 0.2 Å.

On comparison of the crystal structure of the Q363F/R402A mutant enzyme (Figure 2) with those of the wild-
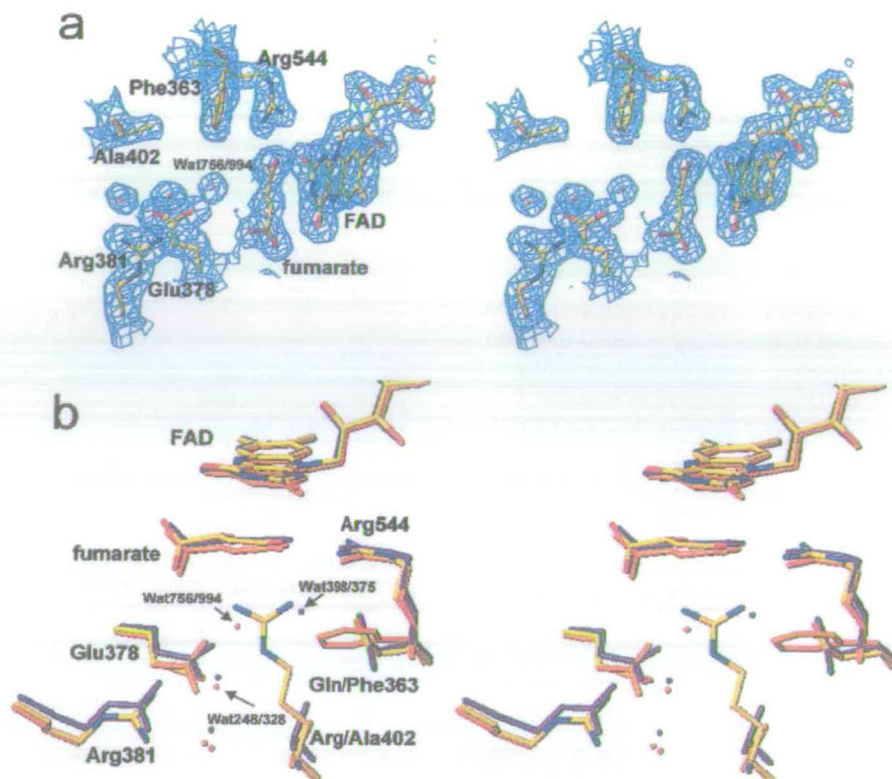
FIGURE 2: Panel a shows a stereodiagram of the active site of the Q363F/R402A double-mutant flavocytochrome c_3. The water which acts as the active site acid catalyst can be clearly seen adjacent to the bound substrate. Electron density was computed using the Fourier coefficients $2F_o - F_c$, where F_o and F_c are the observed and calculated structure factors, respectively, the latter based on the final model. The contour level is 1σ, where σ is the rms electron density. Panel b shows an overlay of the active sites of the wild-type (atom color), R402A (purple), and Q363F/R402A (orange) flavocytochromes c_3. The catalytic water in the Q363F/R402A mutant enzyme can be seen occupying the space designated as position A, which is occupied by one of the NH2 groups of Arg402 in the wild-type enzyme, while the water in the R402A mutant enzyme active site occupies the space taken by the other Arg402 NH2 group in the wild-type enzyme known as position B. The proton pathway residues (Arg381 and Glu378) are also shown, along with the water molecules in the two mutant enzyme structures which result from the movement of the Glu378 side chain in each. This diagram was generated using TURBO-FRODO (*16*).

type enzyme and the R402A single-mutant enzyme, it is clear that there are no unexpected structural changes as a result of the mutation. The phenyl ring of Phe363 is found to occupy the space around position B vacated by the substitution of Arg402 with alanine. What is also apparent is the introduction of a water molecule adjacent to the bound fumarate in both protein molecules of the asymmetric unit (WAT756 in molecule A and WAT994 in molecule B) some 3.5 Å from C3 of the substrate. This water molecule is 3.0 Å from another water molecule (WAT248 in molecule A and WAT328 in molecule B) and 2.7 Å from the carboxylate group of the side chain of Glu378. Glu378 is one of the residues of the proposed proton delivery pathway (Figure 2b). The water molecule which is found at position B in the active site of the R402A single-mutant enzyme (WAT398 in molecule A and WAT375 in molecule B), which forms hydrogen bonding interactions with the side chain of Gln363 and the fumarate C4 carboxylate group, is absent in the structure of the Q363F/R402A double mutant. This absence is due to the steric bulk of the phenylalanine side chain (Figure 2b). The substrate, fumarate, is bound in the same twisted conformation observed in the structure of the wild-type enzyme and other mutant forms of flavocytochrome c_3 (*6, 9, 10*). Also, the hydride transfer distance from C2 of fumarate to N5 of the FAD isoalloxazine ring is 3.4 Å, the same as observed in the wild-type and R402A enzyme

structures. The integrity of the proton transfer pathway involving residues Arg381 and Glu378 is slightly compromised by the rotation and movement of Glu378 in occupying some of the space vacated by the removal of Arg402, and this movement, similar to that observed in the structure of the R402A mutant flavocytochrome c_3, results in a distance of 4.5 Å between the side chains of Arg381 and Glu378 (compared to 3.1 Å in the wild-type enzyme). However, as a consequence of this change in the orientation of Glu378, a water molecule (WAT248 in molecule A and WAT328 in molecule B) is introduced between Glu378 and Arg381 2.9 Å from Arg381 and 3.8 Å from Glu378, which may serve to mediate in the proton delivery mechanism.

Comparison of the crystal structure of the Q363F mutant enzyme with that of the wild-type enzyme reveals some important changes at the active site as a result of the substitution (Figure 3). The phenyl ring at position 363 can clearly be seen, but it is apparent that the introduction of this steric bulk at the active site has caused Arg402 to swing away from the active site toward the surface of the protein where the guanidinium group resides between Gln201 and Lys404; this has led to significant changes in backbone position between residues Ile399 and Ala405. These changes have allowed a water molecule (WAT300 in molecule A and WAT399 in molecule B) to enter the active site and bind adjacent to the substrate, in position A, 3.4 Å from the
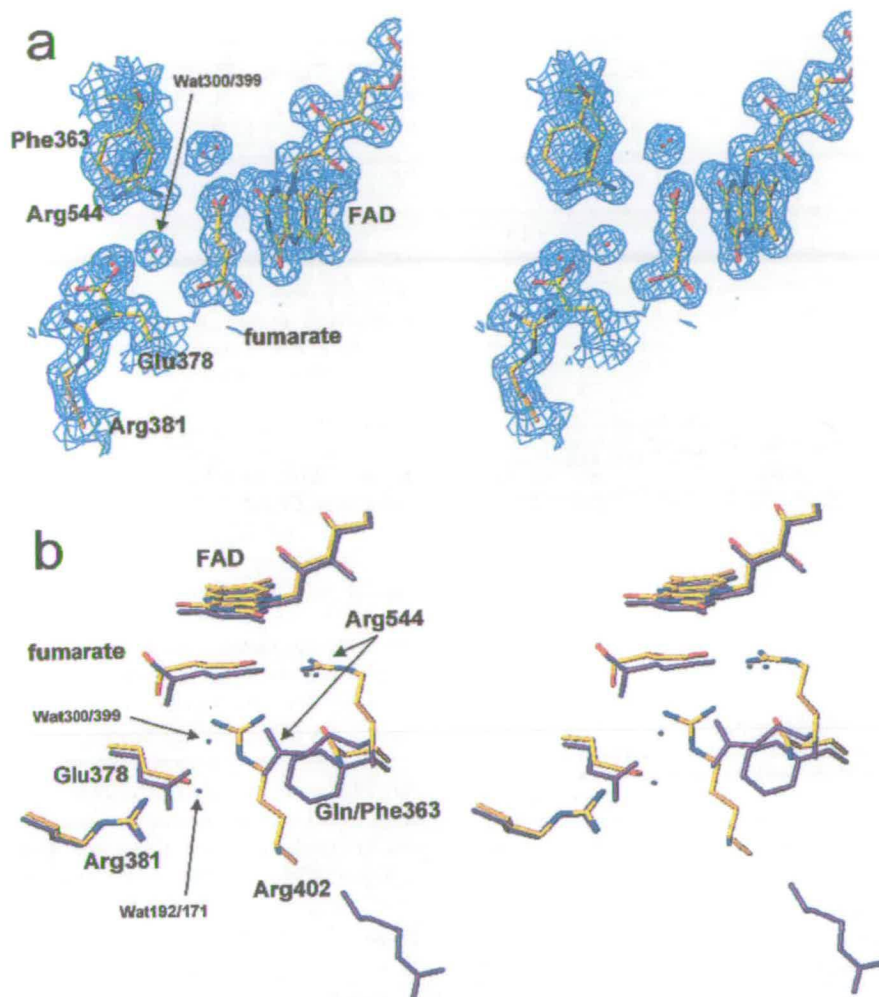
FIGURE 3: Panel a shows a stereodiagram of the active site of the Q363F mutant flavocytochrome c_3. The water which acts as the active site acid catalyst can be clearly seen adjacent to the bound substrate. Electron density was computed using the Fourier coefficients $2F_o - F_c$, where F_o and F_c are the observed and calculated structure factors, respectively, the latter based on the final model. The contour level is 1σ, where σ is the rms electron density. Panel b shows an overlay of the active sites of the wild-type (atom color) and Q363F (purple) flavocytochromes c_3. The side chain of Arg402 in the Q363F mutant enzyme is seen at the bottom right of the figure, and the catalytic water in the Q363F mutant enzyme can be seen occupying the space designated as position A. The movement of Arg544 is also obvious, and the two resulting water molecules are shown adjacent to the fumarate C4 carboxylate group. This diagram was generated using TURBO-FRODO (16).

fumarate C3 atom. As in the Q363F/R402A structure, this water is found to be close to the side chain of Glu378 (2.7 Å), and the slight movement of Glu378 has allowed another water molecule (WAT192 in molecule A and WAT171 in molecule B) to bind 3.6 Å from the Glu378 side chain and 2.9 Å from the Arg381 side chain (as seen in the double-mutant enzyme structure); this may mediate the proton delivery process.

In addition to these changes, Arg544, a residue that is important for the formation of the Michaelis complex, has moved to occupy some of the space vacated by the reorientation of Arg402, exhibiting a stacking interaction with Phe363 and a hydrogen bonding interaction with the water molecule located at position A (2.9 Å). The Arg544 side chain is also found to be 3.2 Å from the C4 carboxylate moiety of the bound fumarate. This movement of Arg544 has resulted in the introduction of a further two water molecules, each forming a hydrogen bonding interaction with one of the fumarate C4 carboxylate oxygen atoms.

DISCUSSION

The mechanism for the Fcc$_3$-catalyzed reaction, as originally proposed by Taylor et al. (6), is shown in Figure 4a, and we believe that this mechanism operates throughout the family of fumarate reductase enzymes. The role of Arg402 as the active site acid catalyst has been confirmed by mutagenesis experiments, and its efficiency in this role is explained in terms of its unique ability to simultaneously occupy positions A and B at the active site of the enzyme and act as both a Brønsted acid and a Lewis acid at each site (10). This is corroborated by recent work on a related enzyme, L-aspartate oxidase from *E. coli*, which is structurally similar to fumarate reductase and in which Arg290, the residue equivalent to Arg402 in flavocytochrome c_3, acts as the active site base, abstracting a proton from the substrate during catalysis (18).

Substitution of Arg402 with alanine in flavocytochrome c_3 leads to an enzyme which has no measurable catalytic activity. This is attributed to the lack of a species capable of

FIGURE 5: Schematic representation of positions A and B in the active site of (a) R402A and (b) Q363F/R402A mutant flavocytochrome c_3. The water in position B of the R402A mutant enzyme is shown in purple, while the water in position A of the Q363F/R402A enzyme is shown in orange along with Phe363. Hydrogen bonding interactions are shown as dashed lines. The direction of proton transfer in Q363F/R402A flavocytochrome c_3 is shown using a blue arrow.
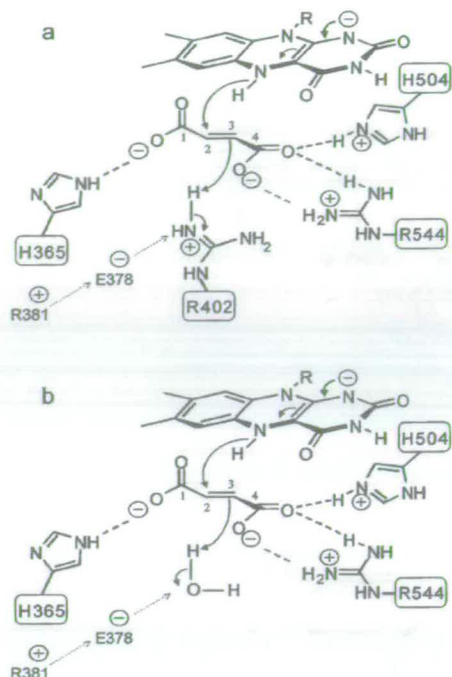
FIGURE 4: Panel a shows the reaction mechanism for fumarate reduction in the wild-type enzyme [this is an abbreviated version of the mechanism proposed by Taylor et al. (6)]. The substrate is polarized by interactions with charged residues facilitating hydride transfer from N5 of the reduced FAD to C2 of the substrate. Arg402 is ideally positioned to donate a proton to C3 of the substrate, resulting in the formation of succinate. Arg402 is immediately reprotonated via a proton pathway involving Arg381 and Glu378. Panel b shows the mechanism of fumarate reduction in the Q363F/R402A double-mutant enzyme. The water molecule introduced at position A of the mutant enzyme is shown to function as the active site acid catalyst as part of the proton delivery pathway.

proton transfer in position A of the active site. In this case, however, a water molecule is found in position B, hydrogen bonding with the side chain of Gln363 and the C4 carboxylate group of the bound fumarate. Clearly, it is these hydrogen bonding interactions which result in the preferential occupation of position B in the R402A mutant enzyme, with steric constraints precluding the simultaneous occupation of position A by a second solvent molecule. The construction of the double-mutant enzyme incorporating the R402A substitution in conjunction with the introduction of phenylalanine at position 363 was designed to force a water molecule to preferentially occupy position A rather than position B (Figure 5). Since water is capable of acting as a Brønsted acid, its occupancy of position A should permit fumarate reductase activity to occur via the mechanism shown in Figure 4b. The kinetic and structural characterization of the Q363F/R402A flavocytochrome c_3 confirmed both the presence of the water molecule at position A and its ability to function as an acid catalyst, albeit with a low level of activity. The fact that the k_{cat} value for the Q363F/R402A enzyme is some 1000-fold lower than that seen for the wild-type enzyme could, at least in part, be due to the inability of water to function as a Lewis acid. There may also be an effect arising from the observed perturbation in the relative positions of "proton pathway" residues Arg381 and Glu378.

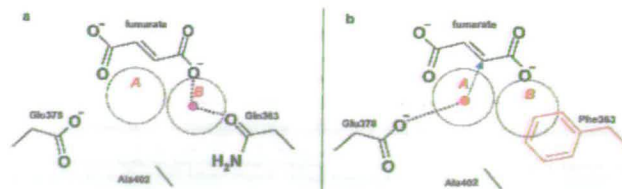Construction of the Q363F single-mutant enzyme as a control has proven to be illuminating, leading to a mutant enzyme with unexpected characteristics. Although the enzyme was found to display fumarate reductase activity at a low level, the high K_M value for fumarate results in an inefficient enzyme (in terms of k_{cat}/K_M). In this case, the crystal structure that was obtained has been crucial in accounting for the kinetic observations, showing that Arg402, the active site acid, has moved away from the active site as a result of the introduction of a phenylalanine residue at position 363. This has allowed a water molecule to occupy position A of the active site in the mutant enzyme, resulting in the measured fumarate reductase activity. In addition, Arg544, a residue that is important for substrate binding, has moved into the active site, and is no longer involved in the Michaelis complex formation, thus explaining the high substrate K_M value that is observed. Interestingly, the value of k_{cat} measured for the Q363F mutant enzyme is ~3-fold greater than that seen with the Q363F/R402A double-mutant form.

In conclusion, by generating the Q363F/R402A double-mutant form of flavocytochrome c_3, we have succeeded in the novel engineering of a water molecule as the active site acid in a fumarate reductase.

REFERENCES

1. Iverson, T. M., Luna-Chavez, C., Cecchini, G., and Rees, D. C. (1999) *Science 284*, 1961–1966.

2. Körtner, C., Lauterbach, F., Tripier, D., Unden, G., and Kröger, A. (1990) *Mol. Microbiol. 4*, 855–860.

3. Gordon, E. H. J., Pealing, S. L., Chapman, S. K., Ward, F. B., and Reid, G. A. (1998) *Microbiology 4*, 937–945.

4. Lancaster, C. R. D., Kröger, A., Auer, M., and Michel, H. (1999) *Nature 402*, 377–385.

5. Lancaster, C. R. D., Gross, R., and Simon, J. (2001) *Eur. J. Biochem. 268*, 1820–1827.

6. Taylor, P., Pealing, S. L., Reid, G. A., Chapman, S. K., and Walkinshaw, M. D. (1999) *Nat. Struct. Biol. 6*, 1108–1112.

7. Leys, D., Tsapin, A. S., Nealson, K. H., Meyer, T. E., Cusanovich, M. A., and Van Beeumen, J. J. (1999) *Nat. Struct. Biol. 6*, 1113–1117.

8. Bamford, V., Dobbin, P. S., Richardson, D. J., and Hemmings, A. M. (1999) *Nat. Struct. Biol. 6*, 1104–1107.

9. Doherty, M. K., Pealing, S. L., Miles, C. S., Moysey, R., Taylor, P., Walkinshaw, M. D., Reid, G. A., and Chapman, S. K. (2000) *Biochemistry 39*, 10695–10701.

10. Mowat, C. G., Moysey, R., Miles, C. S., Leys, D., Doherty, M. K., Taylor, P., Walkinshaw, M. D., Reid, G. A., and Chapman, S. K. (2001) *Biochemistry 40*, 12292–12298.

11. Pealing, S. L., Cheesman, M. R., Reid, G. A., Thomson, A. J., Ward, F. B., and Chapman, S. K. (1995) *Biochemistry 34*, 6153–6158.

12. Pealing, S. L., Lysek, D. A., Taylor, P., Alexeev, D., Reid, G. A., Chapman, S. K., and Walkinshaw, M. D. (1999) *J. Struct. Biol. 127*, 76−78.

13. Macheroux, P. (1999) in *Flavoprotein Protocols: Methods in Molecular Biology* (Chapman, S. K., and Reid, G. A., Eds.) Vol. 131, pp 1−7, Humana Press, Totowa, NJ.

14. Turner, K. L., Doherty, M. K., Heering, H. A., Armstrong, F. A., Reid, G. A., and Chapman, S. K. (1999) *Biochemistry 38*, 3302−3309.

15. Otwinowski, Z., and Minor, W. (1997) *Methods Enzymol. 276*, 307−326.

16. Roussel, A., and Cambillau, C. (1991) TURBO-FRODO, in *Silicon Graphics Geometry Partners Directory 86*, Silicon Graphics, Mountain View, CA.

17. Murshudov, G. N., Vagin, A. A., and Dodson, E. J. (1997) *Acta Crystallogr. D53*, 240−255.

18. Bossi, R. T., Negri, A., Tedeschi, G., and Mattevi, A. (2002) *Biochemistry 41*, 3018−3024.

BI0203177